

Supplemental information for The Neural Sources of N170:
Understanding Timing of Activation in Face-Selective Areas

John E. Richards¹

Chuanji Gao¹

Stefania Conte¹

Margaret Guy²

Wanze Xie³

¹*Department of Psychology, University of South Carolina, Columbia, SC*

²*Department of Psychology, Loyola University, Chicago, IL*

³*Laboratories of Cognitive Neuroscience, BCH, Harvard University, Boston, MA*

Supplemental information for The Neural Sources of N170: Understanding Timing of Activation
in Face-Selective Areas

The understanding of the neural sources of the N170 is an important addition to studies of face processing using fMRI and ERP as neuroimaging tools. This issue was addressed in a recent paper submitted to *Psychophysiology* (Gao, under review). This article reported a study of the presentation of faces and houses to adults along with recording of structural MRI, fMRI, and high-density ERPs. The study showed that the middle and posterior fusiform gyrus were the primary locations of the neural sources for the face-sensitive aspects of the N170.

The current paper is supplemental information supporting the results in that study. In this paper we review the locations of face sensitive areas found in the literature and provide tables of locations for the “fusiform face area”, studies of the N170 cortical sources, and other face sensitive areas. We present some methods of the study that were not included in the article. This includes a discussion of the methods used in prior studies for determine the “fusiform face area” with fMRI localizers and an analysis of three methods of error protection used for defining anatomical and functional ROIs for the analyses in the article. We report some analyses of data from that study not reported in the article, including an analysis of the reaction time and P1 ERP component. Finally we include some graphs and figures providing supporting information for analyses in the article and several supplementary analyses not reported in the article. A goal of this paper is to provide extra supplemental information and discussion not included in the article and methods and supplemental results specific to the article.

Locations of face sensitive areas in the literature

The locations in the brain of face sensitive areas has been studied with a number of several imaging modalities. We were interested in detailing a list of stereotaxic neuroanatomical

coordinates that could be used to guide our initial localization of the face sensitive areas in the fMRI and CDR analyses. We were particularly interested in the “fusiform face area” (FFA) studied in the literature. Müller et al. summarize the FFA in studies of face processing: “First described by Sergent, Ohta, and MacDonald (1992) and (Puce, Allison, Gore, & McCarthy, 1995) and labeled by N. Kanwisher et al. (1997) as the “Fusiform face area” (FFA), this region has been recognized as one of the most important regions in face processing. However, while originally the FFA has been described as one face-selective region (N. Kanwisher et al., 1997), it has been argued that there are two distinct face preferential cluster, one located in mid-FFG and the other in the more posterior FFG (Haxby et al., 1994; Pinsk et al., 2009; Rossion et al., 2000; Weiner & Grill-Spector, 2010).” To this end we surveyed studies of face sensitive areas in the brain to acquire lists of coordinates for these analyses. We also found coordinates from a recent meta-analysis of fMRI studies of face processing (Veronika I. Müller, 2018), and a study of functional localizers of the fusiform face area (FFA) (Berman et al., 2010). Table 1 contains the coordinates from all the analyses reported in this section.

The first task involved one of us (Guy) doing a literature search of fMRI studies of face processing. Sixty-seven studies were found that used fMRI neuroimaging and compared face processing to a control condition (Table 2). The anatomical coordinates of the face-sensitive areas were extracted from the studies and are listed in the Table 1 and Table 2 (147 coordinates). The coordinates in Table 2 contain both Talairach (Talairach, 1988) and MNI (Collins, Neelin, Peters, & Evans, 1994) space. The Talairach and MNI spaces have slightly different AC origin, size, and rotation (Lancaster et al., 2007). The differences in coordinate space were resolved with an affine transformation to/from the Talairach to the MNI space (e.g., <http://www.brainmap.org/icbm2tal/>). Table 1 (“Averages” tab) has a list of the FFA sources

found in this search. The average Talairach coordinates for the locations were [39.15, 51.83, -12.99] and [-38.86, -50.99, and -14.76] for the right and left FFA, respectively.

A second source of coordinates for the FFA came from a study that examined the coordinates of face localizer tasks in the FFG (Berman et al., 2010). They found 50 studies that used a face-control comparison to define a FFA localizer and report coordinates and task conditions for that study (Table 1 in (Berman et al., 2010); 83 coordinates). The coordinates in that study were presented in Talairach space and are presented in Table 1 (“Berman” and “Averages” tabs). The average Talairach coordinates for the locations in this study were [38.88, -51.84 -15.58] and [-39.33, -53.30, -17.15] for the right and left FFA, respectively. A third set of coordinates came from a recent meta-analysis of fMRI studies that detailed a number of locations for face-sensitive brain locations (Veronika I. Müller, 2018). That study included 77 studies with a face-control comparison and included any brain area. The meta-analysis clusters locations reported in the main paper and Supplemental paper that were located in the FFG were extracted and are contained in Table 1 (“Müller”, MNI, and “Averages”, Talairach, tabs; 29 coordinates). The average Talairach coordinates for the locations in this study were [36.71, -50.81, -17.51] and [-39.51, -56.09, -17.47] for the right and left FFA, respectively. Table 1 (“Averages” tab) also has a list of the coordinates from all three sources (259 coordinates). The average Talairach coordinates from all three sources were [38.80, -51.73, -14.35] and [-39.06, -56.27, -15.79] for the right and left FFA, respectively. It is not surprising that the three sources (Guy, Berman, Müller) have consistent average locations and were in the mFFG. The location of the FFA in these studies often was constrained to face-sensitive areas located in the anatomical location of the mFFG.

The second task involved two of us (Guy, Conte) examining the fMRI studies of face processing originally found for the FFA and extending this to studies that located faces sensitive areas in the lateral IOG, the “OFA”. Twenty studies were found that used fMRI neuroimaging, compared face processing to a control condition, and reported face-sensitive areas in the IOG (Table 3). Table 1 (“Averages” tab) also has a list of the coordinates from these studies (126 coordinates). The average Talairach coordinates were [38.23, -77.24, -9.25] and [-35.47, 79.22, -9.49], for the right and left OFA, respectively.

Third, we surveyed all the studies we could find that studied the cortical sources of the N170. These were primarily studies using EEG/ERP recording, though a few MEG “M170” studies were included. Twenty-five studies were found that recorded the N170 or M170 and used cortical source analysis to estimate the brain areas generating the scalp activity (Table 4). There were 71 brain locations that were reported as cortical sources for the ERP in a variety of different areas. However, they were predominantly in the fusiform gyrus (23 in right FFG; 22 in left FFG). Table 1 (“Averages” tab) has a list of the Talairach locations for the FFG and the average coordinates were [37.48, -49.50, -12.95] and [-37.30, -51.95, -10.10], for the right and left cortical source locations, respectively. The locations of the cortical sources designated as being location in the FFG were very close to the FFA found with fMRI studies.

The coordinates from the literature sources were translated into the MNI average template and into an average template from 20-24 year olds from the Neurodevelopmental MRI Database (J. E. Richards, Sanchez, Phillips-Meek, & Xie, 2015; John E. Richards & Xie, 2015). The Talairach coordinates for all the FFA locations, the OFA locations, and the N170 source locations (Table 1) were translated separately into the MNI coordinate system using an affine transformation relating Talairach coordinate space to MNI coordinate space (e.g.,

<http://www.brainmap.org/icbm2tal/>; (Lancaster et al., 2007)). The locations were placed into the corresponding voxels of the MNI coordinate space with the value of the voxel being the number of times that coordinate was found in the list. The average MNI template was registered to the average template of the 20-24 year olds with affine (FSL flirt; (Jenkinson & Smith, 2001)) and nonlinear (ANTS; (Avants et al., 2011; Klein et al., 2009)) registration. The registration parameters were used to transform the FFA/OFA/N170 volumes into the 20-24 year old average template space. Figure 1 shows the historical FFA locations overlaid on an atlas delineation of the mFFG (see following section on atlas ROIs). The FFA locations fall almost exclusively in the mFFG. Figure 2 shows the historical FFA locations (red) and the locations from the FFG for the N170 source analysis studies in a 2D representation, and Figure 1 of the main paper shows the same plot in a 3D rendering. The N170 source locations were spread more widely than the FFA locations. However, consistent with the similar average Talairach locations, there was substantial overlap in their overall location.

Lastly, a meta-analysis map was generated using Neurosynth (<http://www.neurosynth.org>; Yarkoni et al., 2011). Neurosynth is, a database containing fMRI activation coordinates from over 11406 studies (as of 06/2018). The meta-analysis map is an association test map showing brain regions that are preferentially related to the prespecified search term “face ffa”. The generated image was then thresholded using a false discovery rate criterion of .01 to correct for multiple comparisons. The output from the Neurosynth www site was a FDR-corrected MRI volume in the MNI spatial coordinate system. This MRI volume was translated into the 20-24 year old average MRI template. Figure 3 shows the distribution of the Neurosynth “face ffa” areas. Both the mFFG and IIOG heightened activations may be seen in this figure.

The MRI volumes from the historical coordinates (FFA, OFA, N170 sources, Neurosynth) were translated into each participant MRI. These were used in ROI analyses of the CDR. The registration parameters between each participant and the average 20-24 year template were used to transform the historical location volumes to the individual participant volumes.

Role of Attention in Face Processing—Background, Methods

The role of attention on face perception is still an open question (Cauquil, Edmonds, & Taylor, 2000; Palermo & Rhodes, 2007; Vuilleumier, Armony, Driver, & Dolan, 2001; H. Wang, Sun, Ip, Zhao, & Fu, 2015). Some early study found that face perception is automatic and cannot be influenced by attention. For example, Cauquil et al. (2000) examined the effect of attention on face processing by measuring the N170 component. They found that neither the latency nor the amplitude of the peaks of N170 was sensitive to the attention manipulation, suggesting an automatic nature of face processing. In contrast, some studies found that attention could influence face processing (Jacques & Rossion, 2006; Mohamed, Neumann, & Schweinberger, 2009; H. Wang et al., 2015). For example, one study investigated the effect of attentional resources on configural and featural face processing using attentional blink paradigm. They found that the amplitude of N170 was sensitive to attentional resources (H. Wang et al., 2015). Consistently, the influences of manipulation of attention on fusiform responses to faces were also found using fMRI (Vuilleumier et al., 2001; Wojciulik, Kanwisher, & Driver, 1998).

The behavioral data from the fMRI experiment were analyzed for mean accuracy and median reaction times (for correct trials only) using a Stimuli Category (face, house) \times Orientation (upright, inverted) mixed-model ANOVA. The behavioral data from the ERP experiment were analyzed for mean accuracy and median reaction times (for correct trials only)

using a Task (zero-back orientation, one-back orientation, one-back stimulus) \times Stimuli Category (face, house) \times Orientation (upright, inverted) mixed-model ANOVA.

Anatomical Regions of Interest (ROI)

Anatomical “Regions of Interest” (ROIs) were constructed that would be used in the analysis of the current density reconstruction (CDR) data. We were interested in a set of anatomical locations that would be useful for studying face sensitive areas found in the CDR, paralleling those typical found in fMRI studies of face processing. These areas include several ventral temporal and ventral temporal-occipital areas known to be part of the visual ventral processing stream. We also included some areas outside of the temporal-occipital areas that were known to be involved in face processing (e.g., STS) or were close to the typical FFA areas. These ROIs were constructed from individualized stereotaxic atlases based on the participants structural MRI and on atlas locations from the MNI.

First, we defined the ROIs based on anatomical stereotaxic atlases based on the individual structural MRI (Richards, 2013, Supplemental Information). These ROIs were based the LONI Probabilistic Brain Atlas (LPBA; (Shattuck et al., 2008) and the Hammers atlas, based on MRIs from the Information Exchange for the Internet (Hammers atlas (Heckemann, Hajnal, Aljabar, Rueckert, & Hammers, 2006; Heckemann et al., 2003)). These atlases were used to define 18 anatomical ROIs (Table 5). For this study, we selected a subset that would be of interest to the hypotheses about the N170 sources and FFA locations (e.g., source of N170 in the fFFG; FFA in mFFG; OFA in lIOG). We also selected several around these areas (e.g., parahippocampal gyrus, PPG; lingual gyrus, LG; anterior fusiform gyrus, aFFG; posterior inferior temporal gyrus, pITG; superior temporal sulcus, STS). Figure 4 (Guy, Zieber, &

Richards, 2016) shows the lateral posterior ROIs and temporal ROIs that could be important for this analysis.

Second, we used a recent study of the anatomy of the ventral temporal-occipital visual areas (eg., FG1, FG2, FG3, FG4; (Rosenke et al., 2018)) to define ROIs. There are differences in the delineation of the fusiform gyrus between atlases. The FFG extends from its anterior section of the temporal lobe to the posterior portion of the temporal-occipital area. However, some atlases (e.g., LPBA; (Shattuck et al., 2008)) define the FFG only to the temporal-occipital border at the temporal-occipital notch (left figure in Figure 5). This area would be described more appropriately as the aFFG and mFFG. It is likely that most studies of the FFA actually restrict their analysis of face-localizers to this anatomical ROI. However, the extension of face-sensitive areas into the pFFG (Veronika I. Müller, 2018) would include areas that extend beyond the LPBA definition of the fusiform gyrus. Figure 5 shows the LPBA atlas ROIs compared to the ventral occipital temporal areas described in Rosenke et al. “vcAtlas” (Rosenke et al., 2018). Two of the areas defined in the are the areas (FG3, FG4) are located in both the aFFG and mFFG and have substantial overlap with the mFFG defined from the individual participant atlas. Two other areas areas (FG1, FG2) provide an explicit anatomical location for the pFFG (Caspers et al., 2013; Rosenke et al., 2018). This area is not explicitly defined in the individual participant atlas.

Rosenke et al. (Rosenke et al., 2018) provided MNI coordinates for the FG and other areas described as the visual ventral temporal-occipital processing stream. The MNI coordinates for these anatomical locations were placed into the corresponding voxels of the MNI volume and transformed into the average template of the 20-24 year olds with affine (FSL flirt; (Jenkinson & Smith, 2001)) and nonlinear (ANTS; (Avants et al., 2011; Klein et al., 2009)) registration

parameters. The registration parameters were used to transform the FFA/OFA/N170 volumes into the 20-24 year old average template space. Figure 6 shows the overlap of the anatomically mFFG ROI and the four FG areas. It can be seen that areas FG3 and FG4 substantially overlap the mFFG and aFFG, whereas the FG1 and FG2 areas are primarily in the pFFG. Figure 1 in the main paper show both the anatomical ROI defined by the individual participant atlases and the vcAtlas. The affine and non-linear registration parameters between each participant and the average 20-24 template were used to transform the vcAtlas ROIs from the average template to the individual participant volumes.

The overlap of the anatomical ROI for each participant and the historical location volumes for each participant was computed for each participant and summed over all the participants. The overlap was computed from the Fieldtrip-formatted atlas files. The historical FFA locations were predominantly in the mFFG (right, 27%; left 10%), pITG (25%), IIOG (12%) with less than 10% in any other locations. The historical OFA locations were predominantly in the IIOG gyrus (right, 43%; left 9%) and in the middle occipital lobe (MOL; right, 24%; left 18%), and located primarily on the right (71%). The historical N170 source locations were predominantly in the mFFG (24%), IIOG (23%) and the right medial inferior occipital gyrus (17%; e.g., posterior FFG), and located predominantly on the right (N, 65%).

The overlap of the anatomical ROI for each participant and the resulting Neurosynth transformed volume was computed and summed over all the participants. The overlap analysis showed that the Neurosynth voxel locations were primarily in the mFFG (30%), MOL (N, 18%), IIOG (17%), with less than 10% in any of the other anatomical ROIs. There were more voxels on the right than on the left mFFG and overall more voxels on the right than on the left side of the brain (57 and 43%). The voxels on the mFFG had more voxels on the right than on the left,

whereas the pFFG and the IIOG had voxels in approximately equal amounts on the left and right sides.

Faces and Houses Stimuli

The main paper describes the source for the stimuli for the faces and houses. The faces were taken from the neutral and happy faces from the NimStim database (Tottenham et al., 2009). The houses were taken from the internet and contained only the house structure. Figure 7 shows exemplar stimuli for the faces and houses categories.

Placement of HGSN and 10-10 Electrodes

The electrode locations for the EGI hydrocel geodesic sensor net (HGSN) were done for each participant with the structural MRI and a “Geodesic Photogrammetry System” (GPS; (Russell, Jeffrey Eriksen, Poolman, Luu, & Tucker, 2005)). We have described the steps for this procedure in other publications (J. E. Richards, Boswell, Stevens, & Vendemia, 2015). The participant was placed in the GPS dome to acquire photographic images of the net on the head. A program was used that identifies each HGSN electrode location on the head and then provides 3D coordinates of each electrode position (Russell et al., 2005). The electrodes were then co-registered to the head mask of the anatomical MRI based on a set of fiducial electrodes on the MRI and the corresponding GPS coordinates. Coherent point set registration (CPD version 2; (A. Myronenko, & Song, X., 2010; A. Myronenko, Song, X., & Carreira-Perpinan, M., 2007)) registered the MRI and the GPS fiducials, and the resulting affine matrix was used to translate the GPS electrode coordinates into the MRI volume space ((J. E. Richards, 2013; J. E. Richards,

Boswell, et al., 2015), Supplemental Information). This procedure provided a set of realistic electrode placement positions for individual participants.

The electrode locations for the 10-10 recording system were done for each participant on the structural MRI (J. E. Richards, Boswell, et al., 2015). A set of external head locations that define the 10-10 system (Nz, Iz, LMA, RMA, LPA, RPA, Vz) were identified on the participant T1W head volume with a mask in the MRICron programs (Rorden, 2012a, 2012b). The voxel location of these masks were used with the MRI to compute the scalp locations of the 10-10 system using the “Unambiguously Illustrated 10/10 System” ((Jurcak, Okamoto, Singh, & Dan, 2005; Jurcak, Tsuzuki, & Dan, 2007); cf. (Oostenveld & Praamstra, 2001)). This provided a set of 10-10 EEG locations for each participant.

The HGSN and 10-10 locations were used in the analysis of the ERP and CDR data. In order to provide ERP analyses comparable to past results, we report all ERP analyses in the 10-10 coordinate system. Some studies using the EGI HGSN translate their data into 10-10 coordinates by linear combinations of ERP data at multiple HGSN locations, a “Virtual 10-10 System” (e.g. Figure 1, (Reynolds & Richards, 2005); Figure 2, (Henderson, Luke, Schmidt, & Richards, 2013)). However, the relation between individual 10-10 locations and the HGSN locations is not constant across participants due to head size, session net placement, and differential stretching of the HGSN filament connectors. We adopted a new procedure for this study that used the individual participant HGSN and 10-10 locations. A spherical spline interpolation algorithm was adopted from EEGLab (Delorme & Makeig, 2004). The participant’s HGSN locations and the 128-channel EEG/ERP binary data were transformed with a spherical spline interpolation program into the participant’s 10-10 locations and resulting 81-channel EEG/ERP data. This allows for individual HGSN net placement and head shapes and

other factors influencing the relation between HGSN and 10-10 locations. The program used for this analysis is presented in Table 6. Figure 7 shows the EGI and 10-10 locations plotted on a 2D map.

Functional localizers from the fMRI

Previous work defining the “fusiform face area” and other functional ROIs has generally used group-based fMRI locations translated to individual for the fROIs. However, recent work suggests that a localizer based on the individual fMRI results has advantages due to differences across participants in absolute BOLD levels and individual differences in functional anatomical localization (Fedorenko, Hsieh, Nieto-Castanon, Whitfield-Gabrieli, & Kanwisher, 2010; Glezer & Riesenhuber, 2013; Gorgolewski, Storkey, Bastin, & Pernet, 2012; Julian, Fedorenko, Webster, & Kanwisher, 2012; Nieto-Castanon & Fedorenko, 2012; J. X. Wang et al., 2014). This is consistent with our emphasis on individual ERP and source analysis based on realistic models for individual participants and insure that each participant had fROIs from the fMRI for the CDR analysis.

There are many merits of using individualized ROIs, but thresholding in single subject fMRI is challenging given the lower signal-to-noise ratio compared to group analyses. Thus, control of both false positives and false negatives are important for single subject analyses. We tried three methods for estimating thresholds based on individual fMRI volumes for faces gt houses, and houses gt faces contrasts: family-wise error (FWE) found by random field theory; adaptive thresholding designed for single subject fMRI analysis (Gorgolewski et al., 2012) in which voxels from the mFFG were used as input of this thresholding method; $p < .001$ without multiple comparison correction. In a series of simulations, Gorgolewski et al. (2012) demonstrated that adaptive thresholding performs better than fixed thresholding in terms of total

number of false positive and false negative error rates, over and underestimation of the true activation border.

We examined the three methods for thresholding. Figure 8 shows the average BOLD responses for the group average for faces > houses and houses > faces. The three methods produced varying results. Figure 9, Figure 10, and Figure 11 show the application of the three methods to our data and individual subjects. We found that several participants did not have a defined FFA in the fusiform gyrus with the FEW method, as well as the other functional ROIs. Given the role that the mFFG and pFFG plays in face processing, we want to have at least one left or right FFA for each participant in order to test the CDR data. We found that the adaptive thresholding method achieved an intermediate criterion compared to either FWE correction found by random field theory (more strict) or $p < .001$ without multiple comparison correction (more lenient). This suggests it had a good balance between the false positive and false negative error rates. Figure 12 shows the application of the adaptive thresholding to one subject; the gamma distribution correctly picked out the values of BOLD that had faces > houses in the fusiform gyrus.

We defined four ROIs for each participant based on this method: face-sensitive areas with significant thresholded voxels in the middle fusiform gyrus and adjacent areas (FFA); house-sensitive areas with significant thresholded voxels in the lingual gyrus and adjacent areas (LGHA); after removing the FFA and LGHA voxels, face sensitive areas in the occipital lobe and adjacent areas (OFA) and house-sensitive areas in the occipital lobe and adjacent areas (OHA). These were defined for individual participants using a threshold based on the Gauss-gamma adaptive threshold (Gorgolewski et al., 2012).

Fieldtrip Methods for Source Localization

The source analysis methods used the Fieldtrip MATLAB programs (Oostenveld, Fries, Maris, & Schoffelen, 2011). The Fieldtrip programs are a set of procedures for MATLAB that do segmentation, head model and source model generation, lead field and inverse spatial filter calculation, and source analysis. These methods have been previously detailed (Supplemental Information in (Buzzell et al., 2017)), and a precis of the Fieldtrip macros used is presented in Table 7. The majority of the CDR work was done in the coordinate space of the individual participant rather than participants being translated to an average MRI template.

The ROIs from the anatomical atlases, historical atlases, and functional ROIs were transformed in the Fieldtrip format for storing MRI volume data (Oostenveld et al., 2011). This format defines a MATLAB “struc” that has the position of the MRI voxels (“pos”), a vector of logical values that define if each position is used in the analysis (“inside”), and then information about the voxels relevant to the MRI volume (e.g., amplitude of the T1; MRI BOLD value; CDR amplitude). We used this member to extract the 1mm locations of each non-zero voxel in the individual anatomical or vcAtlas describing a stereotaxic ROI type. The values of the ROI type were assigned to the “inside” vector, and a “labelnumbers” and “labels” arrays that described an arbitrary label no and label name for each ROI type.

This Fieldtrip format for storing MRI volumes was also used with the CDR values. The source analysis function in Fieldtrip (ft_sourceanalysis) takes the structures necessary for input (electrode positions, forward model, lead field, inverse spatial filter, ERP data) and produces output in the Fieldtrip volume (e.g., “pos”, “inside”, CDR “power”). The source volume was based on a 3 mm voxel grid of the GM locations in the brain, so the “pos” locations were in 3 mm resolution but in the spatial coordinate system of the 1 mm MRI volume. This format allows

the extraction of summed ROI values by computing the overlap of atlas ROI positions with the corresponding positions of the CDR values directly from the original resolution without transforming them into 1 mm resolution. The mean CDR per mm ($\mu\text{A}/\text{mm}^3$) was computed as the summed CDR divided by the number of grid points making up that atlas segment. Thus for each msec of the ERP data put into the model, we have the CDR values for each ROI in our atlas segments. These calculations were done in the coordinate space of the individual participant.

The Fieldtrip format for storing MRI volumes was applied to the fMRI BOLD contrast volumes. The SPM GLM procedure results in MRI volumes that represent the contrast between the experimental condition contrasts (e.g., faces > houses; faces > rest). The fMRI acquisition was based on 2 mm resolution volumes. The voxels in the 2 mm volumes were translated into the spatial coordinates of the 1 mm MRI volume with the BBR registration results and stored in the “pos” values. The contrast levels from the fMRI BOLD contrasts were stored in the “contrast” member of the struc. All computations involving the fMRI data were done with the original 2mm results from the fMRI pipeline.

Some of the 3D rendered display data were derived from the fMRI BOLD volume and the CDR volumes. A quadratic polynomial transformation was applied to the sample-by-sample CDR values, centered at the peak latency of the N170 ERP component to emphasize the changes in the CDR similar to the N170. This resulted in a single value representing the quadratic trend in the CDR values. The quadratic polynomial sum trend values were translated into 3D MRI volumes by computing the index of the “pos” values in the 3D image and assigning voxel values in the image from the “pos”-indexed CDR transformed value. The CDR MRI volumes were then smoothed similar to the fMRI with a 6 mm full-width at half-maximum (FWHM) Gaussian kernel using FSL `fslmaths` (Jenkinson, Beckmann, Behrens, Woolrich, & Smith, 2012; Smith et

al., 2004). The individual participant volumes were translated into the average 20-24 year MRI template using affine (FSL flirt; (Jenkinson & Smith, 2001)) and nonlinear (ANTS; (Avants et al., 2011; Klein et al., 2009)) registration parameters. The transformed values were then averaged resulting in 3D MRI volumes in the coordinate space of the average MRI template.

Role of Attention in Face Processing—Results and Discussion

An analysis was conducted to examine the behavioral responses in the ERP experiment to the stimuli as a function of task, stimulus type, and stimulus orientation. Mean accuracy and median reaction times were analyzed respectively as a function of Stimulus Type (face, house), Stimulus Orientation (upright, inverted), and Task Group (0-back, 1-back stimulus, 1-back orientation) with a mixed-design ANOVA. For mean accuracy, a main effect of Task Group was found, $F(2, 30) = 51.69, p < 0.001, \eta^2 = .66$. The accuracy of the 0-back task was higher than either the 1-back stimulus or 1-back orientation task (median accuracy = 93.9, 54.9, and 56.0, respectively; StdErr = 2.08, 2050, and 2.84). No other main effects or interactions were significant ($ps > 0.05$). Figure 13 shows the reaction times for the fMRI and the three ERP conditions, separately for the stimuli X orientation conditions. There were no significant main effects or interactions on the median reaction time (median RTs = 211.0, 195.0, 210.0, and 202.5, StdErr = 20.62, 20.60, 17.05, and 19.06 for the upright faces, inverted faces, upright houses, inverted houses, respectively). Figure 14 shows the response probability for the fMRI and the three ERP conditions, separately for the stimuli X orientation conditions.

An analysis was conducted to examine the behavioral responses in the fMRI experiment to the stimuli as a function of stimulus type, and stimulus orientation. Mean accuracy and median reaction times were analyzed respectively as a function of Stimulus Type (face, house) and Stimulus Orientation (upright, inverted) with a repeated measures ANOVA. There were no main

effects or interactions for mean accuracy. Figure 14 shows response accuracy for the fMRI experiment. Accuracy was greater than 97% for all four conditions, similar to that for the EEG 0-back condition. There was a main effect of orientation on median reaction time, $F(1, 29) = 6.94$, $p = 0.01$, $\eta^2 = 0.04$. Figure 15 shows the reaction times for the fMRI experiment. The reaction times for the upright stimuli were faster than the inverted stimuli, for both faces and houses (median RT, 's = 239.5 and 234.75 for the upright faces and houses [stderr = 16.83, 27.21], 252.0 and 251.5 for the inverted faces and houses [stderr = 22.53, 35.5]). Overall the RTs in the fMRI experiment were longer than those in the ERP experiment.

The results of the current study did not show influences of attention on face processing in either behavior, ERP, or cortical source analyses, differing from some previously report results (Jacques & Rossion, 2006; Mohamed et al., 2009; H. Wang et al., 2015). Mohamed et al. (2009) examined whether selective attention influences neural processing of faces by assessing the sensitivity of the N170 for attention. They presented faces or houses as distractors while participants identified superimposed target letters. The targets were embedded in six identical (low load) or six different (high load) letters. They hypothesized that if N170 is not influenced by selective attention, there would be equivalent N170 amplitudes to distractor faces for high compared to low load condition. However, they found a prominent N170 responses under low load condition, whereas the N170 responses were lost under high load condition. Our results were more similar to those of Cauquil et al. (2000). They found that neither the latency nor the amplitude of the peaks of N170 was sensitive to the attention manipulation. The task conditions in the present study did not have a clear effect on the N170 ERP component. Although we did find some non-significant differences in the 0-back and the two 1-back tasks, these did not interact with either stimulus type nor stimulus orientation. The overall CDR level for the ERP

component was larger in the 1-back stimulus condition than in the other two conditions. However, this was not different for any of the stimulus type or stimulus orientation factors. A likely explanation for our findings is that our manipulation affected overall cognitive load during the task but did not affect selective attention.

P1 ERP Component Results

Amplitude values of P1 component were identified as the maximum amplitude within 100-200 ms over occipital and parietal cluster of electrodes (see Figure 7). Similar to analyses of the N170 component, we considered P1 amplitudes as a function of Stimulus Type (Face, House), Stimulus Orientation (upright, Inverted), and Task Group (0-back, 1-back stimulus, 1-back orientation), performing a Multivariate Analysis of Variance (MANOVA). Results showed a significant main effect of Stimulus Type, Wilk's $\Lambda = 0.4230$, $F(12,20) = 2.27$, $p = .0504$. Figure 15 shows a topographical scalp potential map and the ERP tracings for the faces vs houses stimuli. The P1 was of larger amplitude for faces compared to houses. No main effect or interactions involving the factor Task Group were found ($ps > .2679$), therefore amplitude values of the three groups were collapsed for the subsequent analyses. Figure 16 shows the P1 for the four stimulus conditions (stimulus type X orientation).

Separate univariate ANOVAs were performed on each cluster of electrodes to test the peak amplitude of the P1 component as a function of Stimulus Type and Stimulus Orientation. The main effect of Stimulus Type was significant over the lowest line of occipital channels (i.e., I1, IZ, and OZ, $ps < .0476$), showing that greater P1 amplitudes were elicited by faces compared to houses; whereas, inverted then upright stimuli produced greater peaks over O1 (Stimulus Orientation: $p = .0397$) and PO3 (Stimulus Orientation: $p = .0354$) cluster of electrodes. Furthermore, a significant interaction between Stimulus Type and Stimulus Orientation was

found for both P1 ($p = .0297$) and PZ ($p = .0439$) clusters. The peak amplitude of the P1 at the peak of the P1 latency is shown in Figure 17.

Simple effects were further examined through the calculation of the eta-squared values, which are reported in Table 9. The maximum value of variance was explained by Stimulus Type ($\eta^2 = .171$) over IZ, while parietal-occipital (i.e., PO3) and parietal (i.e., P1) clusters of electrodes largely explained the effect of Stimulus Orientation ($\eta^2 = .127$) and the interaction ($\eta^2 = .139$), respectively.

N170 ERP Component Results

The analysis of the N170 ERP component is presented in the main paper. Here we include three figures with further illustration of these effects. Figure 18 shows the ERP changes for the N170 comparing faces and houses. There was a larger N170 to the face than to the houses and this occurred in several of the inferior lateral-occipital electrodes. We found that picking the largest N170 peak among these electrodes and summing over the max electrode location resulted in the same pattern of conditions, but with much larger amplitude effects. Figure 19 shows the average ms-by-ms ERP at the peak of the N170 summed across the latency with the maximum amplitude, and Figure 20 shows bar charts for these figures. The largest N170 effects occurred on the right side in response to faces. The N170 to the inverted faces was larger than that to the upright faces.

Cortical Source and Anatomical ROIs

The cortical source analysis of the N170 ERP component was examined in the main paper. We present several detailed figures for these results and secondary analyses. for its relationship to the experimental conditions. Figure 21 shows the average CDR for the upright

and inverted faces stimuli plotted on a 3D rendering of the average MRI template. The activity was larger for the inverted than the upright faces, maximal in the left hemisphere.

The main paper reports a univariate ANOVA was carried out to examine the CDR values as a function of Stimulus Type (Face, House), Stimulus Orientation (Upright, Inverted), anatomical ROI (mFFG, pFFG, LG, and STS), Side (Left, Right) and Task Group (orientation, 1-back stimulus, 1-back orientation). Figures 22 and 23 are supporting figures for this analysis. These figures show the CDR plotted around the peak of the N170 for the four ROIs. The pFFG had the maximum amplitude (i.e., showed the largest CDR values), followed by the mFFG and LG, whereas the STS activity was the smallest. Current density amplitude was greater in response to faces than houses and in response to inverted then upright stimuli.

The main paper reports a univariate ANOVA was carried out to examine the CDR values as a function of Stimulus Type (Face, House), Stimulus Orientation (Upright, Inverted), functionally defined ROI (FFA, LGHA, OFA, OHA), Side (Left, Right) and Task Group (orientation, 1-back stimulus, 1-back orientation). Figures 24 and 25 are supporting figures for this analysis; Figure 26 is a bar chart of the average CDR at the peak of the N170 for these analyses. Figures 24 and 25 show the CDR plotted around the peak of the N170 for the four ROIs. The CDR for faces was larger than houses in the FFA, OFA, and LGHA ROIs, and was larger for inverted than upright stimuli.

Figures 27 and 28 show several some analyses of the CDR for the N170. Figure 27 shows the results of the CDR analyses (faces/houses, upright/inverted) for the anatomical areas defined by the historical literature studies of the FFA and the sources of the N170 (See Table S1). A similar pattern of faces > houses, inverted faces > upright faces, as found with the anatomical and function ROIs (Figure 7 in main paper; Figures 22 through 25). Figure 28 shows bar graphs

representing these results for the historical FFA, historical cortical sources of the N170, the Neurosynth areas, and the anatomical/functional ROIs in the main paper. All four ROIs based on historical findings duplicated those found with the anatomical and functional ROIs from this study.

Current Density Reconstruction and BOLD Contrast

We did not do formal quantitative comparisons between the current source analysis and the fMRI BOLD analyses due to the differences in methodology for quantifying the BOLD contrasts and the ERP CDR values. Figure 29 (bottom) shows a result of the CDR to the faces and houses on the right and left sides of the head as a function of the ventral temporal occipital areas. This figure is a supporting figure for one of the analyses in the main paper. There was a clear increase from the anterior to the middle FFG in the contrast values across these ROIs, and then a decrease in the values for the mFFG to the posterior occipital ROIs. The contrast values on the right were larger than on the left. The response to faces was larger than the response to houses. This figure also shows the BOLD contrast values for the faces and houses, right and left sides of the head, for these anatomical areas. The same kind of peak in the response at the middle and posterior FFG was found, and similar differences for left/right and faces/houses as the CDR. The CDR values showed more gradual increases and decreases than the BOLD contrast values.

Second, we plotted the average from all participants for the CDR to faces and the BOLD contrast values for the faces > rest contrast. Figure 30 shows 3D rendered MRIs for the BOLD contrast values for faces > rest, the CDR for faces, and a multiplication of the CDR by the BOLD values. The more compact peakedness of the BOLD contrast distribution may be seen in this figure compared to the CDR distribution, and both show larger activity on the right than on the

left. The peak of the combined CDR * BOLD values was in the same location as the peak CDR values (e.g., pFFG).

We did one supplementary analysis comparing the BOLD and CDR. We noticed (e.g., Figure 5 main paper) some substantial individual differences in the distribution of the N170 on the scalp. One finding was that most of the participants had a larger N170 on the right side, and a few had either equal N170 amplitude on the left and right, or had a larger N170 on the left side. The participant data were separated into left > right, left == right, and right > left and the fMRI BOLD from those groups was displayed. Figure 31 shows these results over the ventral temporal-occipital ROIs from the most anterior to posterior. The “typical” ERP right > left group had a similar pattern of responses for the fMRI—the BOLD on the right side was larger than on the left side, and the right side shows a more peaked response across the anterior to middle to posterior locations. The left = right ERP group showed a smaller fMRI response, approximately equivalent on the right and left sides. Some of the “left = right” ERP group had very small ERPs, reflecting the smaller BOLD response. The results from the left > right ERP group were the most different. The BOLD response was larger, was not different on the left and right sides, and was located in the more posterior regions of the ventral occipital areas than the other two groups. These results suggest there may be individual differences in the hemispheric specialization to faces that is found both in fMRI and ERP.

- Avants, B. B., Tustison, N. J., Song, G., Cook, P. A., Klein, A., & Gee, J. C. (2011). A reproducible evaluation of ANTs similarity metric performance in brain image registration. *Neuroimage*, *54*(3), 2033-2044. doi:10.1016/j.neuroimage.2010.09.025
- Berman, M. G., Park, J., Gonzalez, R., Polk, T. A., Gehrke, A., Knaffla, S., & Jonides, J. (2010). Evaluating functional localizers: the case of the FFA. *Neuroimage*, *50*(1), 56-71. doi:10.1016/j.neuroimage.2009.12.024
- Buzzell, G. A., Richards, J. E., White, L. K., Barker, T. V., Pine, D. S., & Fox, N. A. (2017). Development of the error-monitoring system from ages 9–35: Unique insight provided by MRI-constrained source localization of EEG. *Neuroimage*, *157*, 13-26. doi:<http://dx.doi.org/10.1016/j.neuroimage.2017.05.045>
- Caspers, J., Zilles, K., Eickhoff, S. B., Schleicher, A., Mohlberg, H., & Amunts, K. (2013). Cytoarchitectonical analysis and probabilistic mapping of two extrastriate areas of the human posterior fusiform gyrus. *Brain structure & function*, *218*(2), 511-526. doi:10.1007/s00429-012-0411-8
- Cauquil, A. S., Edmonds, G. E., & Taylor, M. J. (2000). Is the face-sensitive N170 the only ERP not affected by selective attention? *Neuroreport*, *11*(10), 2167-2171.
- Collins, D. L., Neelin, P., Peters, T. M., & Evans, A. C. (1994). Automatic 3D intersubject registration of MR volumetric data in standardized Talairach space. *J Comput Assist Tomogr*, *18*(2), 192-205.
- Delorme, A., & Makeig, S. (2004). EEGLAB: an open source toolbox for analysis of single-trial EEG dynamics including independent component analysis. *J Neurosci Methods*, *134*, 9-21.
- Fedorenko, E., Hsieh, P. J., Nieto-Castanon, A., Whitfield-Gabrieli, S., & Kanwisher, N. (2010). New method for fMRI investigations of language: defining ROIs functionally in individual subjects. *J Neurophysiol*, *104*(2), 1177-1194. doi:10.1152/jn.00032.2010
- Gao, C., Conte, S., Richards, J.E., Xie, W., & Hanayik, T. (under review). The neural sources of the N170: Understanding timing of activation in face-selective areas. *Psychophysiology*.
- Glezer, L. S., & Riesenhuber, M. (2013). Individual variability in location impacts orthographic selectivity in the "visual word form area". *J Neurosci*, *33*(27), 11221-11226. doi:10.1523/JNEUROSCI.5002-12.2013

- Gorgolewski, K., Storkey, A., Bastin, M., & Pernet, C. (2012). Adaptive thresholding for reliable topological inference in single subject fMRI analysis. *Front Hum Neurosci*, *6*(245). doi:10.3389/fnhum.2012.00245
- Guy, M. W., Zieber, N., & Richards, J. E. (2016). The cortical development of specialized face processing in infancy. *Child Dev*.
- Heckemann, R. A., Hajnal, J. V., Aljabar, P., Rueckert, D., & Hammers, A. (2006). Automatic anatomical brain MRI segmentation combining label propagation and decision fusion. *Neuroimage*, *33*(1), 115-126. doi:10.1016/j.neuroimage.2006.05.061
- Heckemann, R. A., Hartkens, T., Leung, K., Hill, D. L. G., Hajnal, J. V., & Rueckert, D. (2003). *Information extraction from medical images (IXI): Developing an e-Science application based on the globus toolkit*. Paper presented at the the 2nd UK e-Science All Hands Meeting, Nottingham, UK.
- Henderson, J., Luke, S., Schmidt, J., & Richards, J. (2013). Co-registration of eye movements and event-related potentials in connected-text paragraph reading. *Front Syst Neurosci*, *7*(28). doi:10.3389/fnsys.2013.00028
- Jacques, C., & Rossion, B. (2006). Electrophysiological evidence for temporal dissociation between spatial attention and sensory competition during human face processing. *Cerebral cortex*, *17*(5), 1055-1065.
- Jenkinson, M., Beckmann, C. F., Behrens, T. E., Woolrich, M. W., & Smith, S. M. (2012). Fsl. *Neuroimage*, *62*(2), 782-790. doi:10.1016/j.neuroimage.2011.09.015
- Jenkinson, M., & Smith, S. (2001). A global optimisation method for robust affine registration of brain images. *Med Image Anal*, *5*(2), 143-156.
- Julian, J. B., Fedorenko, E., Webster, J., & Kanwisher, N. (2012). An algorithmic method for functionally defining regions of interest in the ventral visual pathway. *Neuroimage*, *60*(4), 2357-2364. doi:10.1016/j.neuroimage.2012.02.055
- Jurcak, V., Okamoto, M., Singh, A., & Dan, I. (2005). Virtual 10-20 measurement on MR images for inter-modal linking of transcranial and tomographic neuroimaging methods. *Neuroimage*, *26*(4), 1184-1192. doi:10.1016/j.neuroimage.2005.03.021
- Jurcak, V., Tsuzuki, D., & Dan, I. (2007). 10/20, 10/10, and 10/5 systems revisited: their validity as relative head-surface-based positioning systems. *Neuroimage*, *34*(4), 1600-1611. doi:10.1016/j.neuroimage.2006.09.024

- Klein, A., Andersson, J., Ardekani, B. A., Ashburner, J., Avants, B., Chiang, M. C., . . . Parsey, R. V. (2009). Evaluation of 14 nonlinear deformation algorithms applied to human brain MRI registration. *Neuroimage*, *46*(3), 786-802. doi:10.1016/j.neuroimage.2008.12.037
- Lancaster, J. L., Tordesillas-Gutierrez, D., Martinez, M., Salinas, F., Evans, A., Zilles, K., . . . Fox, P. T. (2007). Bias between MNI and Talairach coordinates analyzed using the ICBM-152 brain template. *Hum Brain Mapp*, *28*(11), 1194-1205. doi:10.1002/hbm.20345
- Mohamed, T. N., Neumann, M. F., & Schweinberger, S. R. (2009). Perceptual load manipulation reveals sensitivity of the face-selective N170 to attention. *Neuroreport*, *20*(8), 782-787.
- Myronenko, A., & Song, X. . (2010). Point Set Registration: Coherent Point Drift. *IEEE Transactions on Pattern Analysis and Machine Intelligence*, *32*, 2262-2275.
- Myronenko, A., Song, X., & Carreira-Perpinan, M. (2007). Non-rigid point set registration: Coherent point drift. *Advances in Neural Information Processing Systems -- Proceedings of the 2006 Conference*, *19*, 1009-1016.
- Nieto-Castanon, A., & Fedorenko, E. (2012). Subject-specific functional localizers increase sensitivity and functional resolution of multi-subject analyses. *Neuroimage*, *63*(3), 1646-1669. doi:10.1016/j.neuroimage.2012.06.065
- Oostenveld, R., Fries, P., Maris, E., & Schoffelen, J. M. (2011). FieldTrip: Open source software for advanced analysis of MEG, EEG, and invasive electrophysiological data. *Comput Intell Neurosci*, *2011*, 156869. doi:10.1155/2011/156869
- Oostenveld, R., & Praamstra, P. (2001). The five percent electrode system for high-resolution EEG and ERP measurements. *Clin Neurophysiol*, *112*(4), 713-719.
- Palermo, R., & Rhodes, G. (2007). Are you always on my mind? A review of how face perception and attention interact. *Neuropsychologia*, *45*(1), 75-92.
- Reynolds, G. D., & Richards, J. E. (2005). Familiarization, attention, and recognition memory in infancy: an event-related potential and cortical source localization study. *Dev Psychol*, *41*(4), 598-615. doi:10.1037/0012-1649.41.4.598
- Richards, J. E. (2013). Cortical sources of ERP in prosaccade and antisaccade eye movements using realistic source models. *Front Syst Neurosci*, *7*, 27. doi:10.3389/fnsys.2013.00027

- Richards, J. E., Boswell, C., Stevens, M., & Vendemia, J. M. (2015). Evaluating methods for constructing average high-density electrode positions. *Brain Topogr*, *28*(1), 70-86. doi:10.1007/s10548-014-0400-8
- Richards, J. E., Sanchez, C., Phillips-Meek, M., & Xie, W. (2015). A database of age-appropriate average MRI templates. *Neuroimage*. doi:10.1016/j.neuroimage.2015.04.055
- Richards, J. E., & Xie, W. (2015). Brains for All the Ages: Structural Neurodevelopment in Infants and Children from a Life-Span Perspective. In *Adv Child Dev Behav*: JAI.
- Rosenke, M., Weiner, K. S., Barnett, M. A., Zilles, K., Amunts, K., Goebel, R., & Grill-Spector, K. (2018). A cross-validated cytoarchitectonic atlas of the human ventral visual stream. *Neuroimage*, *170*, 257-270. doi:<https://doi.org/10.1016/j.neuroimage.2017.02.040>
- Russell, G. S., Jeffrey Eriksen, K., Poolman, P., Luu, P., & Tucker, D. M. (2005). Geodesic photogrammetry for localizing sensor positions in dense-array EEG. *Clin Neurophysiol*, *116*(5), 1130-1140. doi:10.1016/j.clinph.2004.12.022
- Shattuck, D. W., Mirza, M., Adisetiyo, V., Hojatkashani, C., Salamon, G., Narr, K. L., . . . Toga, A. W. (2008). Construction of a 3D probabilistic atlas of human cortical structures. *Neuroimage*, *39*(3), 1064-1080. doi:10.1016/j.neuroimage.2007.09.031
- Smith, S. M., Jenkinson, M., Woolrich, M. W., Beckmann, C. F., Behrens, T. E., Johansen-Berg, H., . . . Matthews, P. M. (2004). Advances in functional and structural MR image analysis and implementation as FSL. *Neuroimage*, *23 Suppl 1*, S208-219. doi:10.1016/j.neuroimage.2004.07.051
- Talairach, J., & Tournoux, P. . (1988). *Co-planar stereotaxic atlas of the human brain: 3-dimensional proportional system-an approach to cerebral imagin*. New York: Theme Medical Publishers.
- Tottenham, N., Tanaka, J. W., Leon, A. C., McCarry, T., Nurse, M., Hare, T. A., . . . Nelson, C. (2009). The NimStim set of facial expressions: Judgments from untrained research participants. *Psychiatry Res*, *168*(3), 242-249. doi:10.1016/j.psychres.2008.05.006
- Veronika I. Müller, Y. H., Simon B. Eickhoff. (2018). Influence of Task Instructions and Stimuli on the Neural Network of Face Processing: An ALE Meta-analysis. *Cortex*. doi:10.1016/j.cortex.2018.03.011
- Vuilleumier, P., Armony, J. L., Driver, J., & Dolan, R. J. (2001). Effects of attention and emotion on face processing in the human brain: an event-related fMRI study. *Neuron*, *30*(3), 829-841.

Wang, H., Sun, P., Ip, C., Zhao, X., & Fu, S. (2015). Configural and featural face processing are differently modulated by attentional resources at early stages: an event-related potential study with rapid serial visual presentation. *Brain research*, *1602*, 75-84.

Wang, J. X., Rogers, L. M., Gross, E. Z., Ryals, A. J., Dokucu, M. E., Brandstatt, K. L., . . . Voss, J. L. (2014). Targeted enhancement of cortical-hippocampal brain networks and associative memory. *Science*, *345*(6200), 1054-1057. doi:10.1126/science.1252900

Wojciulik, E., Kanwisher, N., & Driver, J. (1998). Covert visual attention modulates face-specific activity in the human fusiform gyrus: fMRI study. *Journal of Neurophysiology*, *79*(3), 1574-1578.

Table Titles

Table 1. List of all coordinates used for our literature review of face-sensitive areas.

Table 2. List of fMRI studies used for our literature review of area reported as sensitive to faces. Table includes the headspace as well as the FFA coordinates for each study.

Table 3. List of fMRI studies used for our literature review of face-sensitive area in the lateral inferior occipital gyrus (OFA). For each study, headspace and respective coordinates are reported.

Table 4. List of studies that explored the cortical sources of N170 and M170 for faces. For each study, we reported the number of channels used to record brain activity as well as the inverse solution algorithm and the head model and space. Whenever reported we listed both coordinates and respective face-sensitive brain regions (otherwise “N/A”).

Table 5. Regions-of-interest (ROIs) and anatomical regions with labels from the lobar, Hammers, and LPBA40 atlases. The left columns are lateralized, and are presented from posterior-anterior and lateral-medial. The right columns are bilateral and presented from posterior to anterior.

Table 6. Matlab code used to transform data from HGSN 128-channels into “virtual 10-10” 81-channels locations by means of a spherical spline interpolation algorithm. \

Table 7. Fieldtrip macros for ERP source analysis.

Table 8. Preprocessing and processing pipeline for fMRI. Taylor Hanyik, March, 2016.

Table 9. Eta-squared values of P1 amplitude over occipital and parietal electrode cluster. Values represent the variance accounted for by Stimulus Type, Stimulus Orientation, and their interaction. The maximum value of variance for each effect is marked with *.

Table 1. Historical localizations for FFA, OFA, and N170.

<https://wp.me/a9YKYg-fk> or

https://jerlab.sc.edu/table_1_historical_localizations_ffa_ofa_n170-publicationversion/

This is an XLSX file with tables of coordinates of localizations from historical studies. It contains the following sheets:

EEG_SA—localization studies and coordinates of the N170—Maggie Guy and Chuangi Gao

FFA_Locations—localization studies and coordinates of the FFA—Maggie Guy and Stefania Conte.

Berman—coordinates for FFA localize studies (Berman et al., 2010)

Müller 2018—coordinates of faces sensitive areas (Müller, Höhner, & Eickhoff, 2018)

fMRI_FFA_coordinates—localization of fMRI FFA coordinates from FFA Locations, Berman, and Müller 2018.

fMRI_FFA_Paperlist—list of papers providing coordinates for the fMRI_FFA_coordinates

Averages—Lists of coordinates for N170, FFA, OFA, and average coordinates separated by right and left side

Berman, M. G., Park, J., Gonzalez, R., Polk, T. A., Gehrke, A., Knaffla, S., & Jonides, J. (2010). Evaluating functional localizers: the case of the FFA. *Neuroimage*, *50*(1), 56-71.
doi:10.1016/j.neuroimage.2009.12.024

Müller, V. I., Höhner, Y., & Eickhoff, S. B. (2018). Influence of task instructions and stimuli on the neural network of face processing: An ALE meta-analysis. *Cortex*, *103*, 240-255.

Table 2. List of fMRI studies used for our literature review of area reported as sensitive to faces.

Table includes the headspace as well as the FFA coordinates for each study.

Study	Head space	x	y	z
Aguirre (1999)	Talairach	37	-62	-17
T. J. Andrews and Ewbank (2004)	Talairach	44	-58	-22
		-46	-61	-27
Timothy J. Andrews and Schluppeck (2004)	Talairach	44	-59	-15
Avidan, Levy, Hendler, Zohary, and Malach (2003)	Talairach	34	-44	-15
		-38	-48	-15
Benuzzi et al. (2007)	MNI	44	-78	-10
		-44	-67	-17
		26	-101	2
		-22	-101	-2
		42	-57	-11
		-36	-67	-20
		44	-48	-18
		48	-52	-21
		30	-55	-11
		-48	-66	-7
Bernstein, Erez, Blank, and Yovel (2018)	MNI	40	-71	12
		-41	-73	9
Bobes et al. (2018)	MNI	54	-50	-17
		-51	-49	-11
		54	-51	-4
		47	-58	-7
		52	-52	-16
		-49	-47	-20
		52	-51	-16
		50	-52	-16
		-51	-48	-20
		32	-48	-16
		-52	-46	-20
Caldara et al. (2006)	Talairach	40	-50	-17
		-38	-52	-17
Caldara and Seghier (2009)	Talairach	41	-52	-17
		-38	-51	-16
Carlson, Grol, and Verstraten (2006)	Talairach	41	-51	-6
		-43	-58	-9
Chen, Kao, and Tyler (2007)	Talairach	28	-57	-14
Clark (1997)	Talairach	37	-55	10
Courtney (1997)	Talairach	31	-60	-20
		-32	-60	-16
Corrigan et al. (2009)	MNI152	-42	-48	-22
		42	-46	-24

Dove, Manly, Epstein, and Owen (2008)	Talairach	42	-51	-14
Downing, Chan, Peelen, Dodds, and Kanwisher (2006)	Talairach	37	-46	-15
Druzgal (2001)	Talairach	41	-56	-25
Eger, Schweinberger, Dolan, and Henson (2005)	Talairach	45	-45	-24
		-45	-45	-23
Eger, Schyns, and Kleinschmidt (2004)	Talairach	40	-54	-24
		-41	-57	-23
Epstein, Higgins, Parker, Aguirre, and Cooperman (2006)	Talairach	42	-52	-15
		-44	-54	-17
Fang, Murray, and He (2007)	Talairach	33	-40	-14
Feng et al. (2011)	MNI	42	-50	-19
		-40	-53	-21
Ganel, Valyear, Goshen-Gottstein, and Goodale (2005)	Talairach	36	-51	-16
Gathers (2004)	Talairach	42	-56	-22
Gauthier (2000)	Talairach	35	-49	-8
		-35	-56	-6
Gauthier et al., 2000b	Talairach	38	-50	-7
		-38	-56	-6
Gauthier (1999)	Talairach	41	-55	-10
		-40	-46	-12
George (1999)	Talairach	52	-60	-24
		-42	-68	-22
Gilaie-Dotan, Perry, Bonnef, Malach, and Bentin (2009)	Talairach	29	-47	-14
		-36	-54	-18
Grill-Spector, Knouf, and Kanwisher (2004)	Talairach	39	-40	-16
		-37	-42	-16
Hadjikhani and de Gelder (2003)	Talairach	35	-55	-14
		-34	-55	-13
Henson and Mouchlianitis (2007)	Talairach	42	-44	-15
		-42	-50	-13
Haxby et al. (1999)		39	-59	-16
		-39	-55	-23
Henson (2003)	MNI	40	-67	-12
		42	-45	-27
		-39	-51	-24
		-39	-48	-24
		-36	-48	-27
		-39	-45	-24
Hoffman and Haxby (2000)	Talairach	39	-55	-22
		-37	-60	-22
Horowitz, Rossion, Skudlarski, and Gore (2004)	Talairach	34.7	-53	12.7
		31	-40	-6
		42	-40	-15
		49	-20	-15

Iacoboni et al. (2004)	Talairach	36	-82	-22
		-20	-72	-12
Tetsuya Iidaka, Yamashita, Kashikura, and Yonekura (2004)	Talairach	60	-40	2
		-46	-34	-6
T. Iidaka, Matsumoto, Haneda, Okada, and Sadato (2006)	Talairach	-44	-62	-24
		-28	-52	-18
		30	-50	-16
		34	-60	-12
		30	-76	-12
Ishai, Bickle, and Ungerleider (2006)	Talairach	40	-57	-17
		-42	-58	-18
Kanwisher (1997)	Talairach	40	-55	10
Kesler (2001)	Talairach	39	-47	-12
		-39	-53	-12
Lehmann et al. (2004)	Talairach	32	-46	-18
		-43	-56	-16
Leibenluft, Gobbini, Harrison, and Haxby (2004)	Talairach	39	-59	-15
		-39	-61	-17
Loffler, Yourganov, Wilkinson, and Wilson (2005)	Talairach	37	-44	-15
Maurer et al. (2007)	Talairach	44	-60	-24
		-48	-60	-28
McCarthy, Puce, Gore, and Allison (1997)	Talairach	36	-52	-19
		-35	-56	-17
Muller, Hohner, and Eickhoff (2018) ¹	MNI	40	-52	-20
		-42	-52	-20
		40	-52	-22
		-44	-58	-20
		-40	-72	-14
		-42	-48	-18
Mur et al. (2012)	Talairach	40	-50	-15
		-37	-48	-13
Nasr and Tootell (2012)	Talairach	40	-52	-12
		-35	-57	-10
Nguyen and Cunnington (2014)	MNI	44	-50	-20
		-42	-52	-18
		30	-50	-8
		-30	-54	-10
		32	-56	-12
O'Craven (2000)	Talairach	37	-36	-18
		-37	-39	-15
Peelen and Downing (2005)	Talairach	41	-47	-17
		-38	-46	-16

¹ Coordinates refer to clusters' localizations identified by using the revised Activation Likelihood Estimation (ALE) algorithm.

Pitcher, Dilks, Saxe, Triantafyllou, and Kanwisher (2011)	Talairach	42	-58	-18
		42	-50	-13
		39	-59	-18
		39	-48	-16
		42	-45	-17
		43	-48	-16
		40	-50	-13
		43	-50	11
		45	-44	-15
		43	-47	-16
		40	-51	-15
		43	-40	-24
		40	-45	-15
		-42	-58	-18
		-42	-50	-13
		-39	-59	-18
		-39	-48	-16
		-42	-45	-17
		-43	-48	-16
		-40	-50	-13
-43	-50	11		
-45	-44	-15		
-43	-47	-16		
-40	-51	-15		
-43	-40	-24		
-40	-45	-15		
Pitcher, Walsh, and Duchaine (2011)		34	-52	-20
G. Pourtois, Schwartz, Seghier, Lazeyras, and Vuilleumier (2005)	Talairach	48	-57	-33
		-45	-51	-27
Pourtois (2005)	Talairach	48	-57	-33
		-45	-51	-27
A. Puce (1995)	Talairach	31	-60	-20
		-32	-60	-16
A. Puce (1996)	Talairach	30	-54	-20
		-38	-59	-21
Aina Puce et al. (2003)	Talairach	33	-58	-26
		-33	-55	-24
Reddy, Moradi, and Koch (2007)	Talairach	38	-50	-13
Reinholz and Pollmann (2005)	Talairach	37	-50	-12
		-41	-50	-14
Bruno Rossion, Schiltz, and Crommelinck (2003)		38	-44	-28
		-42	-50	-26
B. Rossion, Hanseeuw, and Dricot (2012)		36	-57	-15
		-37	-42	-17
		40	-44	-16
		38	-43	-17

		-39	-40	-20
		-42	-49	-17
		36	-48	-15
		38	-64	13
		-39	-46	16
		-35	-67	-15
<hr/>				
B. Rossion et al. (2003)		38	-44	-28
		44	-76	-14
<hr/>				
Rotshtein, Vuilleumier, Winston, Driver, and Dolan (2007)	Talairach	43	-45	-20
<hr/>				
Serences, Schwarzbach, Courtney, Golay, and Yantis (2004)	Talairach	33	-57	-14
<hr/>				
von Kriegstein (2005)	Talairach	42	-45	-24
		-36	-45	-30
<hr/>				
Yi, Kelley, Marois, and Chun (2006)	Talairach	39	-48	-15
		-39	-48	-15
<hr/>				
Zhang (2007)	Talairach	-48	-42	-2

- Aguirre. (1999). Stimulus inversion and the responses of face and object-sensitive cortical areas.
- Andrews, T. J., & Ewbank, M. P. (2004). Distinct representations for facial identity and changeable aspects of faces in the human temporal lobe. *Neuroimage*, *23*(3), 905-913. doi:10.1016/j.neuroimage.2004.07.060
- Andrews, T. J., & Schluppeck, D. (2004). Neural responses to Mooney images reveal a modular representation of faces in human visual cortex. *Neuroimage*, *21*(1), 91-98. doi:10.1016/j.neuroimage.2003.08.023
- Avidan, G., Levy, I., Hendler, T., Zohary, E., & Malach, R. (2003). Spatial vs. object specific attention in high-order visual areas. *Neuroimage*, *19*(2), 308-318. doi:10.1016/s1053-8119(03)00092-2
- Benuzzi, F., Pugnaghi, M., Meletti, S., Lui, F., Serafini, M., Baraldi, P., & Nichelli, P. (2007). Processing the socially relevant parts of faces. *Brain Res Bull*, *74*(5), 344-356. doi:10.1016/j.brainresbull.2007.07.010
- Bernstein, M., Erez, Y., Blank, I., & Yovel, G. (2018). An Integrated Neural Framework for Dynamic and Static Face Processing. *Sci Rep*, *8*(1), 7036. doi:10.1038/s41598-018-25405-9
- Bobes, M. A., Lage-Castellanos, A., Olivares, E. I., Perez Hidalgo-Gato, J., Iglesias, J., Castro-Laguardia, A. M., & Valdes-Sosa, P. (2018). ERP Source Analysis Guided by fMRI During Familiar Face Processing. *Brain Topogr*. doi:10.1007/s10548-018-0619-x
- Caldara, R., & Seghier, M. L. (2009). The Fusiform Face Area responds automatically to statistical regularities optimal for face categorization. *Hum Brain Mapp*, *30*(5), 1615-1625. doi:10.1002/hbm.20626
- Caldara, R., Seghier, M. L., Rossion, B., Lazeyras, F., Michel, C., & Hauert, C. A. (2006). The fusiform face area is tuned for curvilinear patterns with more high-contrasted elements in the upper part. *Neuroimage*, *31*(1), 313-319. doi:10.1016/j.neuroimage.2005.12.011
- Carlson, T., Grol, M. J., & Verstraten, F. A. (2006). Dynamics of visual recognition revealed by fMRI. *Neuroimage*, *32*(2), 892-905. doi:10.1016/j.neuroimage.2006.03.059
- Chen, C. C., Kao, K. L., & Tyler, C. W. (2007). Face configuration processing in the human brain: the role of symmetry. *Cereb Cortex*, *17*(6), 1423-1432. doi:10.1093/cercor/bhl054
- Clark. (1997). Selective Attention to Face Identity and Color Studied With fMRI.
- Corrigan, N. M., Richards, T., Webb, S. J., Murias, M., Merkle, K., Kleinhans, N. M., . . . Dawson, G. (2009). An investigation of the relationship between fMRI and ERP source localized

- measurements of brain activity during face processing. *Brain Topogr*, 22(2), 83-96.
doi:10.1007/s10548-009-0086-5
- Courtney, S. M. (1997). Transient and sustained activity in a distributed neural system for human working memory.
- Dove, A., Manly, T., Epstein, R., & Owen, A. M. (2008). The engagement of mid-ventrolateral prefrontal cortex and posterior brain regions in intentional cognitive activity. *Hum Brain Mapp*, 29(1), 107-119. doi:10.1002/hbm.20378
- Downing, P. E., Chan, A. W., Peelen, M. V., Dodds, C. M., & Kanwisher, N. (2006). Domain specificity in visual cortex. *Cereb Cortex*, 16(10), 1453-1461. doi:10.1093/cercor/bhj086
- Druzgal. (2001). Activity in fusiform face area modulated as a function of working memory load.
- Eger, E., Schweinberger, S. R., Dolan, R. J., & Henson, R. N. (2005). Familiarity enhances invariance of face representations in human ventral visual cortex: fMRI evidence. *Neuroimage*, 26(4), 1128-1139. doi:10.1016/j.neuroimage.2005.03.010
- Eger, E., Schyns, P. G., & Kleinschmidt, A. (2004). Scale invariant adaptation in fusiform face-responsive regions. *Neuroimage*, 22(1), 232-242. doi:10.1016/j.neuroimage.2003.12.028
- Epstein, R. A., Higgins, J. S., Parker, W., Aguirre, G. K., & Cooperman, S. (2006). Cortical correlates of face and scene inversion: a comparison. *Neuropsychologia*, 44(7), 1145-1158.
doi:10.1016/j.neuropsychologia.2005.10.009
- Fang, F., Murray, S. O., & He, S. (2007). Duration-dependent fMRI adaptation and distributed viewer-centered face representation in human visual cortex. *Cereb Cortex*, 17(6), 1402-1411.
doi:10.1093/cercor/bhl053
- Feng, L., Liu, J., Wang, Z., Li, J., Li, L., Ge, L., . . . Lee, K. (2011). The other face of the other-race effect: an fMRI investigation of the other-race face categorization advantage. *Neuropsychologia*, 49(13), 3739-3749. doi:10.1016/j.neuropsychologia.2011.09.031
- Ganel, T., Valyear, K. F., Goshen-Gottstein, Y., & Goodale, M. A. (2005). The involvement of the "fusiform face area" in processing facial expression. *Neuropsychologia*, 43(11), 1645-1654.
doi:10.1016/j.neuropsychologia.2005.01.012
- Gathers, A. D. (2004). Developmental shifts in cortical loci for face and object recognition.
- Gauthier, I. (1999). Activation of the middle fusiform 'face area' increases with expertise in recognizing novel objects.
- Gauthier, I. (2000). Expertise for cars and birds recruits brain areas involved in face recognition.
- George, J. S. (1999). Contrast polarity and face recognition in the human fusiform gyrus.
- Gilaie-Dotan, S., Perry, A., Bonneh, Y., Malach, R., & Bentin, S. (2009). Seeing with profoundly deactivated mid-level visual areas: non-hierarchical functioning in the human visual cortex. *Cereb Cortex*, 19(7), 1687-1703. doi:10.1093/cercor/bhn205
- Grill-Spector, K., Knouf, N., & Kanwisher, N. (2004). The fusiform face area subserves face perception, not generic within-category identification. *Nat Neurosci*, 7(5), 555-562.
doi:10.1038/nn1224
- Hadjikhani, N., & de Gelder, B. (2003). Seeing Fearful Body Expressions Activates the Fusiform Cortex and Amygdala. *Current Biology*, 13(24), 2201-2205. doi:10.1016/j.cub.2003.11.049
- Haxby, J. V., Ungerleider, L. G., Clark, V. P., Schouten, J. L., Hoffman, E. A., & Martin, A. (1999). The effect of face inversion on activity in human neural systems for face and object perception. *Neuron*, 22(1), 189-199.
- Henson, R. N. (2003). Electrophysiological and Haemodynamic Correlates of Face Perception, Recognition and Priming.
- Henson, R. N., & Mouchlianitis, E. (2007). Effect of spatial attention on stimulus-specific haemodynamic repetition effects. *Neuroimage*, 35(3), 1317-1329.
doi:10.1016/j.neuroimage.2007.01.019
- Hoffman, E. A., & Haxby, J. V. (2000). Distinct representations of eye gaze and identity in the distributed human neural system for face perception. *Nat Neurosci*, 3(1), 7.

- Horovitz, S. G., Rossion, B., Skudlarski, P., & Gore, J. C. (2004). Parametric design and correlational analyses help integrating fMRI and electrophysiological data during face processing. *Neuroimage*, *22*(4), 1587-1595. doi:10.1016/j.neuroimage.2004.04.018
- Iacoboni, M., Lieberman, M. D., Knowlton, B. J., Molnar-Szakacs, I., Moritz, M., Throop, C. J., & Fiske, A. P. (2004). Watching social interactions produces dorsomedial prefrontal and medial parietal BOLD fMRI signal increases compared to a resting baseline. *Neuroimage*, *21*(3), 1167-1173. doi:10.1016/j.neuroimage.2003.11.013
- Iidaka, T., Matsumoto, A., Haneda, K., Okada, T., & Sadato, N. (2006). Hemodynamic and electrophysiological relationship involved in human face processing: evidence from a combined fMRI-ERP study. *Brain Cogn*, *60*(2), 176-186. doi:10.1016/j.bandc.2005.11.004
- Iidaka, T., Yamashita, K., Kashikura, K., & Yonekura, Y. (2004). Spatial frequency of visual image modulates neural responses in the temporo-occipital lobe. An investigation with event-related fMRI. *Cognitive Brain Research*, *18*(2), 196-204. doi:10.1016/j.cogbrainres.2003.10.005
- Ishai, A., Bickel, P. C., & Ungerleider, L. G. (2006). Temporal dynamics of face repetition suppression. *Brain Res Bull*, *70*(4-6), 289-295. doi:10.1016/j.brainresbull.2006.06.002
- Kanwisher, N. M., J.; Chun, M.M. (1997). The Fusiform Face Area: A Module in Human Extrastriate Cortex Specialized for Face Perception.
- Kesler. (2001). Neural substrates of facial emotion processing using fMRI.
- Lehmann, C., Mueller, T., Federspiel, A., Hubl, D., Schroth, G., Huber, O., . . . Dierks, T. (2004). Dissociation between overt and unconscious face processing in fusiform face area. *Neuroimage*, *21*(1), 75-83. doi:10.1016/j.neuroimage.2003.08.038
- Leibenluft, E., Gobbini, M. I., Harrison, T., & Haxby, J. V. (2004). Mothers' neural activation in response to pictures of their children and other children. *Biol Psychiatry*, *56*(4), 225-232. doi:10.1016/j.biopsych.2004.05.017
- Loffler, G., Yourganov, G., Wilkinson, F., & Wilson, H. R. (2005). fMRI evidence for the neural representation of faces. *Nat Neurosci*, *8*(10), 1386-1390. doi:10.1038/nn1538
- Maurer, D., O'Craven, K. M., Le Grand, R., Mondloch, C. J., Springer, M. V., Lewis, T. L., & Grady, C. L. (2007). Neural correlates of processing facial identity based on features versus their spacing. *Neuropsychologia*, *45*(7), 1438-1451. doi:10.1016/j.neuropsychologia.2006.11.016
- McCarthy, G., Puce, A., Gore, J. C., & Allison, T. (1997). Face-specific processing in the human fusiform gyrus. *Journal Of Cognitive Neuroscience*, *9*(5), 6.
- Muller, V. I., Hohner, Y., & Eickhoff, S. B. (2018). Influence of task instructions and stimuli on the neural network of face processing: An ALE meta-analysis. *Cortex*, *103*, 240-255. doi:10.1016/j.cortex.2018.03.011
- Mur, M., Ruff, D. A., Bodurka, J., De Weerd, P., Bandettini, P. A., & Kriegeskorte, N. (2012). Categorical, yet graded--single-image activation profiles of human category-selective cortical regions. *J Neurosci*, *32*(25), 8649-8662. doi:10.1523/JNEUROSCI.2334-11.2012
- Nasr, S., & Tootell, R. B. (2012). Role of fusiform and anterior temporal cortical areas in facial recognition. *Neuroimage*, *63*(3), 1743-1753. doi:10.1016/j.neuroimage.2012.08.031
- Nguyen, V. T., & Cunnington, R. (2014). The superior temporal sulcus and the N170 during face processing: single trial analysis of concurrent EEG-fMRI. *Neuroimage*, *86*, 492-502. doi:10.1016/j.neuroimage.2013.10.047
- O'Craven, K. (2000). Mental Imagery of Faces and Places Activates Corresponding Stimulus-Specific Brain Regions.
- Peelen, M. V., & Downing, P. E. (2005). Within-subject reproducibility of category-specific visual activation with functional MRI. *Hum Brain Mapp*, *25*(4), 402-408. doi:10.1002/hbm.20116
- Pitcher, D., Dilks, D. D., Saxe, R. R., Triantafyllou, C., & Kanwisher, N. (2011). Differential selectivity for dynamic versus static information in face-selective cortical regions. *Neuroimage*, *56*(4), 2356-2363. doi:10.1016/j.neuroimage.2011.03.067

- Pitcher, D., Walsh, V., & Duchaine, B. (2011). The role of the occipital face area in the cortical face perception network. *Exp Brain Res*, 209(4), 481-493. doi:10.1007/s00221-011-2579-1
- Pourtois, G., Schwartz, S., Seghier, M. L., Lazeyras, F., & Vuilleumier, P. (2005). View-independent coding of face identity in frontal and temporal cortices is modulated by familiarity: an event-related fMRI study. *Neuroimage*, 24(4), 1214-1224. doi:10.1016/j.neuroimage.2004.10.038
- Puce, A. (1995). Face-Sensitive Regions in Human Extrastriate Cortex Studied by Functional MRI
- Puce, A. (1996). Differential Sensitivity of Human Visual Cortex to Faces, Letterstrings, and Textures: A Functional Magnetic Resonance Imaging Study.
- Puce, A., Syngieniotis, A., Thompson, J. C., Abbott, D. F., Wheaton, K. J., & Castiello, U. (2003). The human temporal lobe integrates facial form and motion: evidence from fMRI and ERP studies. *Neuroimage*, 19(3), 861-869. doi:10.1016/s1053-8119(03)00189-7
- Reddy, L., Moradi, F., & Koch, C. (2007). Top-down biases win against focal attention in the fusiform face area. *Neuroimage*, 38(4), 730-739. doi:10.1016/j.neuroimage.2007.08.006
- Reinholz, J., & Pollmann, S. (2005). Differential activation of object-selective visual areas by passive viewing of pictures and words. *Brain Res Cogn Brain Res*, 24(3), 702-714. doi:10.1016/j.cogbrainres.2005.04.009
- Rossion, B., Caldara, R., Seghier, M., Schuller, A. M., Lazeyras, F., & Mayer, E. (2003). A network of occipito-temporal face-sensitive areas besides the right middle fusiform gyrus is necessary for normal face processing. *Brain*, 126(Pt 11), 2381-2395. doi:10.1093/brain/awg241
- Rossion, B., Hanseeuw, B., & Dricot, L. (2012). Defining face perception areas in the human brain: a large-scale factorial fMRI face localizer analysis. *Brain Cogn*, 79(2), 138-157. doi:10.1016/j.bandc.2012.01.001
- Rossion, B., Schiltz, C., & Crommelinck, M. (2003). The functionally defined right occipital and fusiform "face areas" discriminate novel from visually familiar faces. *Neuroimage*, 19(3), 877-883. doi:10.1016/s1053-8119(03)00105-8
- Rotshtein, P., Vuilleumier, P., Winston, J., Driver, J., & Dolan, R. (2007). Distinct and convergent visual processing of high and low spatial frequency information in faces. *Cereb Cortex*, 17(11), 2713-2724. doi:10.1093/cercor/bhl180
- Serences, J. T., Schwarzbach, J., Courtney, S. M., Golay, X., & Yantis, S. (2004). Control of object-based attention in human cortex. *Cereb Cortex*, 14(12), 1346-1357. doi:10.1093/cercor/bhh095
- von Kriegstein, K. (2005). Interaction of Face and Voice Areas during Speaker Recognition.
- Yi, D. J., Kelley, T. A., Marois, R., & Chun, M. M. (2006). Attentional modulation of repetition attenuation is anatomically dissociable for scenes and faces. *Brain Res*, 1080(1), 53-62. doi:10.1016/j.brainres.2006.01.090
- Zhang, D. (2007). Detecting faces in pure noise images: a functional MRI study on top-down perception.

Table 3. List of fMRI studies used for our literature review of face-sensitive area in the lateral inferior occipital gyrus (OFA). For each study, headspace and respective coordinates are reported.

Study	Head space	x	y	z
Caldara et al. (2006)	Talairach	33	-76	-8
		-36	-79	-14
Caldara and Seghier (2009)		36	-82	-6
Feng et al. (2011)	MNI	39	-77	-13
		-38	-78	-13
Gauthier (2000)	Talairach	31	-75	0
		-30	-77	0
Hoffman and Haxby (2000)		-31	-82	-15
		41	-79	-14
Kovacs, Cziraki, Vidnyanszky, Schweinberger, and Greenlee (2008)	Talairach	47	-71	-7
		-43	-74	-6
Large, Cavina-Pratesi, Vilis, and Culham (2008)	Talairach	-34.3	-69	-15.8
		36	-75	-13
Liu (2010)	Talairach	46	-78	-7
		38	-78	-12
		-38	-78	-12
Muller, Hohner, and Eickhoff (2018)	MNI	30	-92	-8
		-22	-96	-6
		44	-86	-1
		46	-80	-8
		46	-78	-16
		38	-86	-10
		34	-88	-8
		26	-98	-6
		-38	-86	-6
		-40	-80	-12
		46	-80	-6
		46	-92	-8
		32	-90	-10
		30	-96	-8
42	-74	-12		
48	-82	-6		
54	-72	-2		

		46	-70	-10
		-20	-96	-8
		-40	-78	-10
		-20	-96	-8
		-22	-96	-8
		26	-96	-6
		28	-94	-6
		30	-92	-8
		32	-88	-10
		44	-76	-12
		44	-80	-10
		46	-80	-6
		46	-80	-8
		48	-82	-6
		48	-82	-6
		50	-76	-2
<hr/>				
Nichols, Betts, and Wilson (2010)	Talairach	40	-71	-9
		-37	-74	-9
<hr/>				
Pitcher, Dilks, Saxe, Triantafyllou, and Kanwisher (2011)	Talairach	44	-80	-4
		42	-76	-13
		40	-84	-3
		41	-83	3
		36	-85	-2
		45	-74	-10
		40	79	-10
		41	-76	-1
		41	-78	5
		42	-76	-13
		39	-80	-7
		51	-77	7
		39	-75	5
		-44	-80	-4
		-42	-76	-13
		-40	-84	-3
		-41	-83	3
		-36	-85	-2
		-45	-74	-10
		-40	79	-10
		-41	-76	-1
		-41	-78	5
		-42	-76	-13
		-39	-80	-7

		-51	-77	7
		-39	-75	5
Pitcher, Charles, Devlin, Walsh, and Duchaine (2009)	MNI	47	-72	-15
		49	-77	-3
		45	-68	-23
		51	-78	-12
		40	-81	-11
		46	-73	-6
		44	-65	-23
		38	-84	-10
		32	-88	-21
		50	-73	-9
		48	-78	-3
		44	-72	-18
		45	-70	-20
		51	-72	-6
		45	-79	-7
Puce (1996)	Talairach	36	-66	-17
		38	-62	-18
		-40	-66	-17
		-37	-71	-22
Ramon, Dricot, and Rossion (2010)	Talairach	31	-85	-7
		-28	-87	-10
Rhodes, Michie, Hughes, and Byatt (2009)	Talairach	40	-78	-6
		-37	-80	-8
B. Rossion et al. (2003)	Talairach	37	-87	-3
		-33	-80	-11
		-35	-83	-14
		27	-83	0
		-29	-83	-11
		38	-69	-11
		34	-80	-10
		48	-76	3
		-37	-78	-18
		38	-73	-19
		44	-80	-11
		-34	-81	-18
		31	-93	-12
		42	-83	-3
Rossion (2003)	Talairach	46	-80	-16
		44	-76	-14

B. Rossion, Hanseeuw, and Dricot (2012)	Talairach	25	-88	-10
		-20	-90	-12
		29	-84	-12
		-30	-84	-13
		32	-81	-10
		-34	-81	-8
		38	-72	-10
		-36	-72	-15
Rotshtein, Henson, Treves, Driver, and Dolan (2005)	MNI	43	-61	-20
Schiltz and Rossion (2006)	Talairach	39	-77	-11
		-38	-77	-9
		37	-75	-12
		-36	-73	-11

- Caldara, R., & Seghier, M. L. (2009). The Fusiform Face Area responds automatically to statistical regularities optimal for face categorization. *Hum Brain Mapp*, *30*(5), 1615-1625. doi:10.1002/hbm.20626
- Caldara, R., Seghier, M. L., Rossion, B., Lazeyras, F., Michel, C., & Hauert, C. A. (2006). The fusiform face area is tuned for curvilinear patterns with more high-contrasted elements in the upper part. *Neuroimage*, *31*(1), 313-319. doi:10.1016/j.neuroimage.2005.12.011
- Feng, L., Liu, J., Wang, Z., Li, J., Li, L., Ge, L., . . . Lee, K. (2011). The other face of the other-race effect: an fMRI investigation of the other-race face categorization advantage. *Neuropsychologia*, *49*(13), 3739-3749. doi:10.1016/j.neuropsychologia.2011.09.031
- Gauthier, I. (2000).
- Hoffman, E. A., & Haxby, J. V. (2000). Distinct representations of eye gaze and identity in the distributed human neural system for face perception. *Nat Neurosci*, *3*(1), 7.
- Kovacs, G., Cziraki, C., Vidnyanszky, Z., Schweinberger, S. R., & Greenlee, M. W. (2008). Position-specific and position-invariant face aftereffects reflect the adaptation of different cortical areas. *Neuroimage*, *43*(1), 156-164. doi:10.1016/j.neuroimage.2008.06.042
- Large, M. E., Cavina-Pratesi, C., Vilis, T., & Culham, J. C. (2008). The neural correlates of change detection in the face perception network. *Neuropsychologia*, *46*(8), 2169-2176. doi:10.1016/j.neuropsychologia.2008.02.027
- Liu, A. K. (2010).
- Muller, V. I., Hohner, Y., & Eickhoff, S. B. (2018). Influence of task instructions and stimuli on the neural network of face processing: An ALE meta-analysis. *Cortex*, *103*, 240-255. doi:10.1016/j.cortex.2018.03.011
- Nichols, D. F., Betts, L. R., & Wilson, H. R. (2010). Decoding of faces and face components in face-sensitive human visual cortex. *Front Psychol*, *1*, 28. doi:10.3389/fpsyg.2010.00028
- Pitcher, D., Charles, L., Devlin, J. T., Walsh, V., & Duchaine, B. (2009). Triple dissociation of faces, bodies, and objects in extrastriate cortex. *Curr Biol*, *19*(4), 319-324. doi:10.1016/j.cub.2009.01.007

- Pitcher, D., Dilks, D. D., Saxe, R. R., Triantafyllou, C., & Kanwisher, N. (2011). Differential selectivity for dynamic versus static information in face-selective cortical regions. *Neuroimage*, *56*(4), 2356-2363. doi:10.1016/j.neuroimage.2011.03.067
- Puce, A. (1996).
- Ramon, M., Dricot, L., & Rossion, B. (2010). Personally familiar faces are perceived categorically in face-selective regions other than the fusiform face area. *Eur J Neurosci*, *32*(9), 1587-1598. doi:10.1111/j.1460-9568.2010.07405.x
- Rhodes, G., Michie, P. T., Hughes, M. E., & Byatt, G. (2009). The fusiform face area and occipital face area show sensitivity to spatial relations in faces. *Eur J Neurosci*, *30*(4), 721-733. doi:10.1111/j.1460-9568.2009.06861.x
- Rossion, B., Caldara, R., Seghier, M., Schuller, A. M., Lazeyras, F., & Mayer, E. (2003). A network of occipito-temporal face-sensitive areas besides the right middle fusiform gyrus is necessary for normal face processing. *Brain*, *126*(Pt 11), 2381-2395. doi:10.1093/brain/awg241
- Rossion, B., Hanseeuw, B., & Dricot, L. (2012). Defining face perception areas in the human brain: a large-scale factorial fMRI face localizer analysis. *Brain Cogn*, *79*(2), 138-157. doi:10.1016/j.bandc.2012.01.001
- Rossion, B., Schiltz, C., & Crommelinck, M. (2003). The functionally defined right occipital and fusiform "face areas" discriminate novel from visually familiar faces. *Neuroimage*, *19*(3), 877-883. doi:10.1016/s1053-8119(03)00105-8
- Rotshtein, P., Henson, R. N., Treves, A., Driver, J., & Dolan, R. J. (2005). Morphing Marilyn into Maggie dissociates physical and identity face representations in the brain. *Nat Neurosci*, *8*(1), 107-113. doi:10.1038/nn1370
- Schiltz, C., & Rossion, B. (2006). Faces are represented holistically in the human occipito-temporal cortex. *Neuroimage*, *32*(3), 1385-1394. doi:10.1016/j.neuroimage.2006.05.037

Table 4. List of studies that explored the cortical sources of N170 and M170 for faces. For each study, we reported the number of channels used to record brain activity as well as the inverse solution algorithm and the head model and space. Whenever reported we listed both coordinates and respective face-sensitive brain regions (otherwise “N/A”).

Study	Technique	n. of channels	Method	Head model	Head space	x	y	z	Brain region
Batty and Taylor (2003)	EEG	32	LAURA Linear inverse	realistic head model based on MNI	MNI	N/A	N/A	N/A	Superior temporal and middle temporal gyri
Caldara et al. (2003)	EEG	62	LORETA/ BESA	3D spherical model	EC=8.47 VC=0.01 SC=4.89 EC=8.32 VC=0.01 SC=3.89	N/A	N/A	N/A	Occipito-temporal regions
Corrigan et al. (2009)	EEG and fMRI	128	LORETA	3-shell spherical head model	MNI	-44	-46	-22	Left fusiform gyrus
Deffke et al. (2007)	EEG	27	BESA dipole localizations (constrained bilateral)	4-shell ellipsoidal	Talairach	42	-46	-22	Right fusiform gyrus
						+35	-65	-11	Right fusiform gyrus
						-35	-65	-11	Left fusiform gyrus
						+35	-58	-5	Right fusiform gyrus
						-35	-58	-5	Left fusiform gyrus
MEG	93	BESA dipole localizations (constrained bilateral)	single-layer spherical	Talairach	+29	-62	-15	Right fusiform gyrus	
					-29	-62	-15	Left fusiform gyrus	
					+29	-64	-19	Right fusiform gyrus	
					-29	-64	-19	Left fusiform gyrus	
					Gao et al. (2013)	MEG	248	SAM- Beamformer	Template MRI adjusted to each individual head shape
28	-92	-18	Right fusiform gyrus						
32	-82	-12	Right fusiform gyrus						
23	-67	-6	Right lingual gyrus						
28	-74	-10	Right lingual gyrus						
Hadjikhani, Kveraga, Naik, and Ahlfors (2009)	MEG	306	MNE method	T1-weighted MRI images co-	N/A	N/A	N/A	N/A	

Commented [r1]:

Commented [r2]:

				registered with MEG data					
Halgren, Raji, Marinkovic, Jousmaki, and Hari (2000)	EEG and MEG	122	equivalent dipole current	spherical volume conductor, individual MRIs	Talairach	-38	-65	-14	Left occipito-temporal
					(M170)	35	-64	-8	Right occipito-temporal
Herrmann, Ehlis, Muehlberger, and Fallgatter (2005)	EEG	21	LORETA	3-shell spherical	Talairach	46	-25	-27	Right fusiform gyrus
						-38	-39	-27	Left fusiform gyrus
Ibanez et al. (2011)	EEG	128	sLORETA	Considered white matter anisotropy by using a diffusion tensor atlas co- registered with the ICBM model	MNI	40	67	-12	Posterior portions of fusiform gyrus
						25	-86	-18	Posterior portions of fusiform gyrus
Itier, Herdman, George, Cheyne, and Taylor (2006)	MEG	151	SAM- Beamformer	MNI template	Talairach	38	-54	-25	Right fusiform gyrus
						46	-58	-17	Right fusiform gyrus
						35	-60	-30	Right fusiform gyrus
Itier and Taylor (2004)	EEG	35	LAURA Linear inverse	realistic head model	not reported	N/A	N/A	N/A	Superior temporal sulcus
Jemel, George, Olivares, Fiori, and Renault (1999)	EEG	30	BESA dipole localizations (constrained bilateral)	3-shell head model	Talairach	35	-62	-15	Right infero-occipital gyrus
						-35	-62	-15	Left infero-occipital gyrus
Jemel, Coutya, Langer, and Roy (2009)	EEG	58	BESA dipole localizations (constrained bilateral)	4-shell spherical head model	Talairach	+39	-58	-7	Right fusiform gyrus
						-39	-58	-7	Left fusiform gyrus
						+28	-78	-17	Right middle occipital gyrus
						-28	-78	-17	Left middle occipital gyrus
Jung, Kim, Kim, Im, and Lee (2012)	EEG	64	sLORETA	3-shell head model	MNI	-45	-55	10	Left superior temporal gyrus

						-60	-60	0	Left middle temporal gyrus
Kaufmann, Schweinberger, and Burton (2009)	EEG	32	BESA dipole localizations (constrained bilateral)	4-shell spherical head model	Talairach	44.4	-65.6	-10	Right fusiform gyrus
						-44.4	-65.6	-10	Left fusiform gyrus
						51.4	-76.2	-11.3	Right fusiform gyrus
						-51.4	-76.2	-11.3	Left fusiform gyrus
Lopes et al. (2011)	EEG	78	sLORETA	realistic finite element model of the head	N/A	+37	51	25	Right fusiform gyrus
						-37	51	25	Left fusiform gyrus
Mnatsakanian and Tarkka (2004)	EEG	128	BESA dipole localizations (constrained bilateral)	4-shell ellipsoidal head model	Talairach	-37.6	-31.8	-11.1	Left fusiform/hippocampal gyri
						41.4	-34.9	-10	Right fusiform/hippocampal gyri
						-13.3	-67.7	4	Left lingual gyrus
						13.7	-67.9	4	Right lingual gyrus
						-36.6	-58.1	19.6	Left middle temporal gyrus
						45.9	-62.8	4.4	Right middle temporal gyrus
						-10	22.9	24	Left cingulate gyrus
						7.6	9.2	-4.9	Caudate nucleus
Petroni et al. (2011)	EEG	128	ARD	Average Lead Field	N/A	41	-8	-36	Right anterior fusiform gyrus
Pizzagalli et al. (2002)	EEG	27	LORETA	3-shell spherical head model	Talairach	67	-39	29	Supramarginal gyrus
Puce, Allison, Asgari, Gore, and McCarthy (1996)	fMRI	N/A	N/A	N/A	Talairach	30	-54	-20	Right fusiform gyrus
						-38	-59	-21	Left fusiform gyrus
						31	-54	-21	Right fusiform gyrus
						-39	-54	-23	Left fusiform gyrus
Rossion, Joyce, Cottrell, and Tarr (2003)	EEG	53	Constrained multiple dipole fit	realistic 3D head-shaped model	MNI	-65	-35	-8.3	Right inferior occipital gyrus
						-65	35	-8.3	Left inferior occipital gyrus
						-33	-41	-4.4	Inferior temporal gyrus
Santesso et al. (2008)	EEG	128	LORETA	3-shell spherical head model	MNI (84-124ms)	4	59	29	ACC/medial frontal gyrus
						18	66	6	Superior frontal gyrus
						18	59	-20	Superior frontal gyrus
						11	-53	1	Lingual/Parahippocampal gyri
	EEG	32	BESA		Talairach	+44	-42	29	Right-lateral extra-striate areas

Schweinberger, Pickering, Jentsch, Burton, and Kaufmann (2002)			dipole localizations (constrained bilateral)	4-shell spherical head model		-44	-42	29	Left-lateral extra-striate areas
Wong, Fung, Chua, and McAlonan (2008)	EEG	128	BESA dipole localizations (constrained bilateral)	realistic isotropic head model	Talarirach	-32.93	-49.26	-12.24	Left fusiform gyrus
						32.93	-49.26	-12.24	Right fusiform gyrus
Wong, Fung, McAlonan, and Chua (2009)	EEG	128	BESA dipole localizations (constrained bilateral)	realistic isotropic head model	Talairach	17.4	-66.5	-9.7	Right lingual gyrus
						-17.4	-66.5	-9.7	Left lingual gyrus
						37.5	-62.2	-12.3	Right fusiform gyrus
						-37.5	-62.2	-12.3	Left fusiform gyrus
						13.6	-74.2	7.6	Right lingual gyrus
						-13.6	-74.2	7.6	Left lingual gyrus
						32.9	-45.8	1.4	Right parahippocampal gyrus
						-32.9	-45.8	1.4	Left parahippocampal gyrus

- Batty, M., & Taylor, M. J. (2003). Early processing of the six basic facial emotional expressions. *Cognitive Brain Research*, *17*(3), 613-620. doi:10.1016/s0926-6410(03)00174-5
- Caldara, R., Thut, G., Servoir, P., Michel, C. M., Bovet, P., & Renault, B. (2003). Face versus non-face object perception and the 'other-race' effect: a spatio-temporal event-related potential study. *Clinical Neurophysiology*, *114*(3), 515-528. doi:10.1016/s1388-2457(02)00407-8
- Corrigan, N. M., Richards, T., Webb, S. J., Murias, M., Merkle, K., Kleinhans, N. M., . . . Dawson, G. (2009). An investigation of the relationship between fMRI and ERP source localized measurements of brain activity during face processing. *Brain Topogr*, *22*(2), 83-96. doi:10.1007/s10548-009-0086-5
- Deffke, I., Sander, T., Heidenreich, J., Sommer, W., Curio, G., Trahms, L., & Lueschow, A. (2007). MEG/EEG sources of the 170-ms response to faces are co-localized in the fusiform gyrus. *Neuroimage*, *35*(4), 1495-1501. doi:10.1016/j.neuroimage.2007.01.034
- Gao, Z., Goldstein, A., Harpaz, Y., Hansel, M., Zion-Golumbic, E., & Bentin, S. (2013). A magnetoencephalographic study of face processing: M170, gamma-band oscillations and source localization. *Hum Brain Mapp*, *34*(8), 1783-1795. doi:10.1002/hbm.22028
- Hadjikhani, N., Kveraga, K., Naik, P., & Ahlfors, S. P. (2009). Early (N170) activation of face-specific cortex by face-like objects. *Neuroreport*, *20*(4), 403.
- Halgren, E., Raji, T., Marinkovic, K., Jousmaki, V., & Hari, R. (2000). Cognitive response profile of the human fusiform face area as determined by MEG. *Cereb Cortex*, *10*, 69-81.
- Herrmann, M. J., Ehlis, A. C., Muehlberger, A., & Fallgatter, A. J. (2005). Source localization of early stages of face processing. *Brain Topogr*, *18*(2), 77-85. doi:10.1007/s10548-005-0277-7
- Ibanez, A., Petroni, A., Urquina, H., Torrente, F., Torralva, T., Hurtado, E., . . . Manes, F. (2011). Cortical deficits of emotional face processing in adults with ADHD: its relation to social cognition and executive function. *Soc Neurosci*, *6*(5-6), 464-481. doi:10.1080/17470919.2011.620769
- Itier, R. J., Herdman, A. T., George, N., Cheyne, D., & Taylor, M. J. (2006). Inversion and contrast-reversal effects on face processing assessed by MEG. *Brain Res*, *1115*(1), 108-120. doi:10.1016/j.brainres.2006.07.072

- Itier, R. J., & Taylor, M. J. (2004). Source analysis of the N170 to faces and objects. *Neuroreport*, *15*(8), 1261-1265.
- Jemel, B., Coutya, J., Langer, C., & Roy, S. (2009). From upright to upside-down presentation: a spatio-temporal ERP study of the parametric effect of rotation on face and house processing. *BMC Neurosci*, *10*, 100. doi:10.1186/1471-2202-10-100
- Jemel, B., George, N., Olivares, E., Fiori, N., & Renault, B. (1999). Event-related potentials to structural familiar face incongruity processing. *Psychophysiology*, *36*(4), 437-452.
- Jung, H. T., Kim, D. W., Kim, S., Im, C. H., & Lee, S. H. (2012). Reduced source activity of event-related potentials for affective facial pictures in schizophrenia patients. *Schizophr Res*, *136*(1-3), 150-159. doi:10.1016/j.schres.2011.10.023
- Kaufmann, J. M., Schweinberger, S. R., & Burton, A. M. (2009). N250 ERP correlates of the acquisition of face representations across different images. *Journal Of Cognitive Neuroscience*, *21*(4), 625-641. doi:10.1162/jocn.2009.21080
- Lopes, R., Cabral, P., Canas, N., Breia, P., Foreid, J. P., Calado, E., . . . Leal, A. (2011). N170 asymmetry as an index of inferior occipital dysfunction in patients with symptomatic occipital lobe epilepsy. *Clin Neurophysiol*, *122*(1), 9-15. doi:10.1016/j.clinph.2010.05.023
- Mnatsakanian, E. V., & Tarkka, I. M. (2004). Familiar-face recognition and comparison: source analysis of scalp-recorded event-related potentials. *Clin Neurophysiol*, *115*(4), 880-886. doi:10.1016/j.clinph.2003.11.027
- Petroni, A., Canales-Johnson, A., Urquina, H., Guex, R., Hurtado, E., Blenkman, A., . . . Ibanez, A. (2011). The cortical processing of facial emotional expression is associated with social cognition skills and executive functioning: a preliminary study. *Neuroscience Letters*, *505*(1), 41-46.
- Pizzagalli, D. A., Lehmann, D., Hendrick, A. M., Regard, M., Pascual-Marqui, R. D., & Davidson, R. J. (2002). Affective Judgments of Faces Modulate Early Activity (~160 ms) within the Fusiform Gyri. *Neuroimage*, *16*(3), 663-677. doi:10.1006/nimg.2002.1126
- Puce, A., Allison, T., Asgari, M., Gore, J. C., & McCarthy, G. (1996). Differential sensitivity of human visual cortex to faces, letterstrings, and textures: a functional magnetic resonance imaging study. *J Neurosci*, *16*(16), 5205-5215.
- Rossion, B., Joyce, C. A., Cottrell, G. W., & Tarr, M. J. (2003). Early lateralization and orientation tuning for face, word, and object processing in the visual cortex. *Neuroimage*, *20*, 1609-1624. doi:10.1016/S1053-8119(03)00460-9
- Santesso, D. L., Meuret, A. E., Hofmann, S. G., Mueller, E. M., Ratner, K. G., Roesch, E. B., & Pizzagalli, D. A. (2008). Electrophysiological correlates of spatial orienting towards angry faces: a source localization study. *Neuropsychologia*, *46*(5), 1338-1348. doi:10.1016/j.neuropsychologia.2007.12.013
- Schweinberger, S. R., Pickering, E. C., Jentsch, I., Burton, A. M., & Kaufmann, J. M. (2002). Event-related brain potential evidence for a response of inferior temporal cortex to familiar face repetitions. *Cognitive Brain Research*, *14*, 398-409.
- Wong, T. K., Fung, P. C., Chua, S. E., & McAlonan, G. M. (2008). Abnormal spatiotemporal processing of emotional facial expressions in childhood autism: dipole source analysis of event-related potentials. *Eur J Neurosci*, *28*(2), 407-416. doi:10.1111/j.1460-9568.2008.06328.x
- Wong, T. K., Fung, P. C., McAlonan, G. M., & Chua, S. E. (2009). Spatiotemporal dipole source localization of face processing ERPs in adolescents: a preliminary study. *Behavioral And Brain Functions: BBF*, *5*, 16. doi:10.1186/1744-9081-5-16

Table 5. Regions-of-interest (ROIs) and anatomical regions with labels from the lobar, Hammers, and LPBA40 atlases. The left columns are lateralized, and are presented from posterior-anterior and lateral-medial. The right columns are bilateral and presented from posterior to anterior (Guy et al. 2016).

Lateral inferior occipital lobe		Occipital lobe	
LPBA		Lobar	Occipital pole
65	L inferior occipital gyrus, lateral part	Hammers	
66	R inferior occipital gyrus, lateral part	66, 67	Cuneus (left, right)
		LPBA	
Inferior and middle temporal gyrus		67 68	L, R Cuneus
LPBA		Middle occipital lobe	
83	L middle temporal gyrus		
84	R middle temporal gyrus	LPBA	
85	L inferior temporal gyrus	63, 64	L, R middle occipital gyrus
86	R inferior temporal gyrus		
Medial inferior occipital lobe		Superior occipital lobe	
LPBA		LPBA	
65	L inferior occipital gyrus, medial part	61 62	L, R superior occipital gyrus
66	R inferior occipital gyrus, medial part	Superior parietal lobe	
Middle fusiform gyrus		Hammers	
Lobar	Fusiform gyrus, middle part	62, 63	Superior parietal gyrus left, right
Hammers:		LBPA	
15	Lateral occipitotemporal gyrus right, middle part	43, 44	L, R_superior_parietal_gyrus
16	Lateral occipitotemporal gyrus left, middle part	Posterior cingulate gyrus	
LPBA		Hammers	
91	L fusiform gyrus, middle part	26, 27	Cingulate gyrus left, right, posterior part
92	R fusiform gyrus, middle part	LPBA	
Anterior fusiform gyrus		121, 122	L, R_cingulate_gyrus, posterior part
Lobar	Fusiform gyrus, anterior part	Dorsal-anterior cingulate gyrus	
Hammers:		Hammers	
15	Lateral occipitotemporal gyrus right, anterior part	24, 25	Cingulate gyrus, anterior (supragenua), left, right, superior to anterior commissure
16	Lateral occipitotemporal gyrus left, anterior part	LPBA	
LPBA:		121, 122	L R cingulate_gyrus, anterior part, superior to AC
91	L fusiform gyrus, anterior part	Ventral-anterior cingulate	
92	R fusiform gyrus, anterior part	Hammers	
Lingual gyrus		76. 77	Subgenual anterior cingulate gyrus (right, left)
Hammers		78, 79	Subcallosal area (right, left)

64	Lingual gyrus left	80, 81	Pre-subgenual anterior cingulate (right, left)
65	Lingual gyrus right	24, 25	Cingulate gyrus, anterior (supragenual) (right, left), inferior to anterior commissure
LPBA		LPBA	
89	L lingual gyrus	121, 122	L R cingulate_gyrus, anterior part, inferior to AC
90	R lingual gyrus		
Parahippocampal gyrus		Orbito-frontal gyrus	
Hammers		Hammers	
9	Parahippocampal and ambient gyri right	52, 53	straight gyrus (right and left),
10	Parahippocampal and ambient gyri left	68, 69	, medial orbital gyrus (right and left),
LPBA		LPBA	
LPBA		29,30	L, R middle orbitofrontal gyrus
87	L parahippocampal gyrus	33,34	L, R , gyrus rectus
88	R parahippocampal gyrus		
Superior temporal gyrus		Frontal pole	
LPBA		Lobar	Frontal pole
81	L superior temporal gyrus		
82	R superior temporal gyrus		
Temporal pole			
Hammers			
5	Anterior temporal lobe, medial part right		
6	Anterior temporal lobe, medial part left		
7	Anterior temporal lobe, lateral part right		
8	Anterior temporal lobe, lateral part left		
82	Superior temporal gyrus, anterior part left		
83	Superior temporal gyrus, anterior part left		
Superior temporal sulcus			
LBPA			
81 & 83	Intersection (2 mm ea) of L superior temporal gyrus and L middle temporal gyrus		
82 & 84	Intersection (2 mm ea) of R superior temporal gyrus and R middle temporal gyrus		

Table 6. Matlab code used to transform data from HGSN 128-channels into “virtual 10-10” 81-channels

locations by means of a spherical spline interpolation algorithm.

```
%the HGSN electrodes are loaded in electrodes.locations (128, 3)
%the TenTen electrodes are loaded in tentenelectrodes.locations(81,3)
%the ERP data is in ERP1.bindata(128,nsegments,nbins)
%the output is in tempbindata(81,nsegments,nbins);

Gelec=[];
Gsph=[];
disp('begin spheric spline');
for binno=1:ERP1.nbin;
    disp(binno);
    [xx yy zz tempbindata(:,binno) Gelec Gsph] = ...
        JERLab_spheric_spline(electrodes.locations(:,1),electrodes.locations(:,2),electrodes.locations(:,3), ...
            tentenelectrodes.locations(:,1),tentenelectrodes.locations(:,2),tentenelectrodes.locations(:,3), ...
            squeeze(ERP1.bindata(:,binno)),Gelec,Gsph);
end

function [xbad, ybad, zbad, allres, Gelec, Gsph] = JERLab_spheric_spline( xelec, yelec, zelec, xbad, ybad, zbad, values,
    Gelec, Gsph)
%function [xbad, ybad, zbad, allres, Gelec, Gsph] = JERLab_spheric_spline( xelec, yelec, zelec, xbad, ybad, zbad, values,
    Gelec, Gsph)
%x y z elec are original electrudes
%x y z sites to be estimated
%values must be [nelec npoints], but is checked in program
%values are vector of values to interpolate
%if Gelec is an argument, use it rather than compute it
%if Gsph is an argument, use it rather than compute it. Gsph takes a long time for nodes with many locations
%adapted by John E. Richards, July 2017, from EEGLab
% Author: Arnaud Delorme, CERCO, CNRS, Mai 2006-
% Copyright (C) Arnaud Delorme, CERCO, 2006, arno@salk.edu
%
% This program is free software; you can redistribute it and/or modify
% it under the terms of the GNU General Public License as published by
% the Free Software Foundation; either version 2 of the License, or
% (at your option) any later version.
%

%rearrange to make nelec, 1
if size(xelec,1) > size(xelec,2);
    xelec=xelec';
    yelec=yelec';
    zelec=zelec';
end

if size(xbad,1) > size(xbad,2);
    xbad=xbad';
    ybad=ybad';
    zbad=zbad';
```

```

end

if size(values,1) ~= size(xelec,2);values=values';end;

if size(values,1) ~= size(xelec,2);
disp(['elect size and values size does not match ' num2str(size(xelec,2)) ' ' num2str(size(values,1))]);
return
end;

size(xelec);
size(xbad);
size(values);

newchans = length(xbad);
numpoints = size(values,2);

%SPHERERES = 20;
%[x,y,z] = sphere(SPHERERES);
%x(1:(length(x)-1)/2,:) = []; xbad = [ x(:)'];
%y(1:(length(x)-1)/2,:) = []; ybad = [ y(:)'];
%z(1:(length(x)-1)/2,:) = []; zbad = [ z(:)'];

if isempty(Gelec);
%disp('compute g');
Gelec = computeg(xelec,yelec,zelec,xelec,yelec,zelec);
Gsph = computeg(xbad,ybad,zbad,xelec,yelec,zelec);
end

% compute solution for parameters C
% -----
meanvalues = mean(values);
values = values - repmat(meanvalues, [size(values,1) 1]); % make mean zero

%disp('compute c');
values = [values;zeros(1,numpoints)];
C = pinv([Gelec;ones(1,length(Gelec))]) * values;
clear values;
allres = zeros(newchans, numpoints);

%disp('apply results');
% apply results
% -----
for j = 1:size(Gsph,1)
    allres(j,:) = sum(C .* repmat(Gsph(j,:)', [1 size(C,2)]));
end
allres = allres + repmat(meanvalues, [size(allres,1) 1]);

% compute G function
% -----
function g = computeg(x,y,z,xelec,yelec,zelec)

unitmat = ones(length(x(:)),length(xelec));
EI = unitmat - sqrt((repmat(x(:),1,length(xelec)) - repmat(xelec,length(x(:)),1)).^2 +...

```

```
(repmat(y(:),1,length(xelec)) - repmat(yelec,length(x(:)),1)).^2 +...  
(repmat(z(:),1,length(xelec)) - repmat(zelec,length(x(:)),1)).^2);
```

```
g = zeros(length(x(:)),length(xelec));  
%dsafds  
m = 4; % 3 is linear, 4 is best according to Perrin's curve  
for n = 1:7  
    if ismatlab  
        L = legendre(n,EI);  
    else % Octave legendre function cannot process 2-D matrices  
        for icol = 1:size(EI,2)  
            tmpL = legendre(n,EI(:,icol));  
            if icol == 1, L = zeros([ size(tmpL) size(EI,2)]); end;  
            L(:,:,icol) = tmpL;  
        end;  
    end;  
    g = g + ((2*n+1)/(n^m*(n+1)^m))*squeeze(L(1,,:));  
end  
g = g/(4*pi);
```

Table 7. Fieldtrip macros for ERP source analysis.

Realign MRI volumes to AC-defined space

```
cfg=[];
cfg.method='fiducial';
cfg.landmark.ac=mriinfo.ac;
cfg.landmark.pc=mriinfo.pc;
cfg.landmark.xzpoint=mriinfo.vertex;
cfg.landmark.right=mriinfo.rpa;
cfg.coordsys='spm';
cfg.parameter='gray';
mri=ft_volumerealign(cfg,mri);
```

Create the source model grid

```
cfg=[];
cfg.mri=mri;
cfg.threshold=.25;
cfg.smooth='no';
cfg.elec=elec;
cfg.grid.resolution=mmresol; % 1 mm or 3 mm
cfg.grid.unit='mm';
grid = ft_prepare_sourcemodel(cfg,mri);
grid=ft_determine_coordsys(grid,'interactive','no')
```

Create a compartment volume mesh

```
cfg = [];
cfg.method = 'projectmesh';
cfg.tissue = 'gray';
cfg.numvertices = 2000;
mesh = ft_prepare_mesh(cfg, mri);
```

Prepare the BEM-DIPOLI head model

```
cfg          = [];
cfg.feedback = false;
cfg.method    = 'dipoli';
cfg.isolatedsource = 'no';
cfg.conductivity = [conductivity(6) conductivity(5) conductivity(3) conductivity(2)];
cfg.tissue      = {'scalp','skull','csf','gray'};
vol            = ft_prepare_headmodel(cfg,mesh);
```

Prepare the FEM mesh

```
cfg = [];
cfg.shift = 0.3;
cfg.method = 'hexahedral';
mesh = ft_prepare_mesh(cfg,mri);
```

Prepate the BEM-SIMBIO head model

```
cfg = [];  
cfg.method='simbio';  
cfg.conductivity=conductivity;  
vol = ft_prepare_headmodel(cfg, mesh);
```

Prepare the lead-field matrix

```
cfg=[]  
cfg.vol=vol;  
cfg.elec=elec;  
cfg.grid=grid;  
cfg.normalize='no';  
lf=ft_prepare_leadfield(cfg);
```

MNE Source reconstruction

```
cfg=[];  
cfg.method='mne';  
cfg.vol=vol;  
cfg.elec=elec;  
cfg.grid=lf;  
cfg.projectnoise='yes';  
cfg.keepcsd='yes';  
cfg.mne.projectnoise='yes';  
cfg.mne.keepcsd='yes';  
cfg.mne.lambda=.000001;;  
cfg.mne.prewhten='no';  
sourcemne=ft_sourceanalysis(cfg,ERPdata);
```

eLORETA source reconstruction

```
cfg=[];  
cfg.method='eloreta';  
cfg.vol=vol;  
cfg.elec=elec;  
cfg.grid=lf;  
cfg.projectnoise='yes';  
cfg.keepcsd='yes';  
cfg.eloreta.projectnoise='yes';  
cfg.eloreta.keepcsd='yes';  
cfg.eloreta.keepmom='yes';  
cfg.eloreta.lambda=1e-5;  
cfg.lambda=cfg.eloreta.lambda;  
sourceft=ft_sourceanalysis(cfg,centermean);
```



```
disp('%%%%%%%%%%%%%%%%%%%%%%%%%%%%%%%%%%%%%%%%%%%%%%%%%%%%%%%%%%%%%%%%%%%%%%%%')
Jenkinson, M., Beckmann, C. F., Behrens, T. E., Woolrich, M. W., & Smith, S. M. (2012). Fsl. Neuroimage, 62(2), 782-790.
doi:10.1016/j.neuroimage.2011.09.015
```

S.M. Smith, M. Jenkinson, M.W. Woolrich, C.F. Beckmann, T.E.J. Behrens, H. Johansen-Berg, P.R. Bannister, M. De Luca, I. Drobnjak, D.E. Flitney, R. Niazy, J. Saunders, J. Vickers, Y. Zhang, N. De Stefano, J.M. Brady, and P.M. Matthews. *Advances in functional and structural MR image analysis and implementation as FSL. NeuroImage*, 23(S1):208-219, 2004.

```
disp('%%%%%%%%%%%%%%%%%%%%%%%%%%%%%%%%%%%%%%%%%%%%%%%%%%%%%%%%%%%%%%%%%%%%%%%%')
disp('stat 1st levelSub, including MOCO regressors')
disp('%%%%%%%%%%%%%%%%%%%%%%%%%%%%%%%%%%%%%%%%%%%%%%%%%%%%%%%%%%%%%%%%%%%%%%%%').
SPM 12 (http://www.fil.ion.ucl.ac.uk/spm)
```

The 14 contrasts were

- 1 'Task_minus_Rest', ...
- 2 'FacesInverted_minus_FacesUpright', ...
- 3 'FacesInverted_minus_HousesInverted', ...
- 4 'FacesInverted_minus_HousesUpright',...
- 5 'FacesUpright_minus_HousesInverted', ...
- 6 'FacesUpright_minus_HousesUpright',...
- 7 'HousesInverted_minus_HousesUpright',...
- 8 'Faces_minus_Houses',...
- 9 'FacesInverted_minus_Rest',...
- 10 'FacesUpright_minus_Rest',...
- 11 'HousesInverted_minus_Rest',...
- 12 'HousesUpright_minus_Rest', ...
- 13 'Faces_minus_Rest', ...
- 14 'Houses_minus_Rest'

Some files were created after the SPM contrast step

- 15—Faces minus houses, > 0, i.e., Faces > houses.
- 16—Houses minus faces, > 0, i.e., Houses > Faces
- 17—Faces minus rest, > 0, i.e., Faces > Rest
- 18—Houses minus rest, > 0, i.e., Houses > Rest
- 19—Faces upright minus inverted, > 0, i.e., Faces Upright > Faces Inverted
- 20—Faces inverted minus upright, > 0, i.e., Faces Inverted > Faces Upright
- 21—Houses upright minus inverted, > 0, i.e., Houses Upright > Houses Inverted
- 22—Houses inverted minus upright > 0, i.e., Houses Inverted > Houses Upright
- 23—Faces upright minus rest, > 0, i.e., Faces Upright > Rest
- 24—Faces inverted minus rest, > 0, i.e., Faces Inverted > Rest
- 25—Houses upright minus rest, > 0, i.e., Houses Upright > Rest
- 26—Houses inverted minus rest, > 0, i.e., Houses Inverted > Rest

Table 9. Eta-squared values of P1 amplitude over occipital and parietal electrode cluster. Values represent the variance accounted for by Stimulus Type, Stimulus Orientation, and their interaction. The maximum value of variance for each effect is marked with *.

Electrode Cluster	Stimulus Type	Stimulus Orientation	Type*Orientation
I1	0.146	0.083	0.002
IZ	0.171*	0.036	0.002
I2	0.109	0.049	0.004
O1	0.091	0.122	0.015
OZ	0.114	0.058	0.063
O2	0.077	0.029	0.030
PO3	0.014	0.127*	0.072
POZ	0.010	0.089	0.089
PO4	0.024	0.033	0.056
P1	0.019	0.109	0.139*
PZ	0.006	0.074	0.121
P2	0.001	0.006	0.111

Figure Titles

Figure 1. Graphical representation of the FFA locations of fMRI studies (red) and N170 cortical sources (green) from our literature review. Both results seem to overlap in the FFG, although N170 sources locations look more widespread than FFA locations.

Figure 3. 3D rendering localization (on an average MRI template) of the face-sensitive areas from the Neurosynth database (<http://www.neurosynth.org>).

Figure 4. Lateral posterior (left) and temporal (right) ROIs relevant for face processing (from Guy, Zieber, & richards, 2016).

Figure 5. Loni Probabilistic Brain Atlas (left; Shattuck et al., 2008) and ventral occipital temporal ROIs (right) described in Rosenke et al. (2018) and transformed into the average adult template.

Figure 6. Relation between mFFG (green) as defined in LPBA (Shattuck et al., 2008) and posterior (FG1, FG2) and middle (FG3, FG4) portions of the fusiform gyrus defined by the cythoarchitectonic cell organization.

Figure 8. Functional localization of faces and houses. Top panel represent the group average response to Faces > Houses, bottom panel show the localization of the group average response to Houses > Faces.

Figure 9. Comparison between three different methods used to estimate thresholds plotted on two individual fMRI volumes. Random filter Theory (RFT), Gaussian-Gamma Adaptive Tresholding (AT), and .001 Bonferroni correction methods produced similar results in Subject 1 (top row), but only AT method performed well in detecting large enough thresholds for the fusiform face area.

Figure 10. Example fROI definitions for family-wise error (red), adaptive thresholding (blue), and $p < .001$ without corrections (green). The volume on the left showed similar coverate for FWE and adaptive thresholding, and liberal coverage for $p < .001$. The figure on the right showed appropriate coverage only for the adaptive thresholding.

Figure 11. Comparison of thresholds for fROI on SPM “Glass plots”. Random Field Theory (RT), Gauss-Gamma Adaptive Thresholt (AT), and .001 Bonferonni correction (.001).

Figure 12. Gauss-Gamma Adaptive Threshold results for one subject. The left graphs are for T-value thresholds taken from the whole brain, and the right graphs are from thresholds taken only from the fusiform and lingual gyri.

Figure 13. Reaction times for the fMRI experiment and the three attention conditions, as a function of the stimulus and orientation stimuli.

Figure 14. Response probability for the fMRI experiment and the three attention conditions, as a function of the stimulus and orientation stimuli.

Figure 15. Topographical maps (left) representing the scalp distribution of the P1 component (at around 130 ms) for faces and houses. Grand average ERP waveforms (right) as a function of Stimulus Type at medial posterior cluster of electrodes. Larger P1 peaks for faces than houses were recorded at the bottom lines of electrodes (I1, IZ, OZ).

Figure 16. Topographical maps (left) representing the scalp distribution of the P1 component (at around 130 ms) for faces and houses. Grand average ERP waveforms (right) as a function of the four conditions at medial posterior cluster of electrodes. Large P1 peaks were recorded at the bottom lines of electrodes (I1, IZ, I2, O1, OZ, O2).

Figure 17. Amplitude values plotted around the peak of P1 as a function of the four stimulus conditions. Overall, larger amplitudes around the peak were found for faces compared to houses and for inverted compared to upright stimuli.

Figure 18. Topographical maps (left) representing the scalp distribution of the N170 component (at around 177 ms) for faces and houses. Grand average ERP waveforms (right) as a function of Stimulus Type at posterior lateral cluster of electrodes. Both the representations show that larger occipital negativity was elicited by faces when compared to houses.

Figure 19. Amplitude values plotted around the peak of N170 as a function of the four stimulus conditions. Larger amplitudes around the peak were found for faces compared to houses and for inverted compared to upright stimuli. Also, N170 amplitude appears to be larger over right than left cluster of channels.

Figure 20. Bar graphs depicting amplitude values around the peak of N170 as a function of the four experimental stimulus types. Larger amplitudes around the peak are shown for faces compared to houses and for inverted compared to upright stimuli. N170 amplitude appears to be larger over right than left cluster of channels.

Figure 21. The figures represent the CDR values on the average template, where the average is found by translating the individual CDR to the space of the average MRI template, smoothing with a 4mm Gaussian filter, and averaging the resulting transformed-smoothed MRI volumes. Individual volumes were entered into a one-way t-test (upright faces CDR < inverted faces CDR) with Monte Carlo permutations controlled by a cluster strategy. The displayed CDRs are above the minimum significant t-value from this analysis.

Figure 22. Current density reconstruction (CDR) values at middle (top) and posterior (bottom) fusiform Gyri plotted around the peak of N170 as a function of the four conditions. Larger CDR values around the peak were found for faces compared to houses, with the largest amplitudes recorded at the posterior fusiform gyrus. All regions showed an inversion effect for faces.

Figure 23. Current density reconstruction (CDR) values at lingual gyrus (top) and superior temporal sulcus (bottom) plotted around the peak of N170 as a function of the four conditions. Larger CDR values around the peak were found for faces compared to houses, with the smallest amplitudes recorded at the superior temporal sulcus. All regions showed an inversion effect for faces.

Figure 24. Current density reconstruction (CDR) values of left and right functional ROIs (FFA top panels, LGHA bottom panels) plotted around the peak of N170 as a function of the four conditions. Larger CDR values around the peak were found for faces compared to houses and all regions showed an inversion effect for faces but not for houses.

Figure 25. Current density reconstruction (CDR) values of left and right functional occipital ROIs (OFA top panels, OHA bottom panels) plotted around the peak of N170 as a function of the four conditions. Larger CDR values and significant inversion effect were found around the N170 peak at OFA. The OHA did not differ significantly for the four conditions.

Figure 26. Current Density Reconstruction (CDR) values around the peak of N170 (left and right) as a function of the four conditions over the four functional ROIs. FFA, LGHA, and OFA functional regions show larger CDR values around the peak and selective inversion effect for faces but not for houses. CDR values at OHA reported nonsignificant differences between conditions.

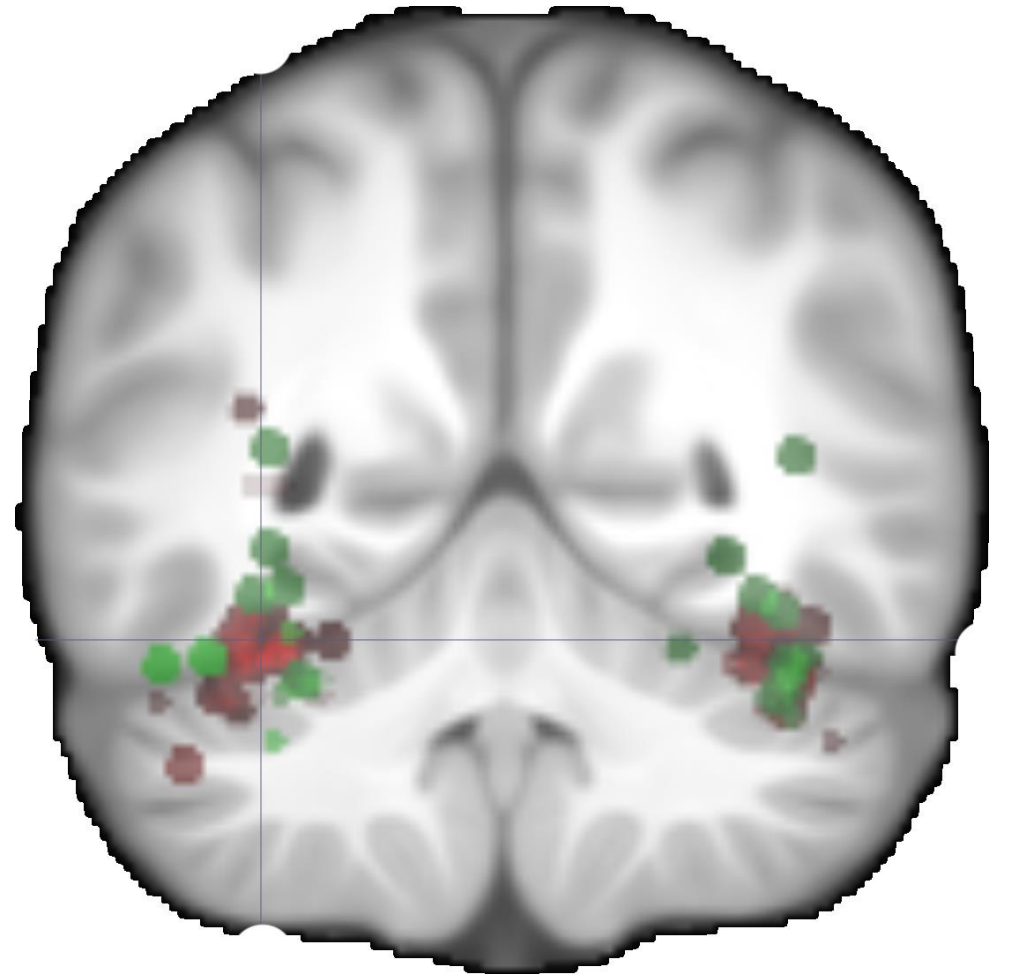
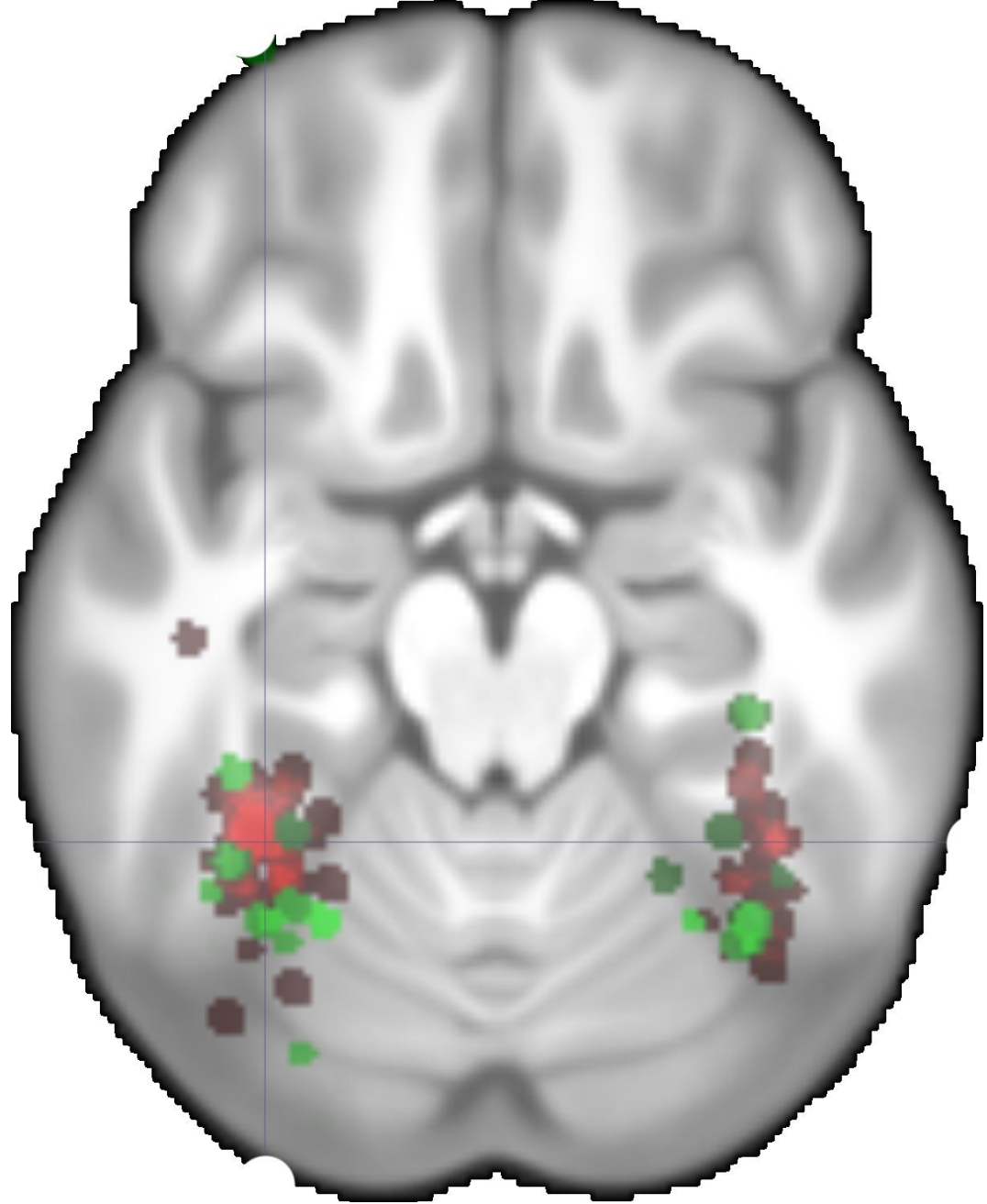
Figure 27. Current Density Reconstruction (CDR) values as a function of the four experimental stimulus types. Top panels depict CDRs over the area (left and right) reported as sensitive to faces in fMRI studies from our literature research. Bottom panels show CDRs of the N170 source locations (left and right) from our literature review.

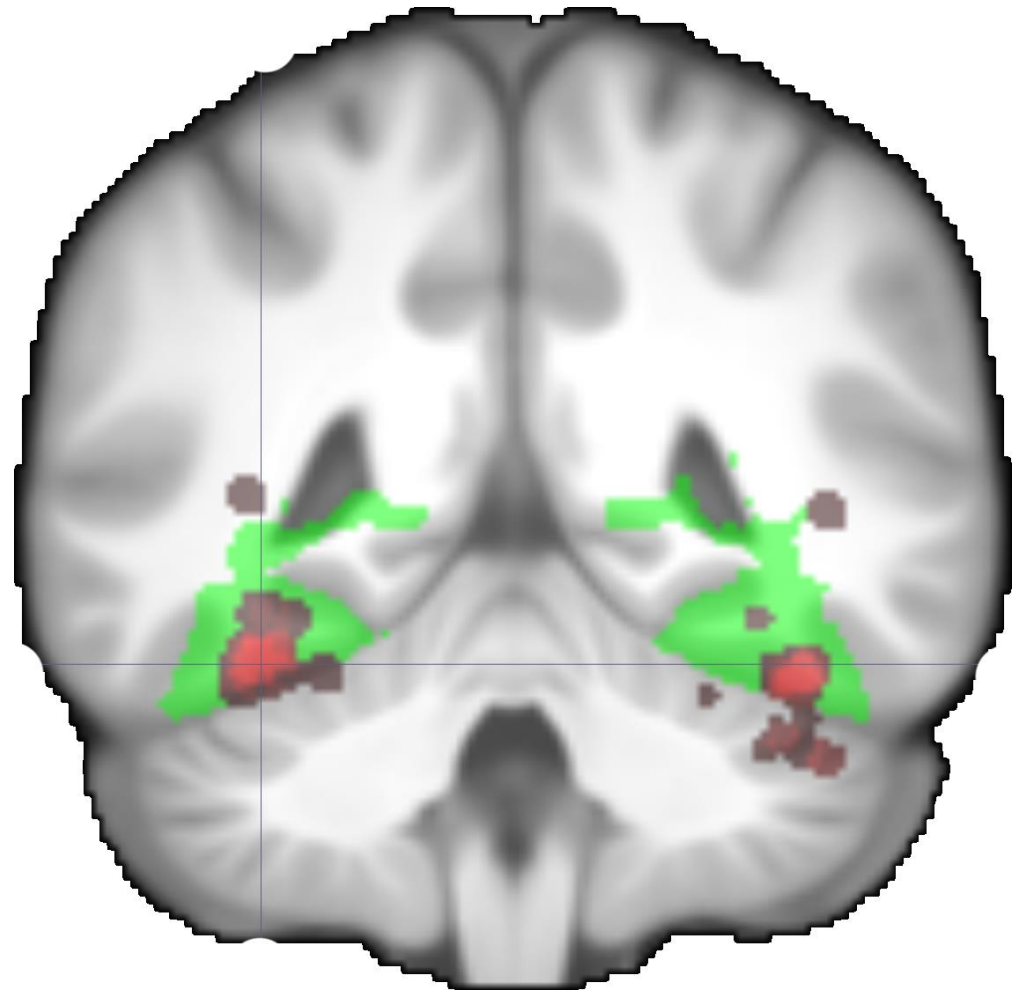
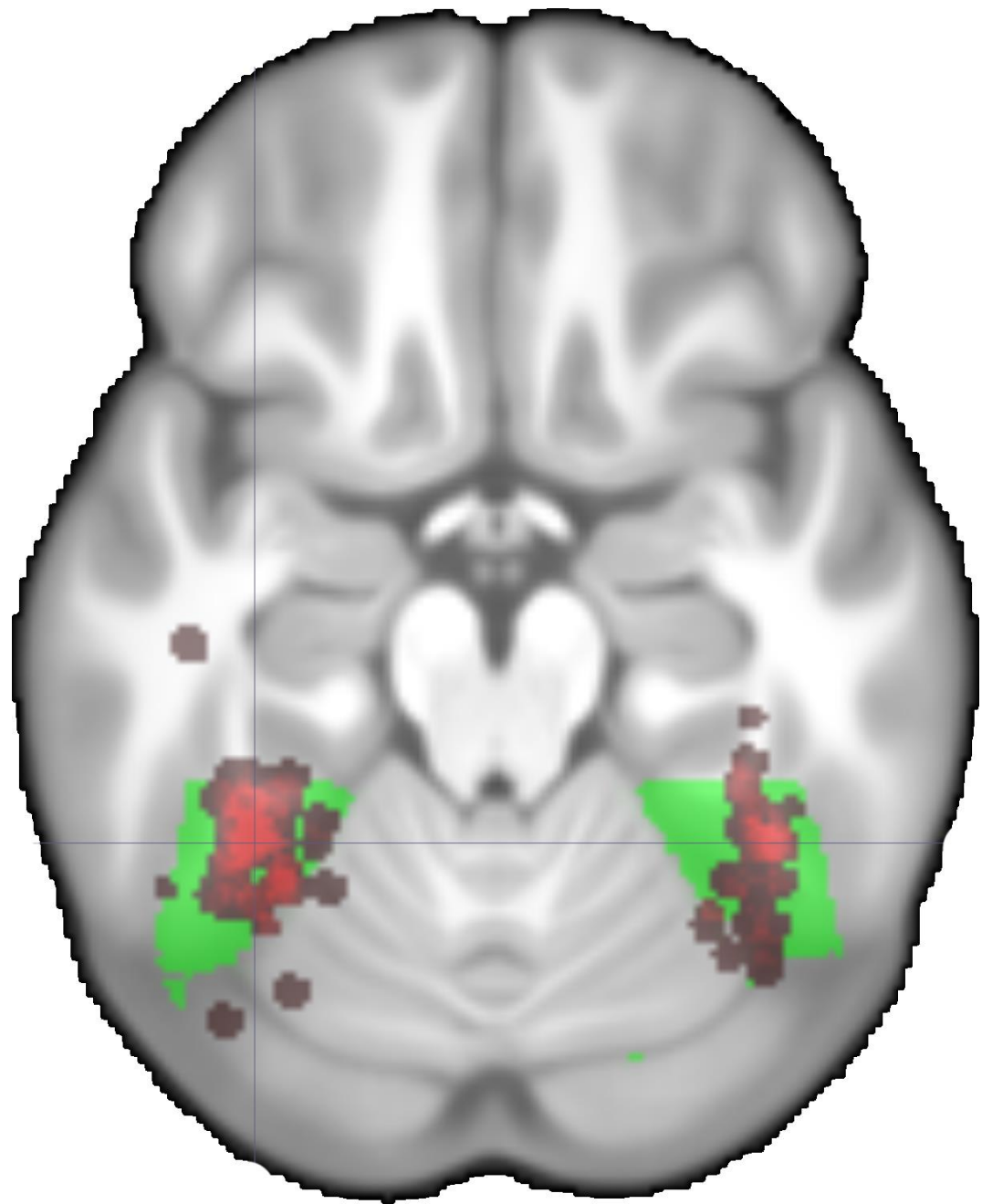
Figure 28. Bar graphs showing the Current Density Reconstruction (CDR) values of faces and houses as a function of the face-sensitive locations reported in literature studies (see also Table S1).

Figure 29. fMRI BOLD Contrast (top) and CDR values (bottom) in response to faces and houses over a series of anatomical ROIs (left and right).

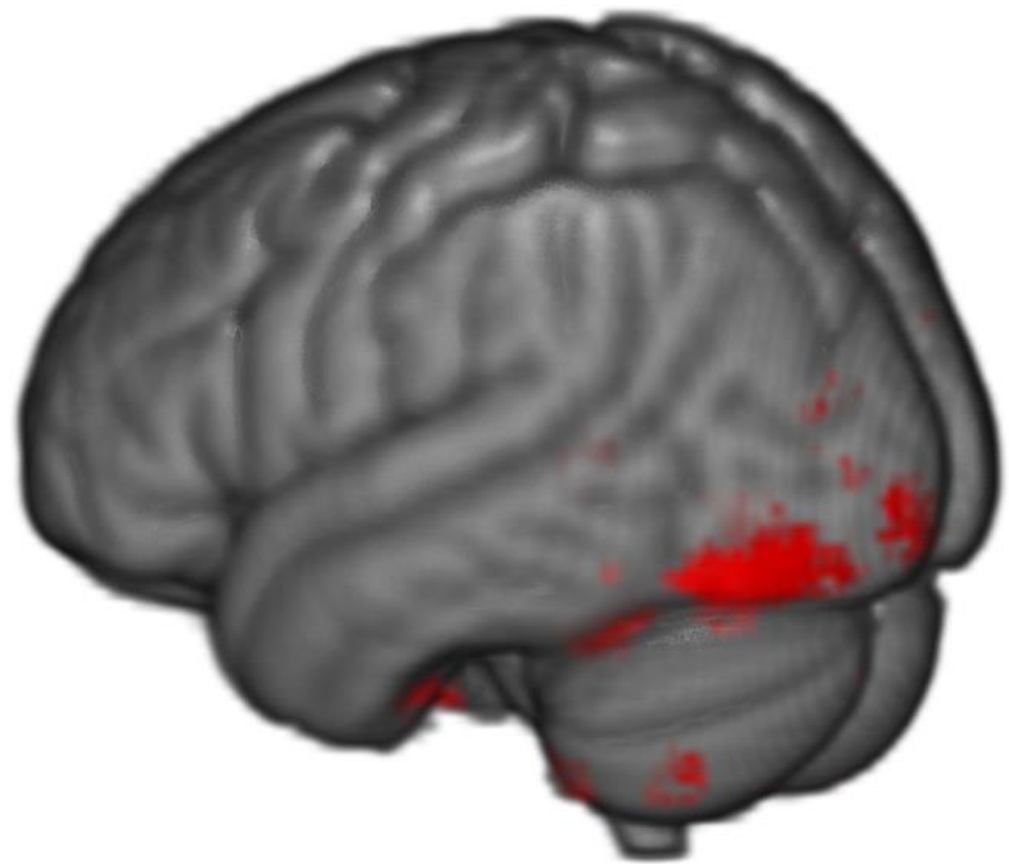
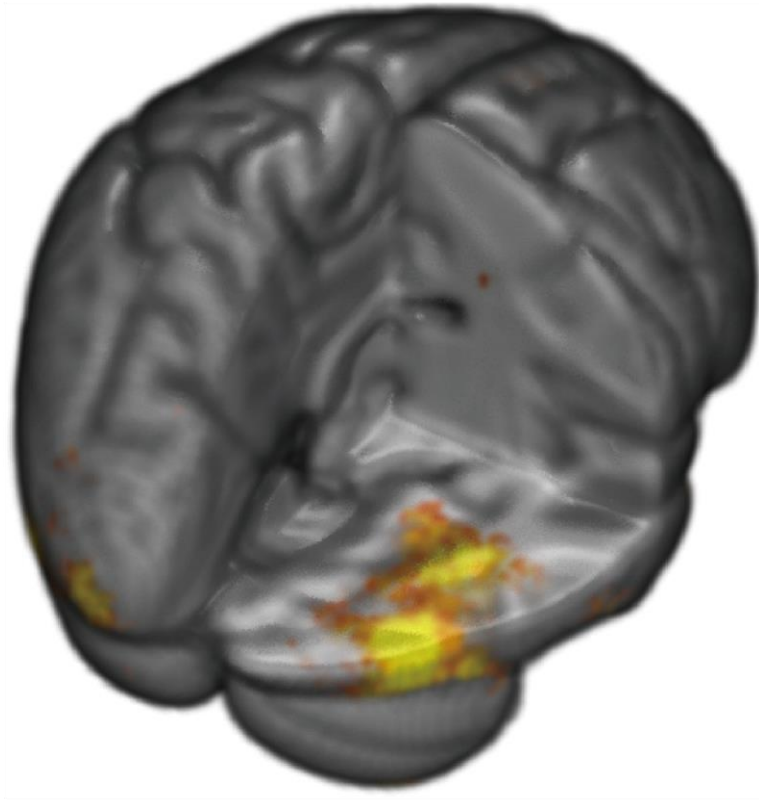
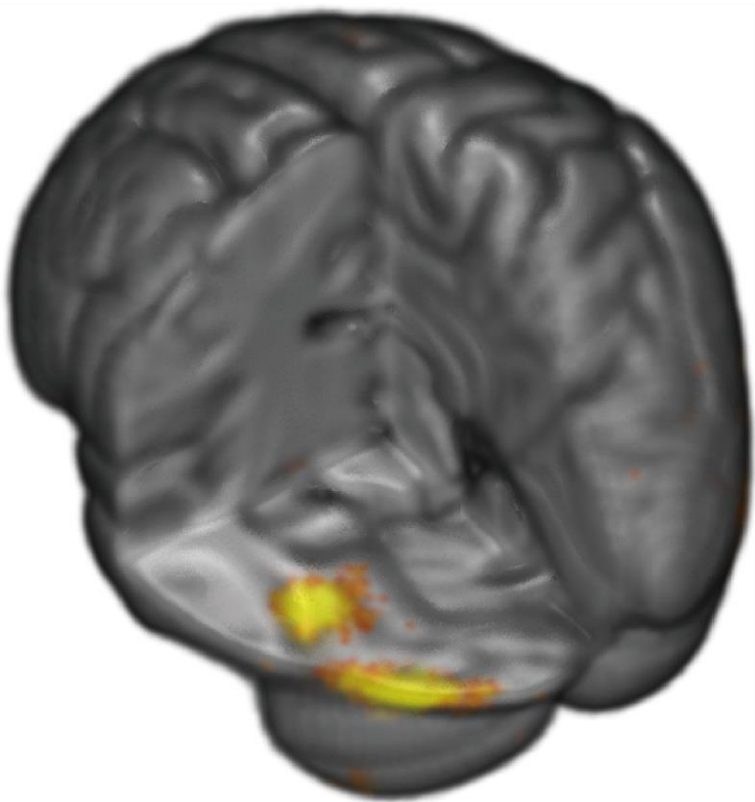
Figure 30. 3D rendering representation on the average MRI volume of the fMRI contrast (left), CDR (middle), and combined fMRI*CDR for faces.

Figure 31. fMRI BOLD Contrast response (left and right) of three different groups defined by participants' N170 ERP response. Specifically, participants were classified as having right ERP > left ERP (N = 18 participants; top panels) equivalent right and left ERP (N = 6; central panels), and left ERP > right ERP (N = 8; bottom panels).

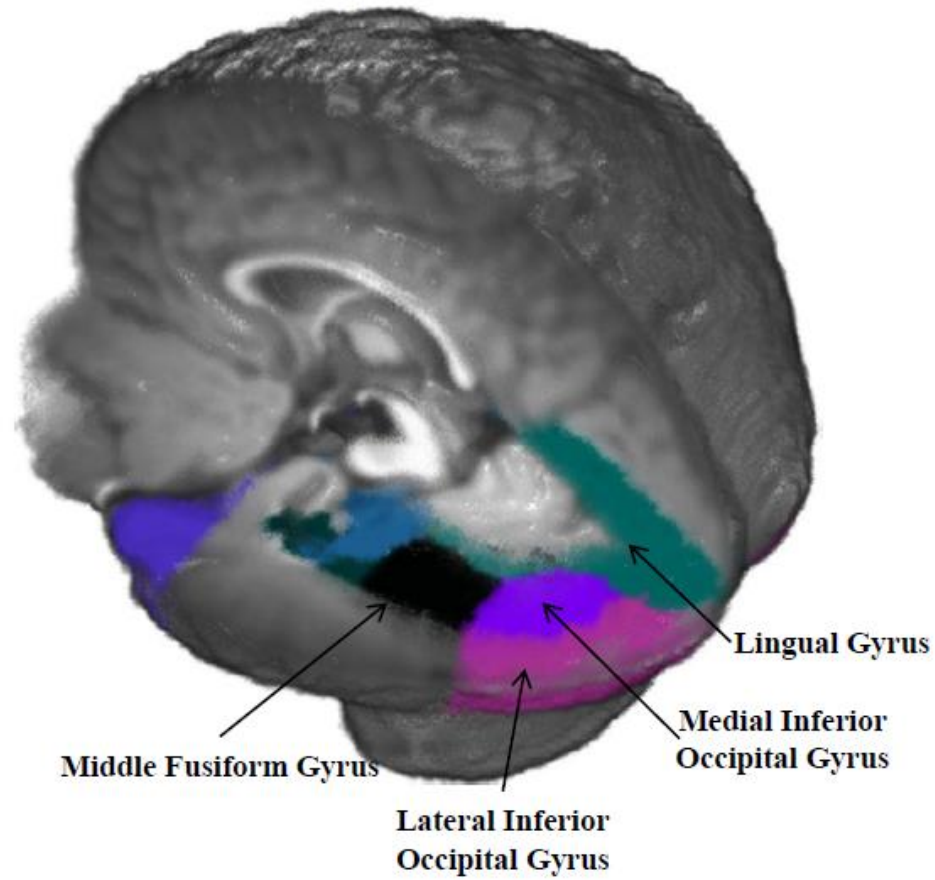




NeuroSynth 'FFA'



Lateral Posterior ROIs



Temporal Lobe ROIs

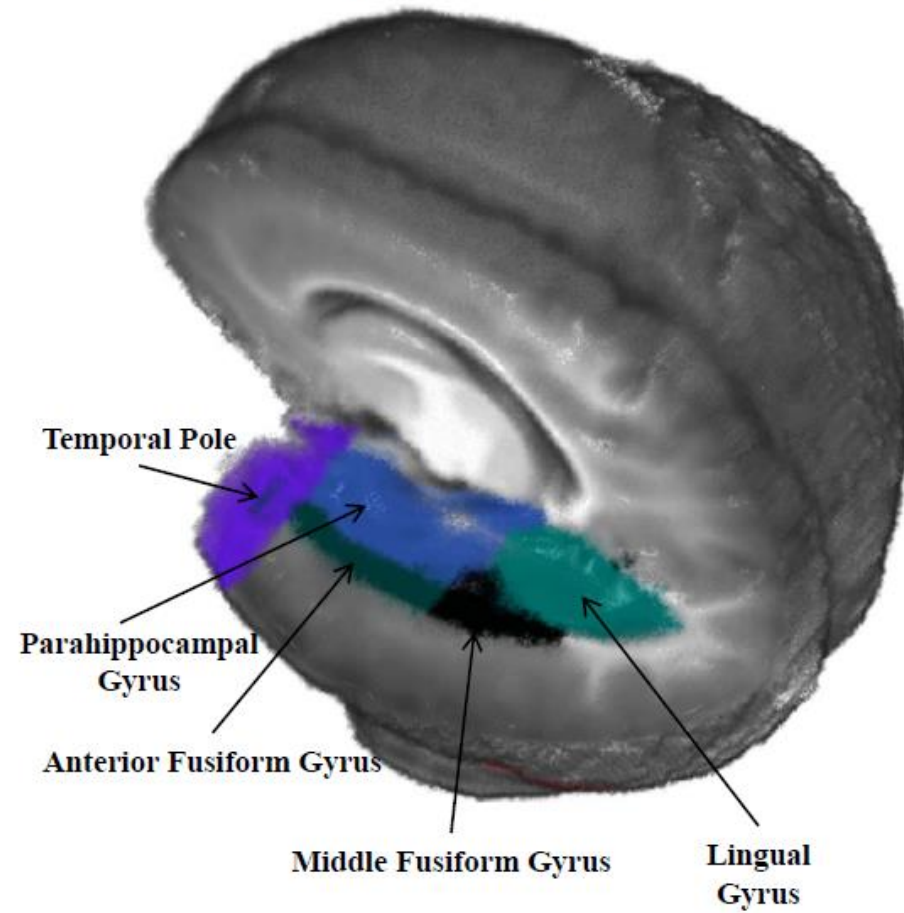
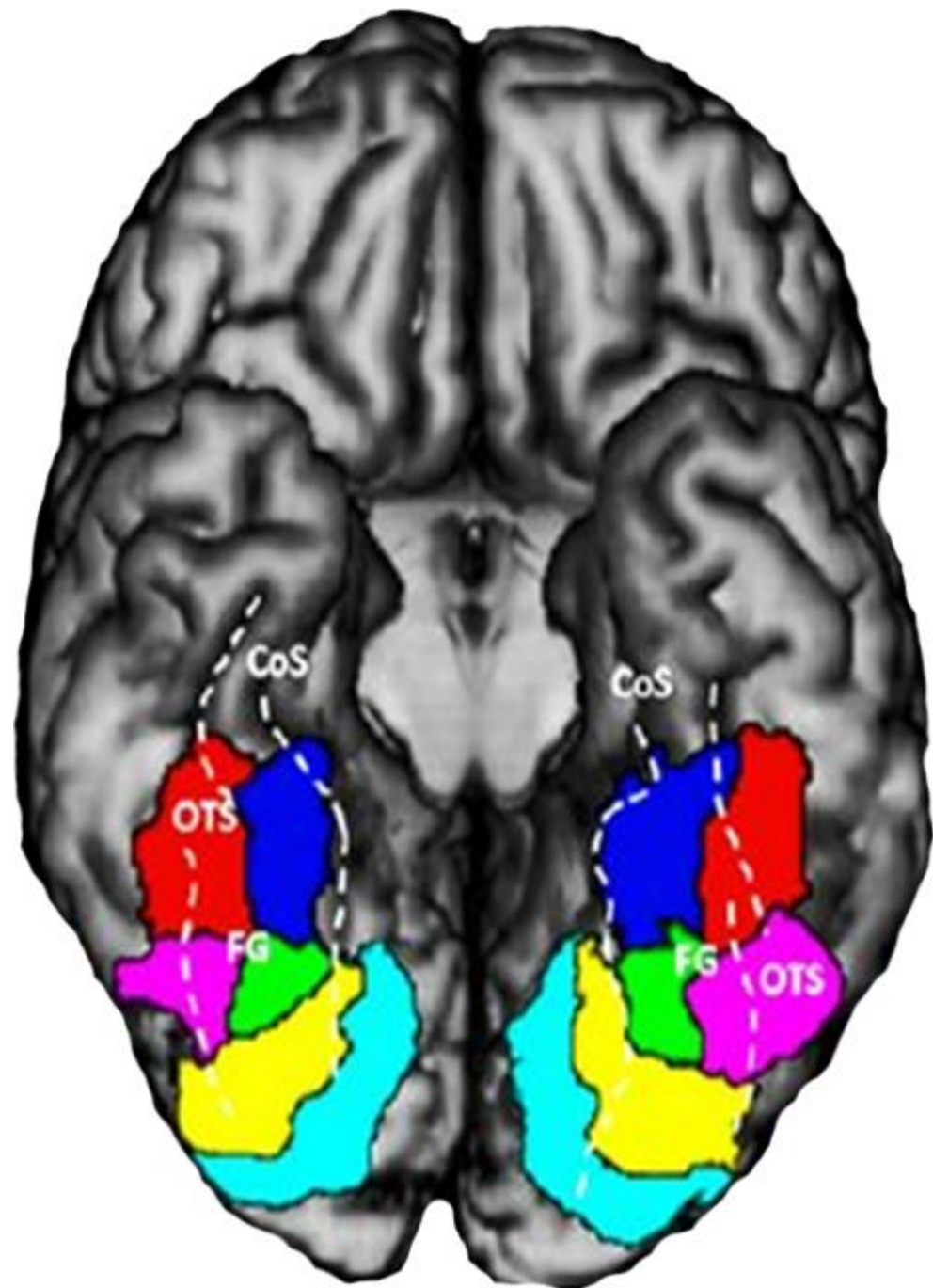
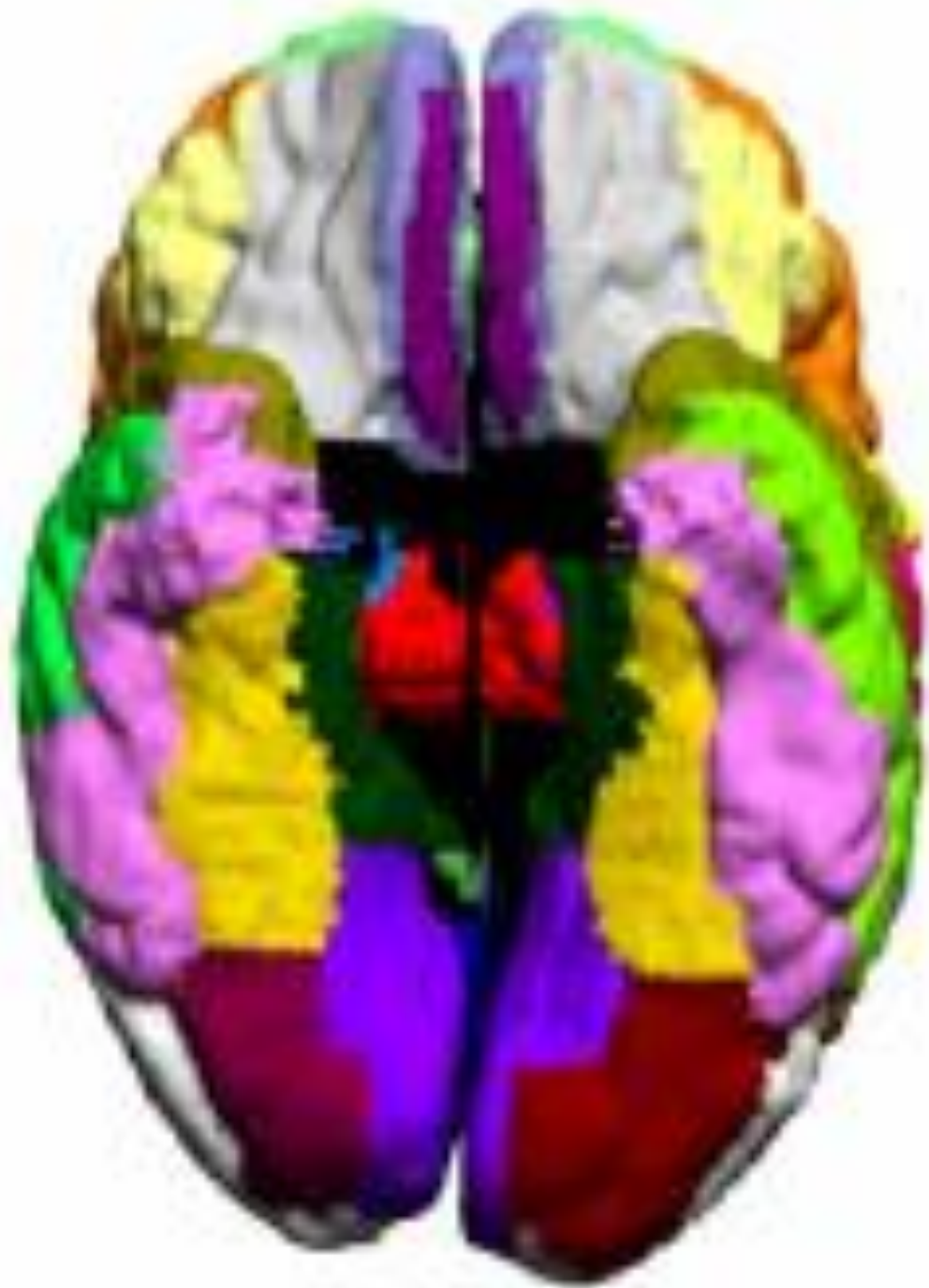
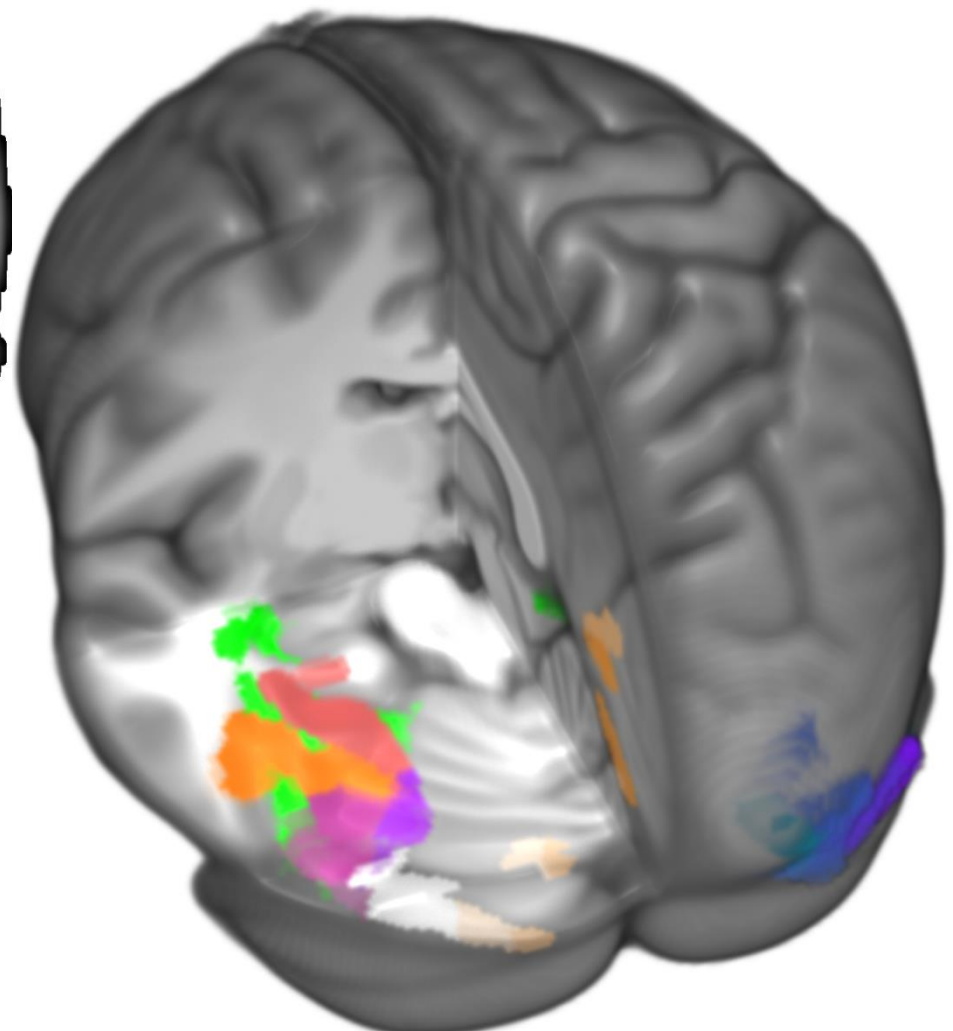
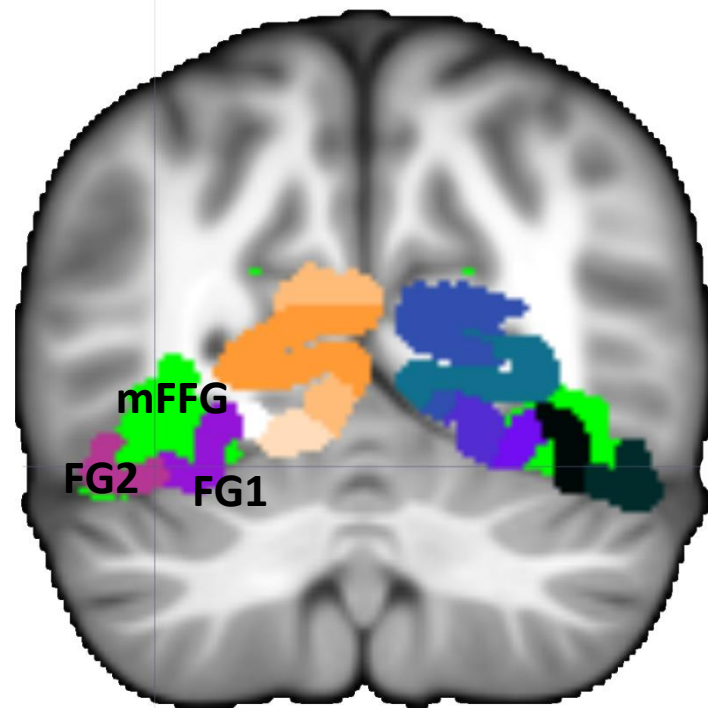
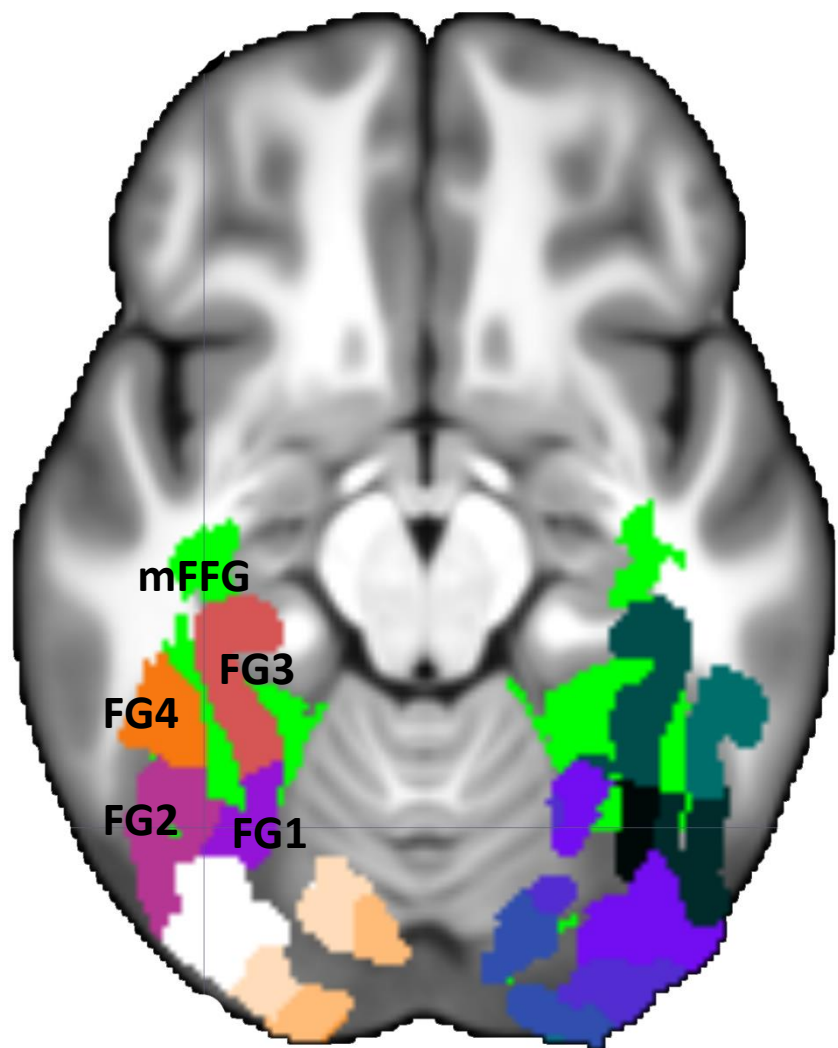


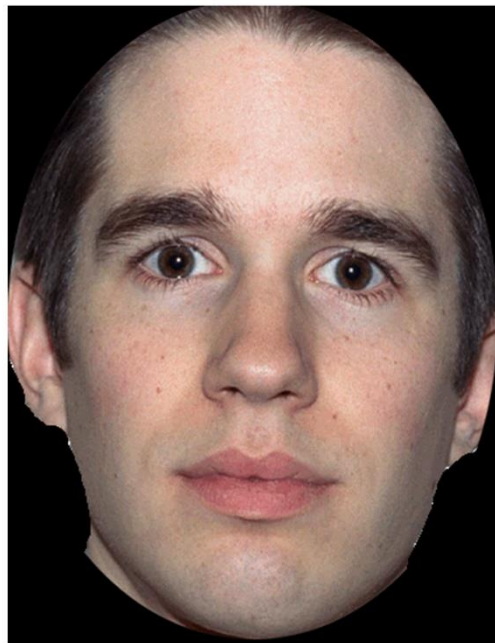
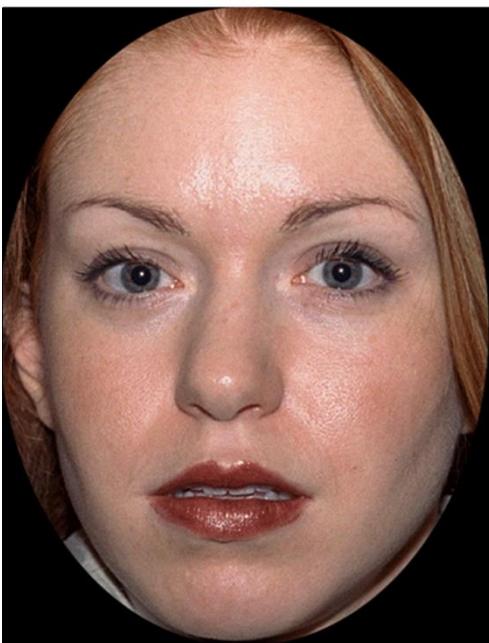
Figure 2. Regions of interests (ROIs) shown on the 6-month-old average age-appropriate template. These regions are the most relevant theoretically for the processing of faces.



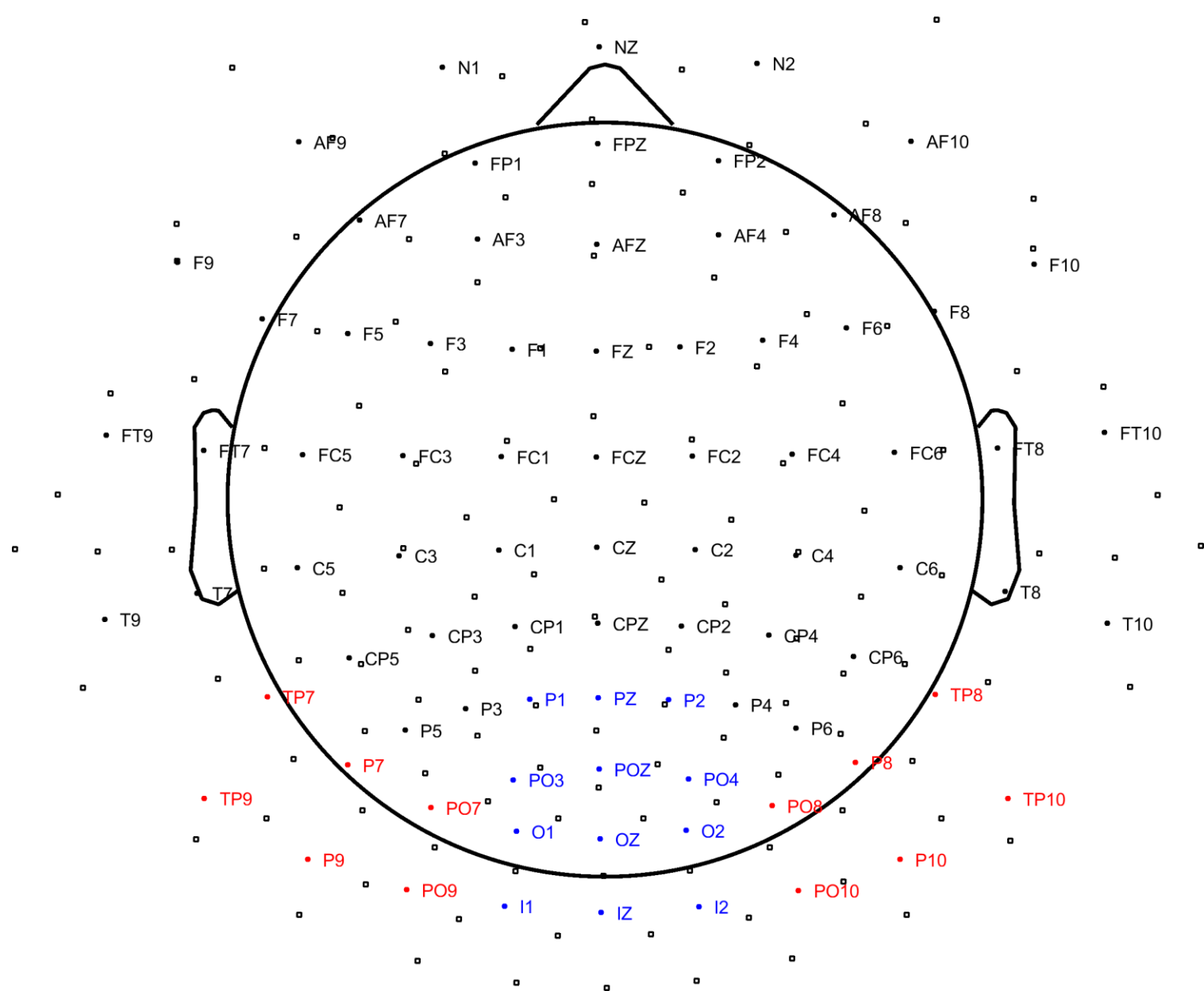
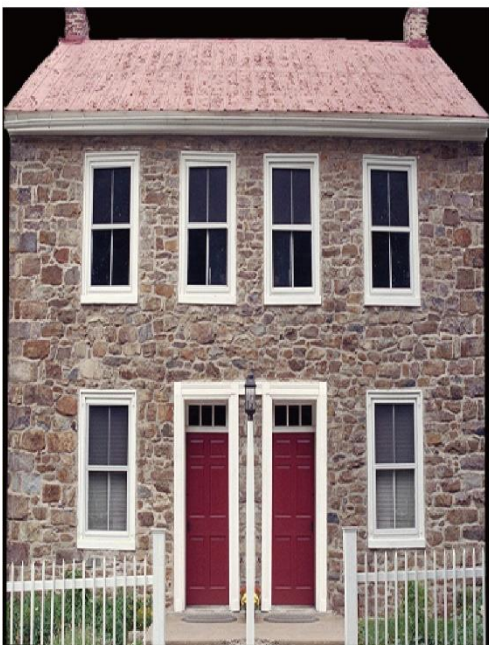
- FG3
- FG4
- FG1
- FG2
- hOc4v
- hOc3v



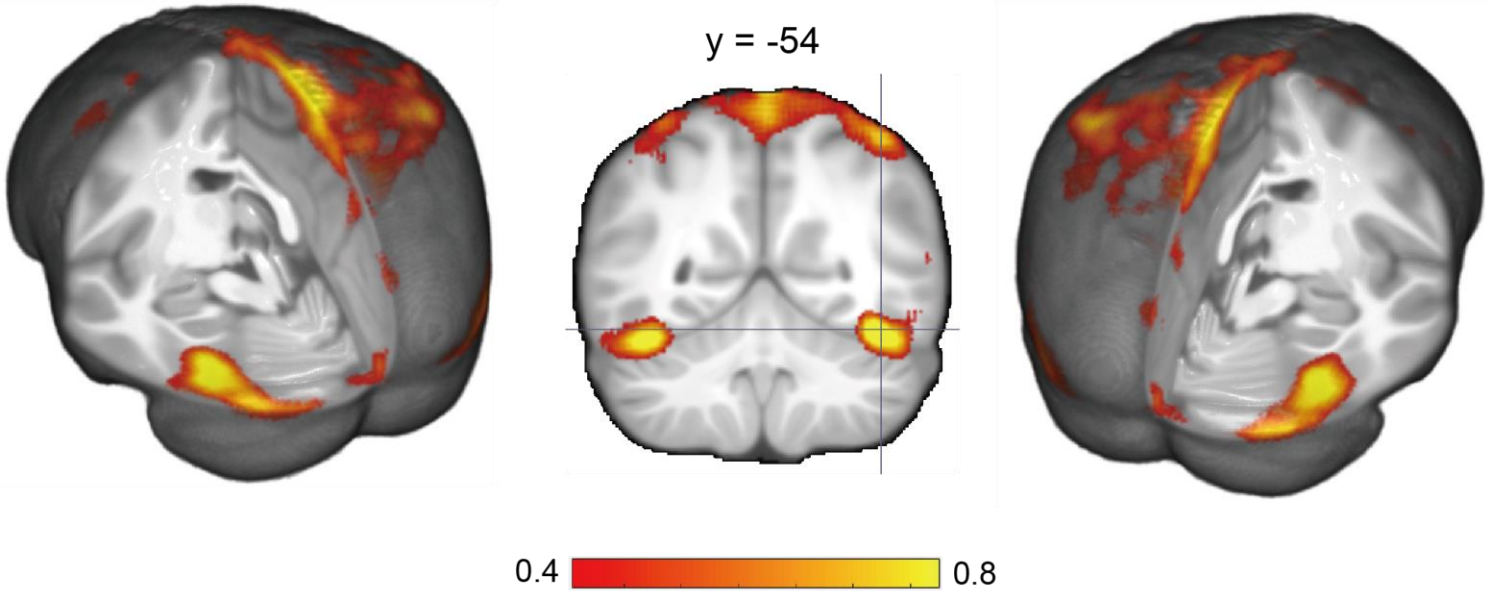
A



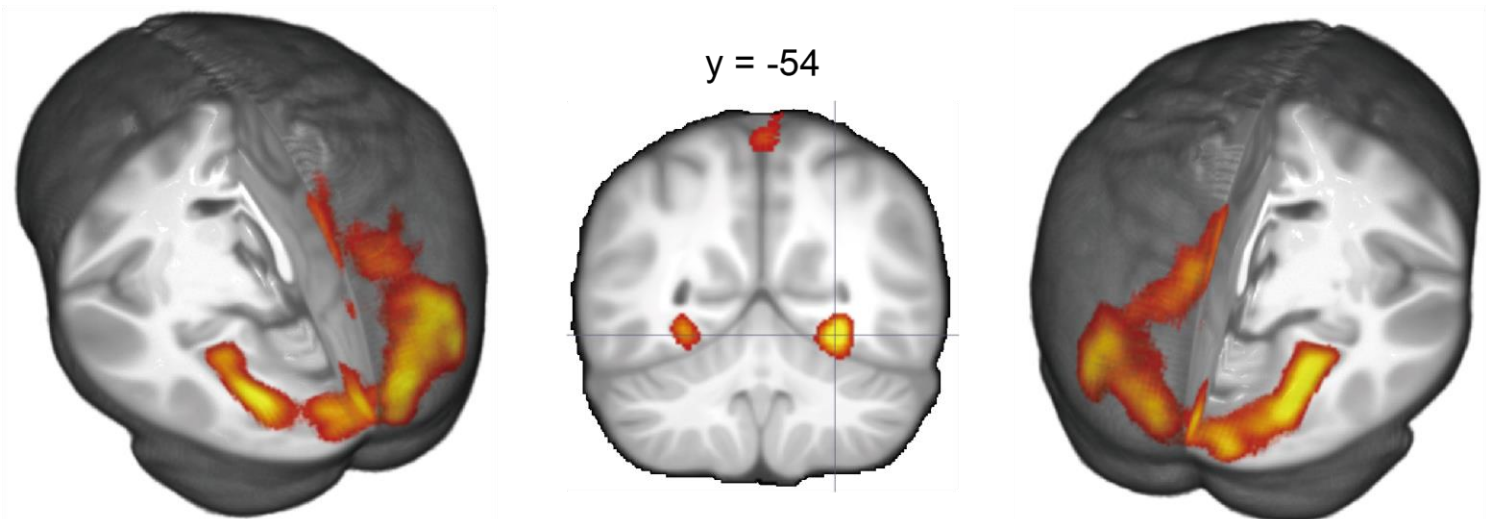
B



Group Mean of Faces > Houses



Group Mean of Houses > Faces

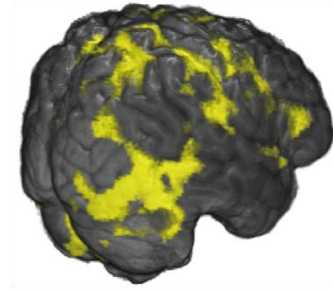
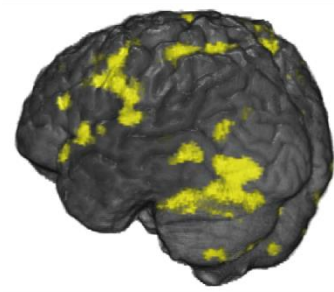
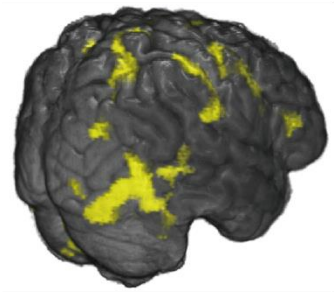
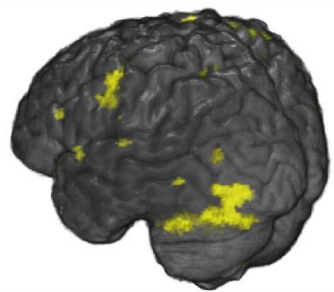
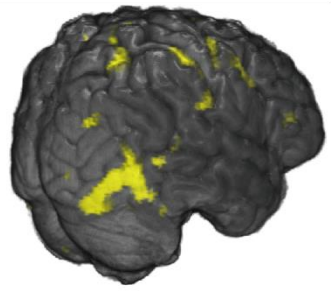
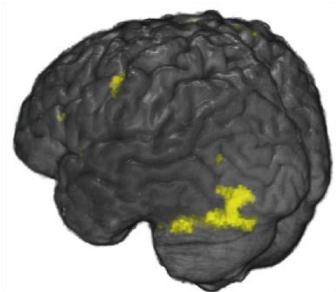


RFT

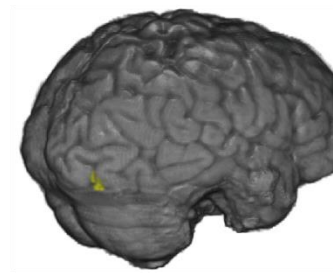
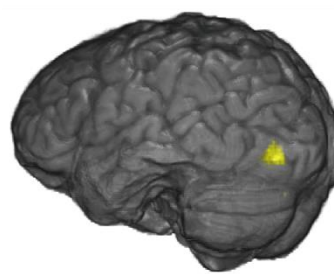
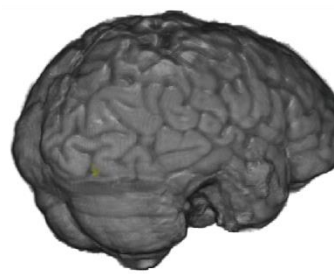
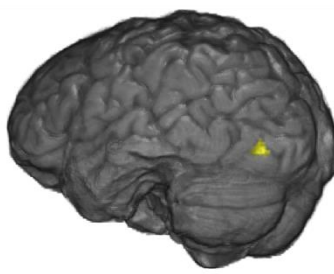
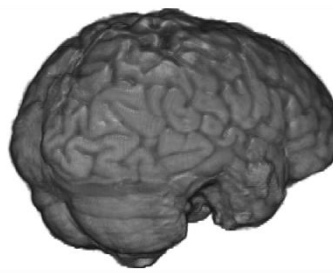
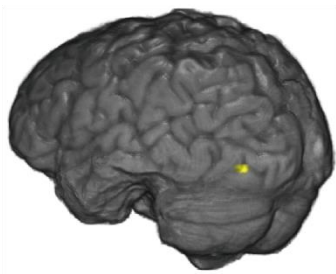
AT

.001

Subject 1

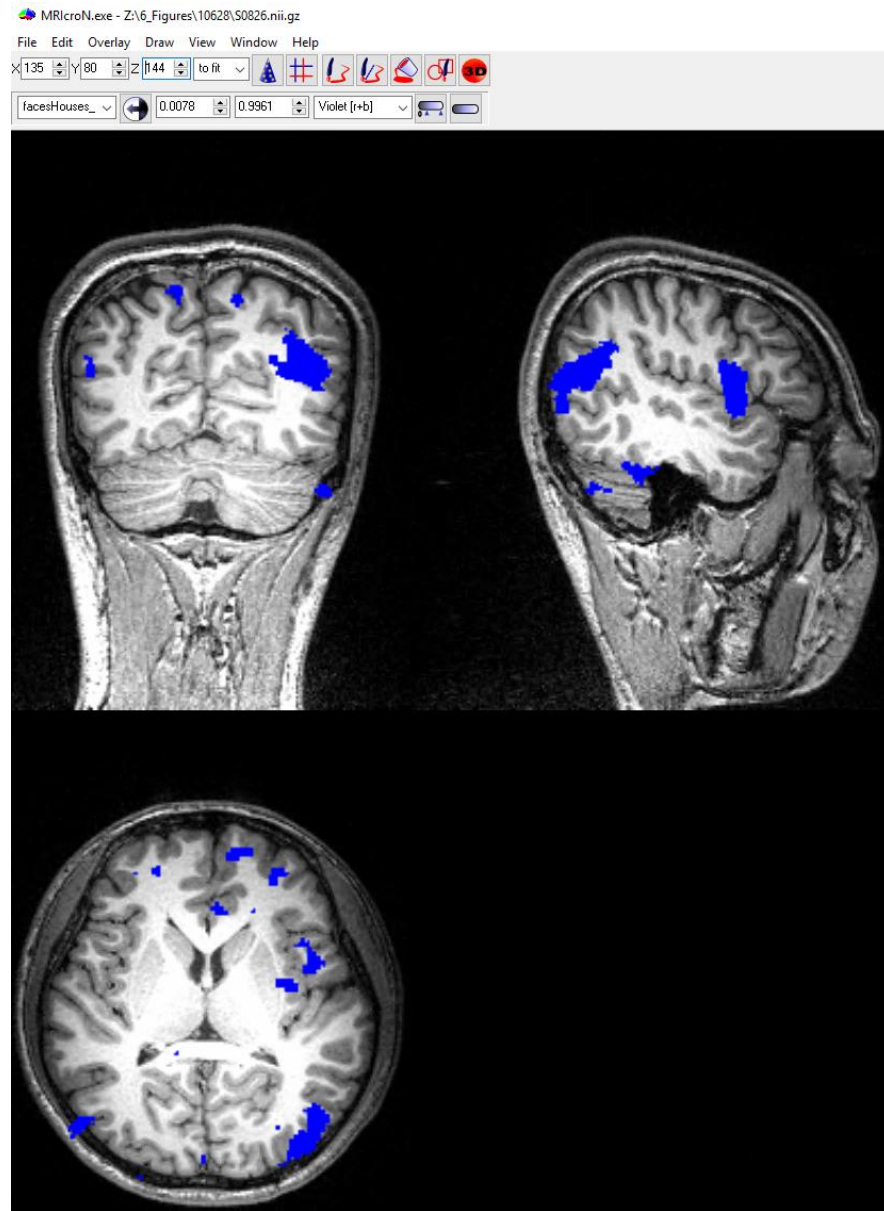
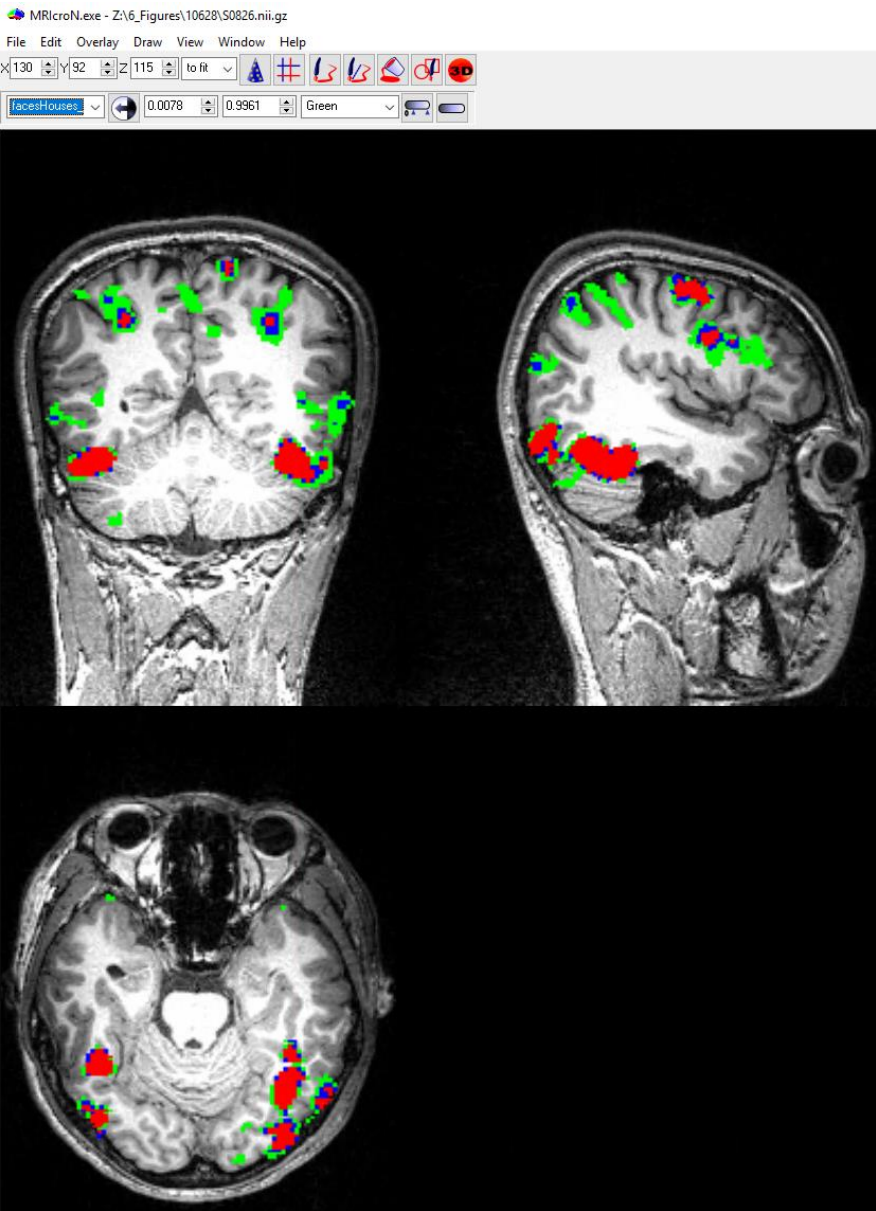


Subject 2



10628

10671



Faces > Houses

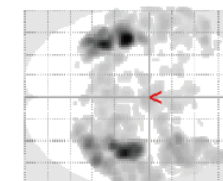
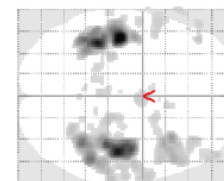
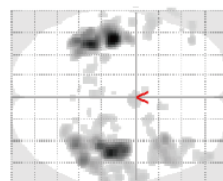
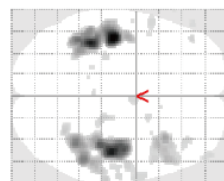
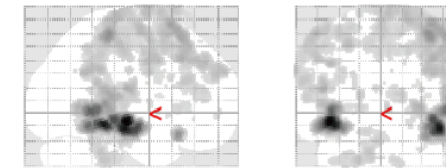
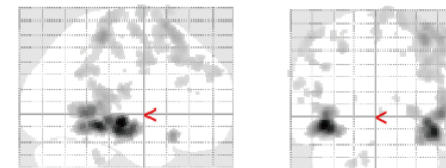
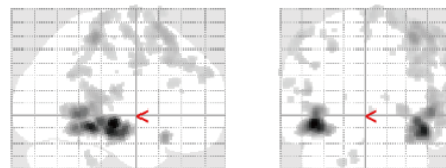
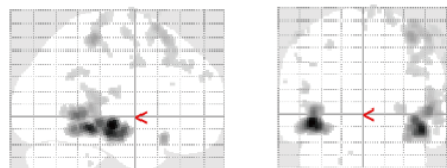
RFT

AT - Whole Brain

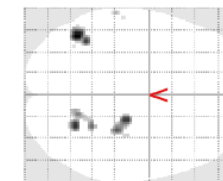
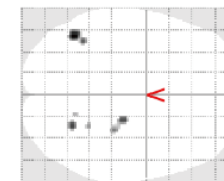
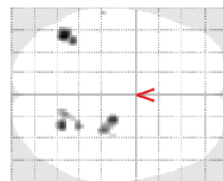
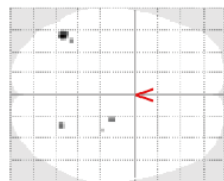
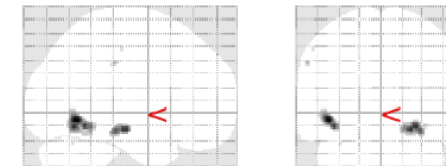
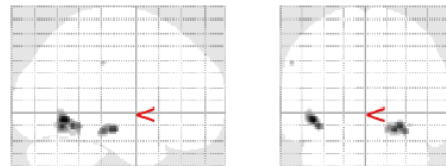
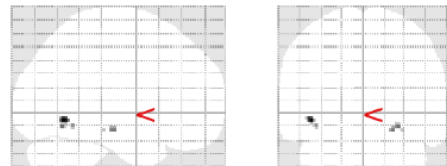
AT - ROI

.001

Subject 1



Subject 2

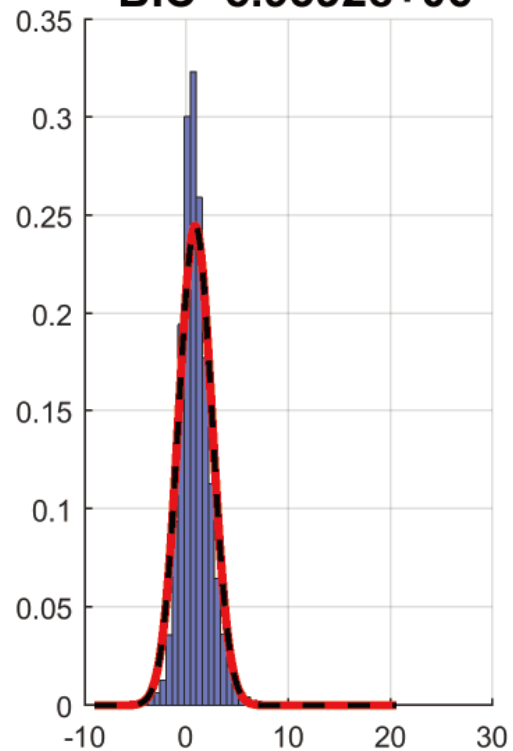


Faces > Houses

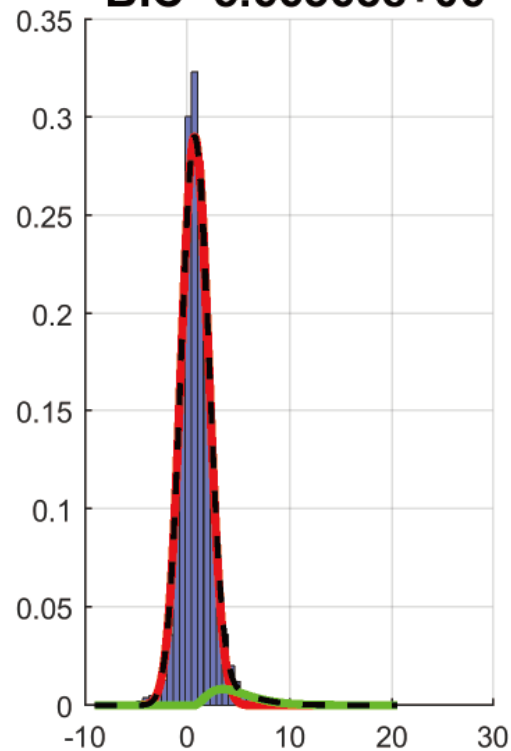
AT - Whole Brain

AT - ROI

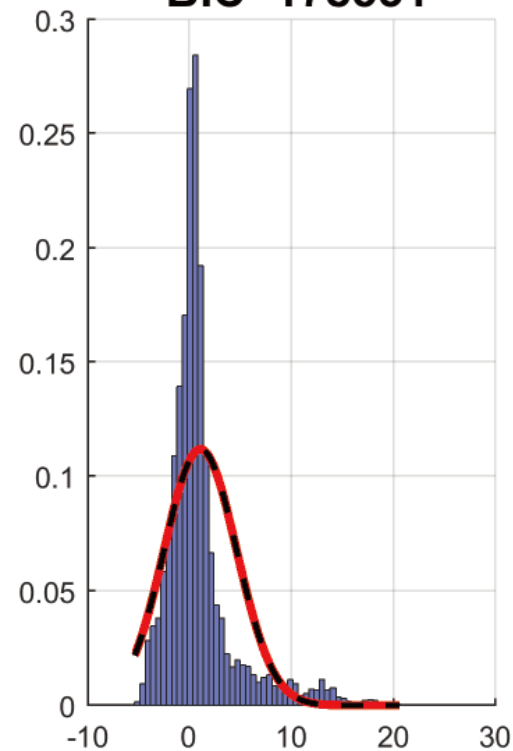
Gaussian only
BIC=5.9392e+06



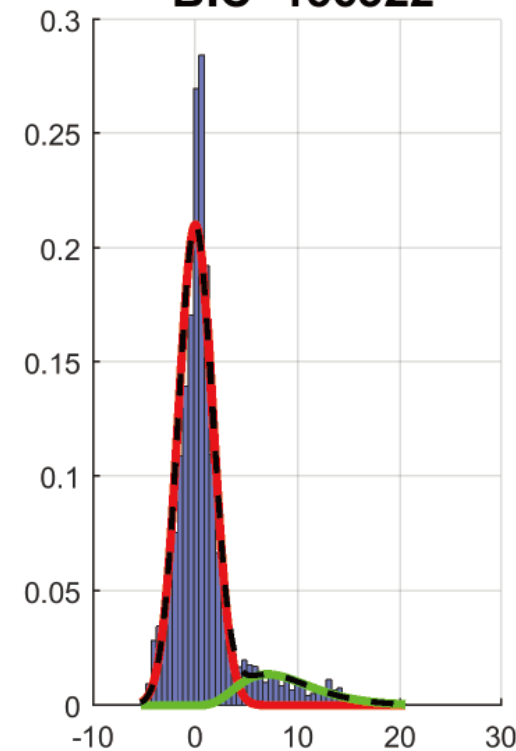
Gaussian & Gamma
BIC=5.66368e+06



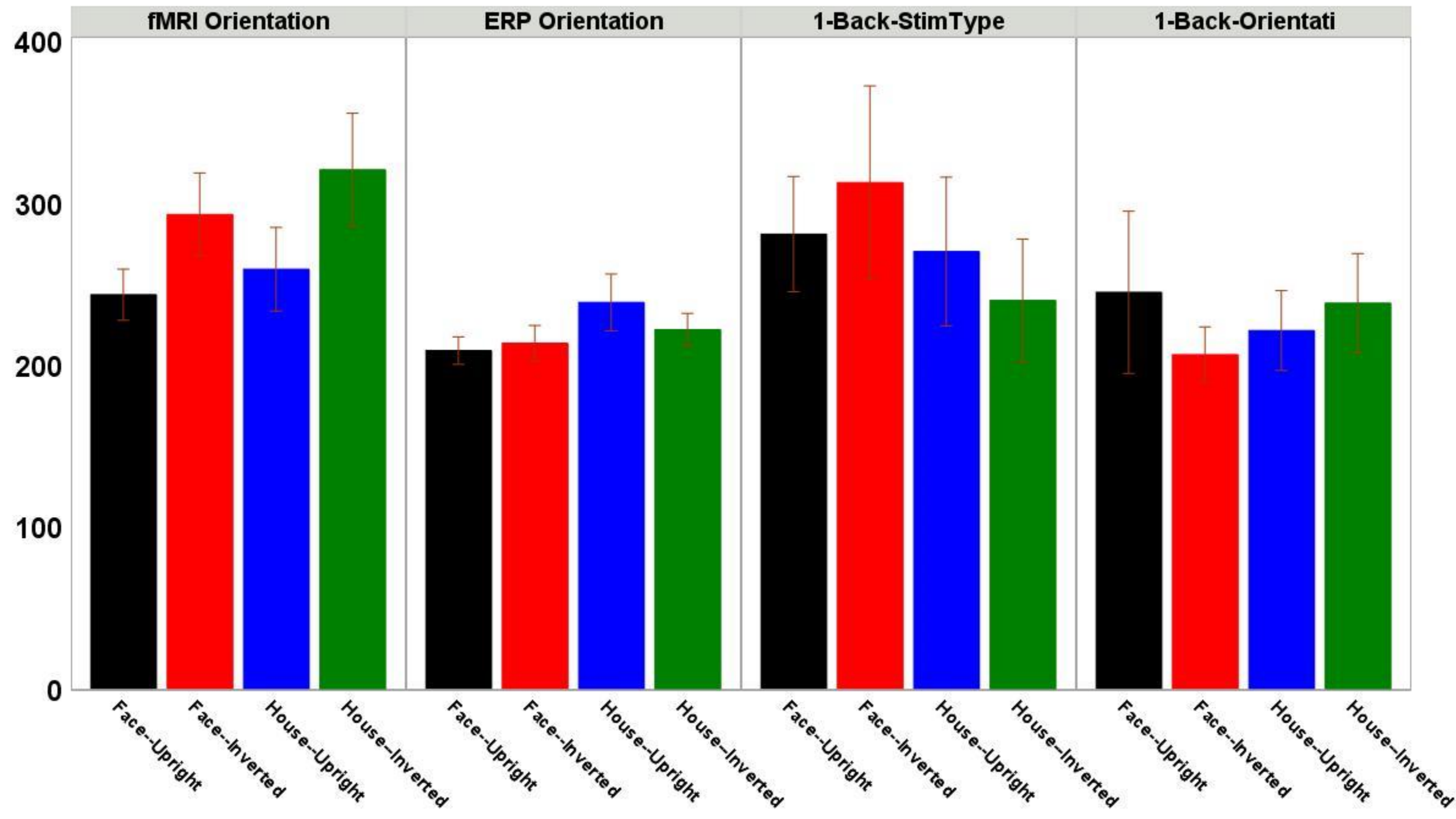
Gaussian only
BIC=178531

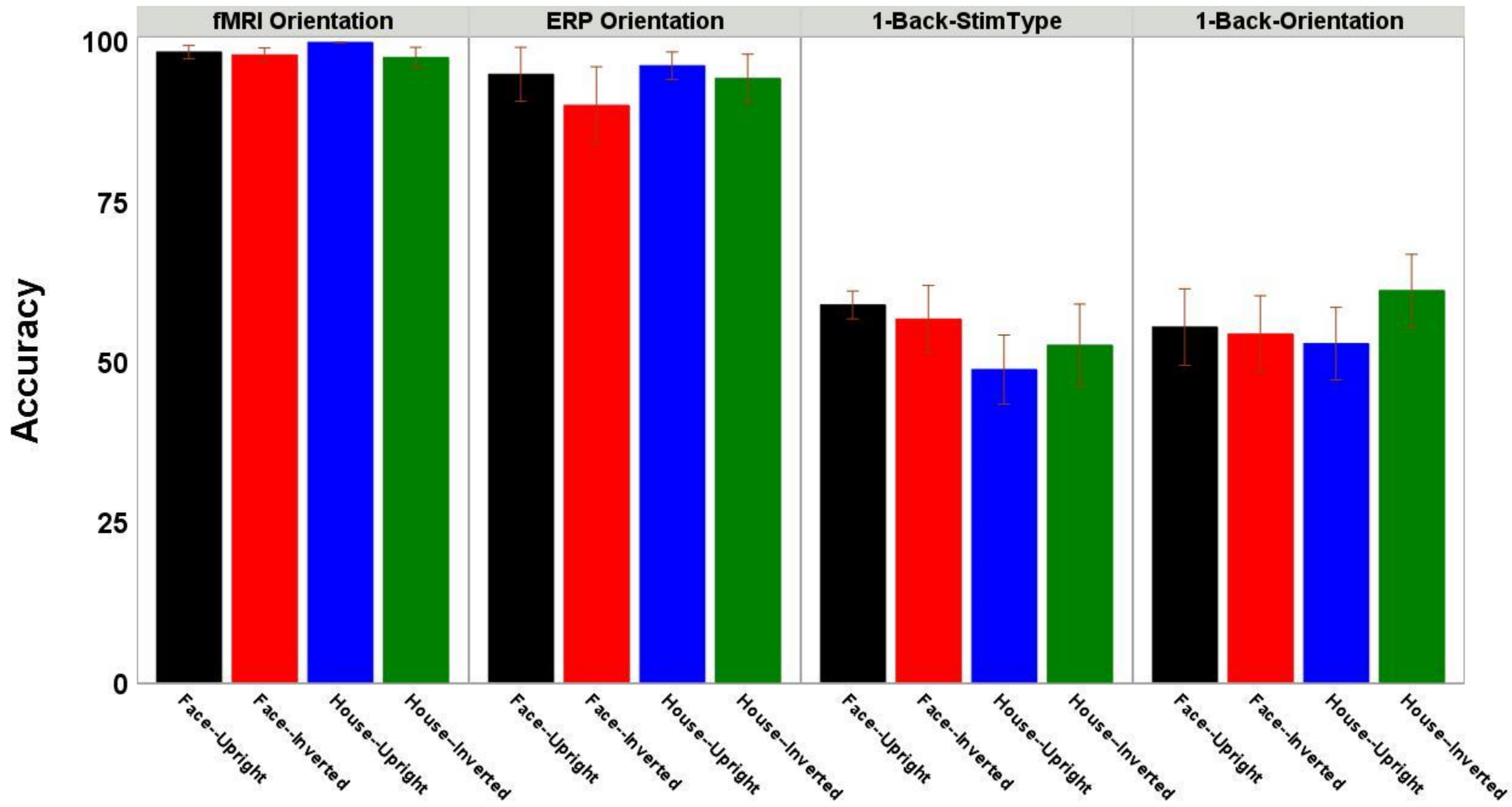


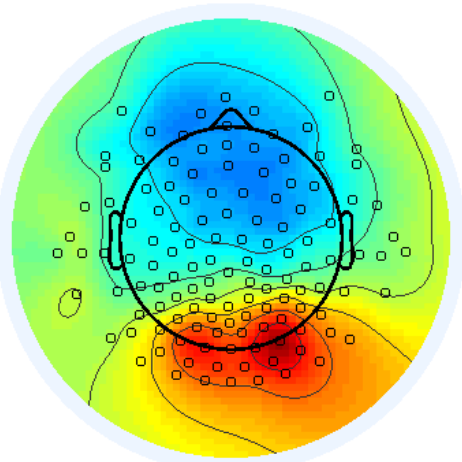
Gaussian & Gamma
BIC=156322



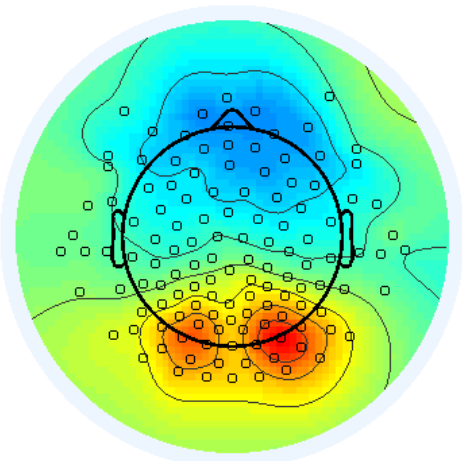
Median RT



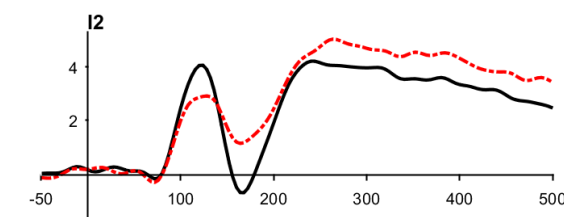
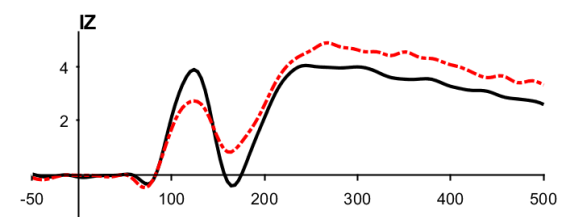
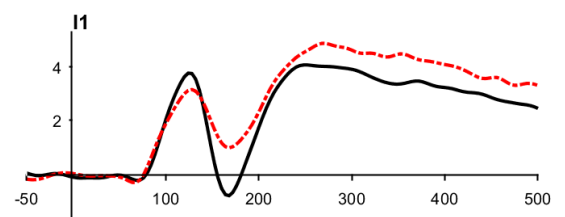
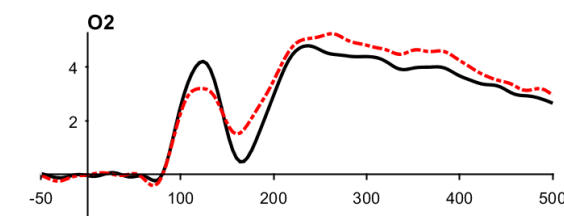
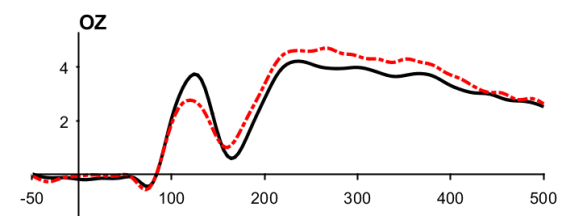
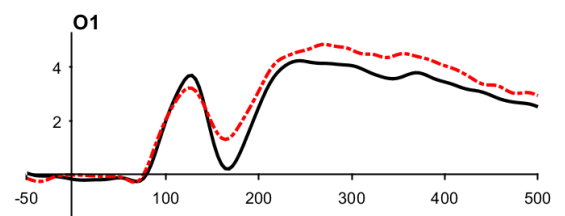
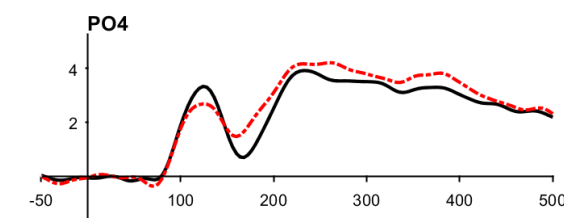
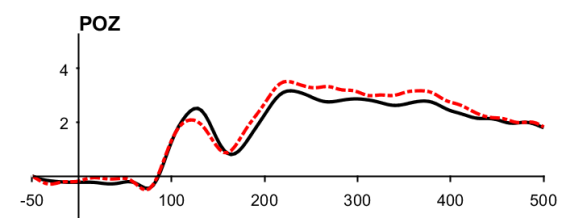
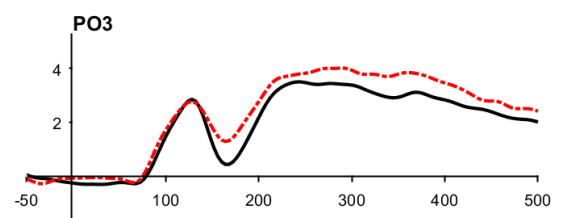
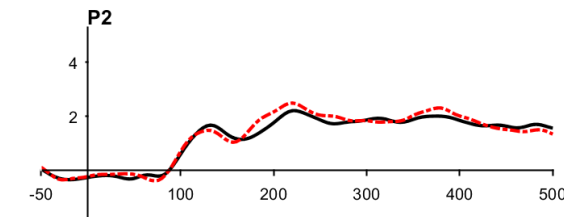
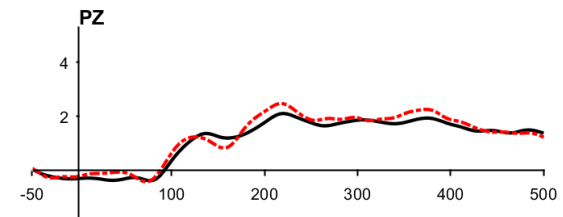
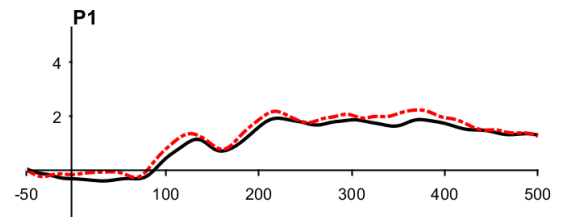
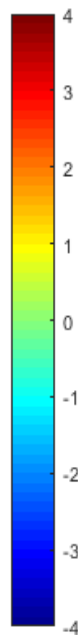


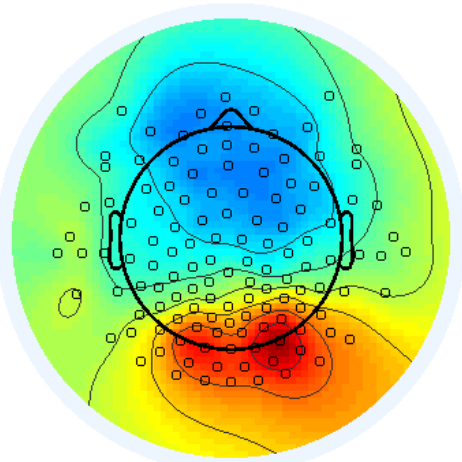


Faces (130 ms)

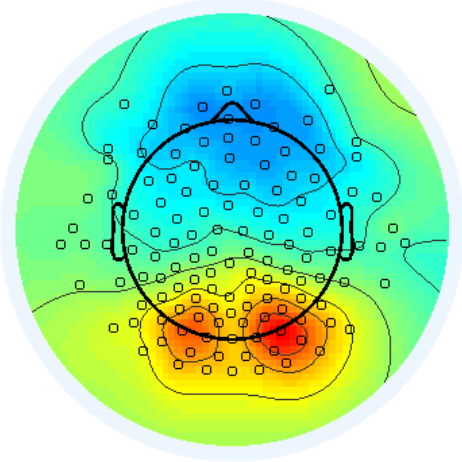


Houses (130 ms)

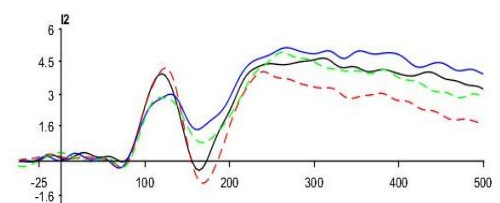
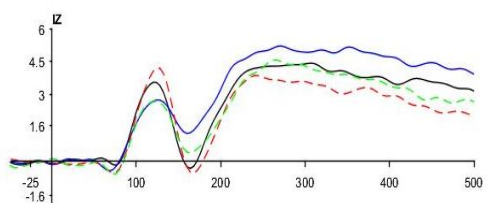
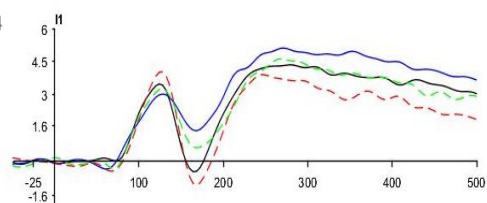
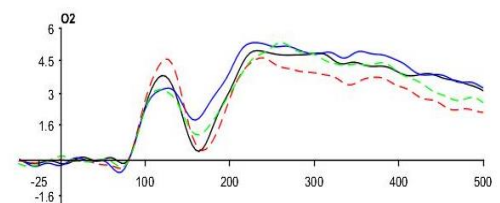
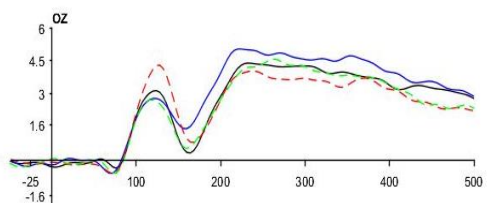
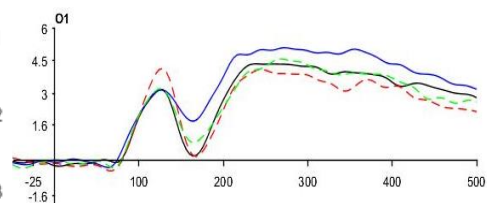
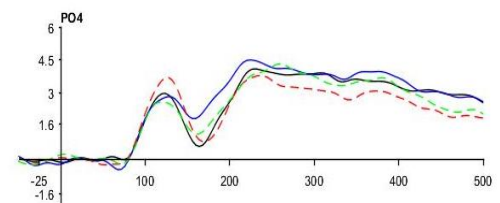
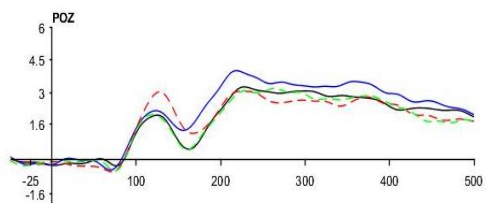
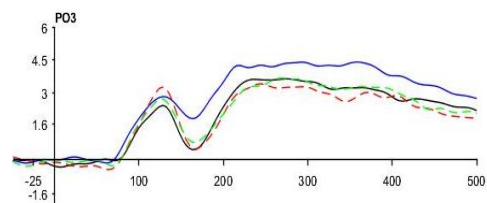
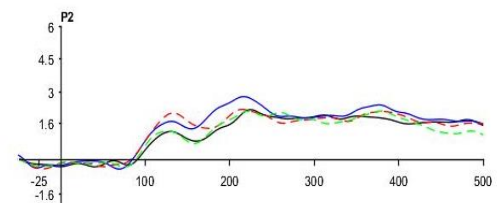
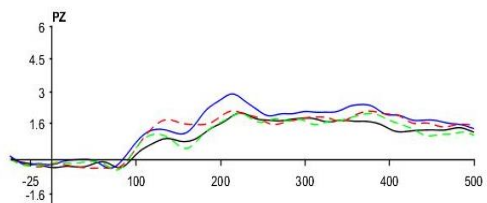
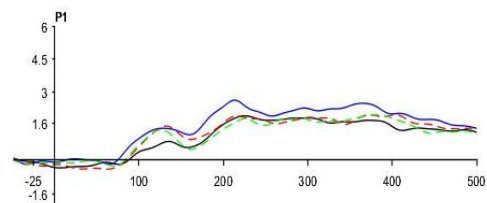
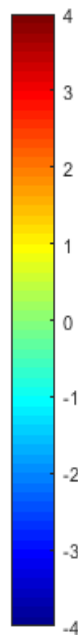




Faces (130 ms)

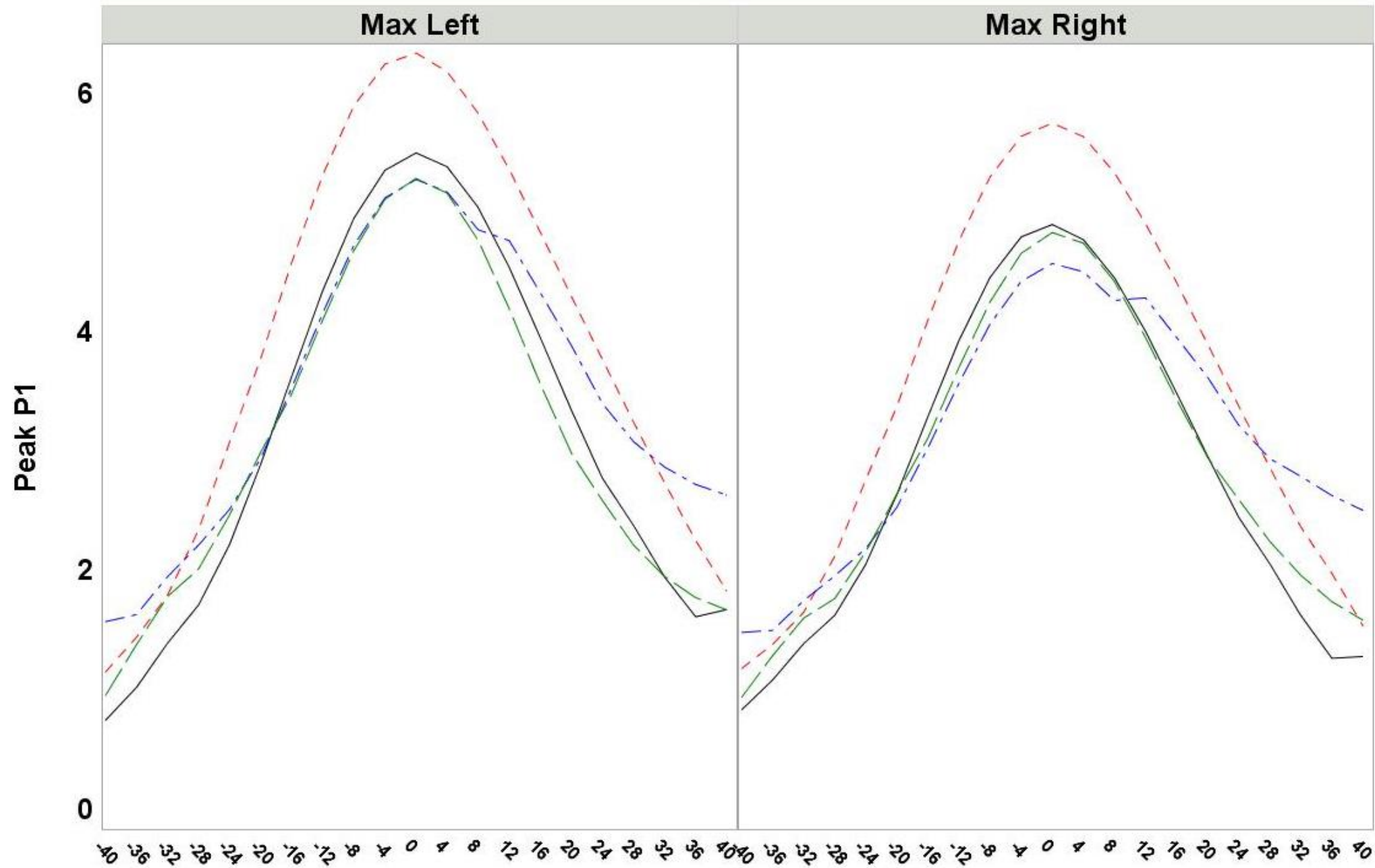


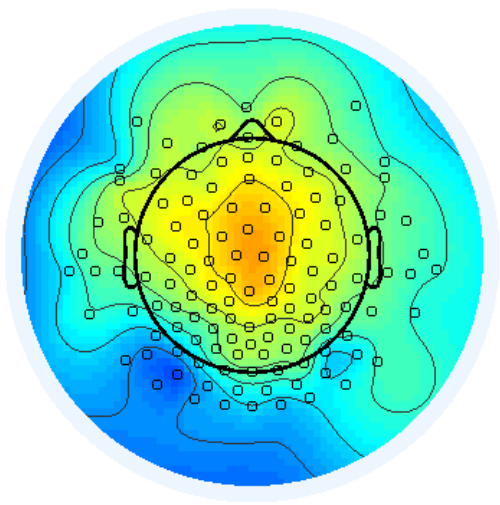
Houses (130 ms)



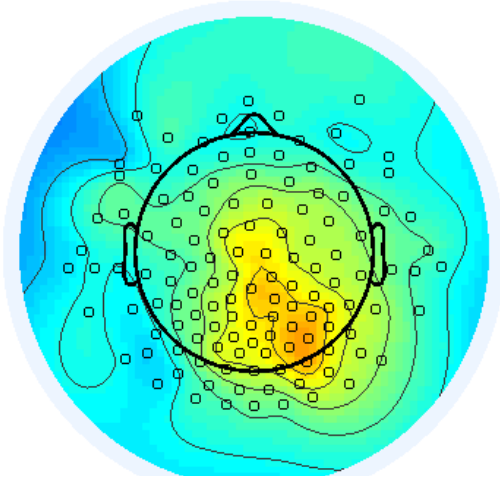
- upright face
- upright house
- - - inverted face
- - - inverted house

Max ERP occipital channels

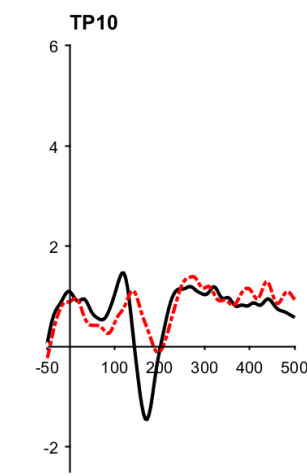
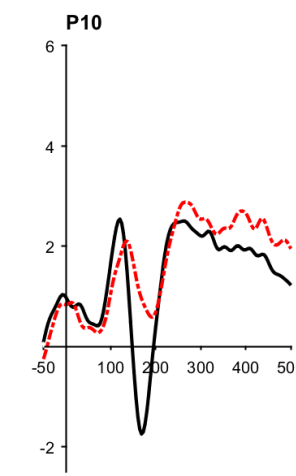
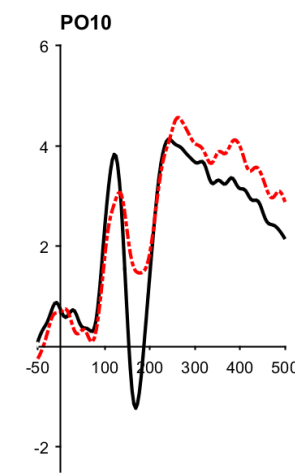
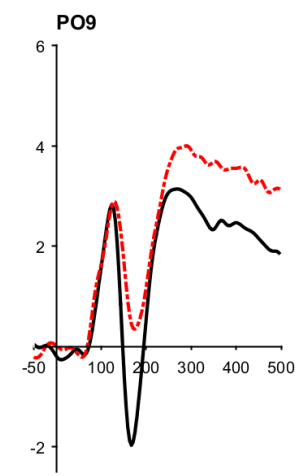
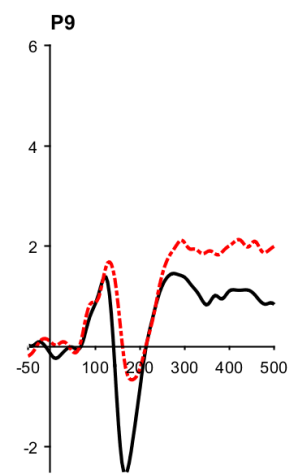
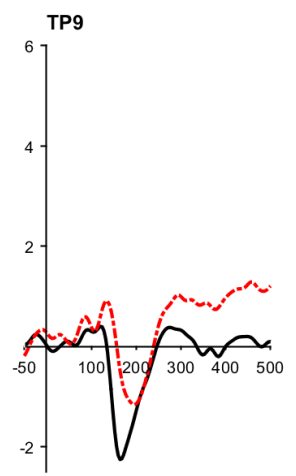
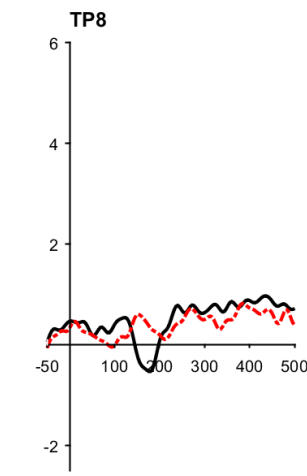
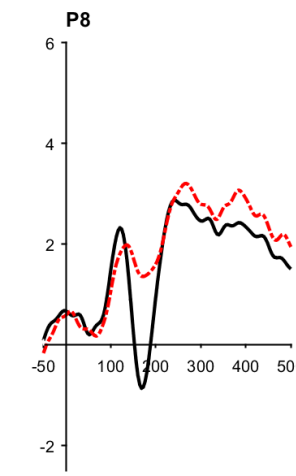
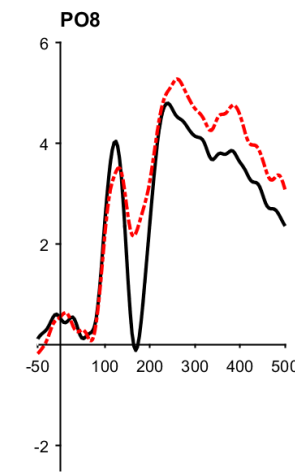
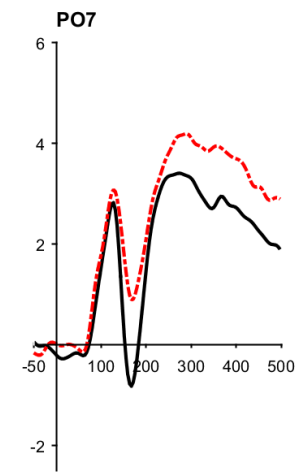
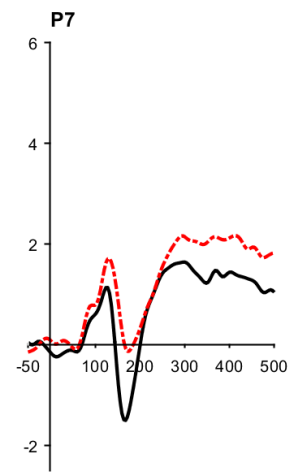
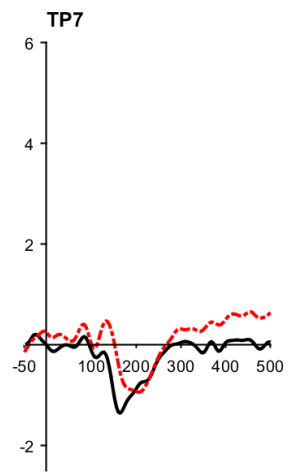
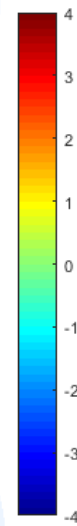


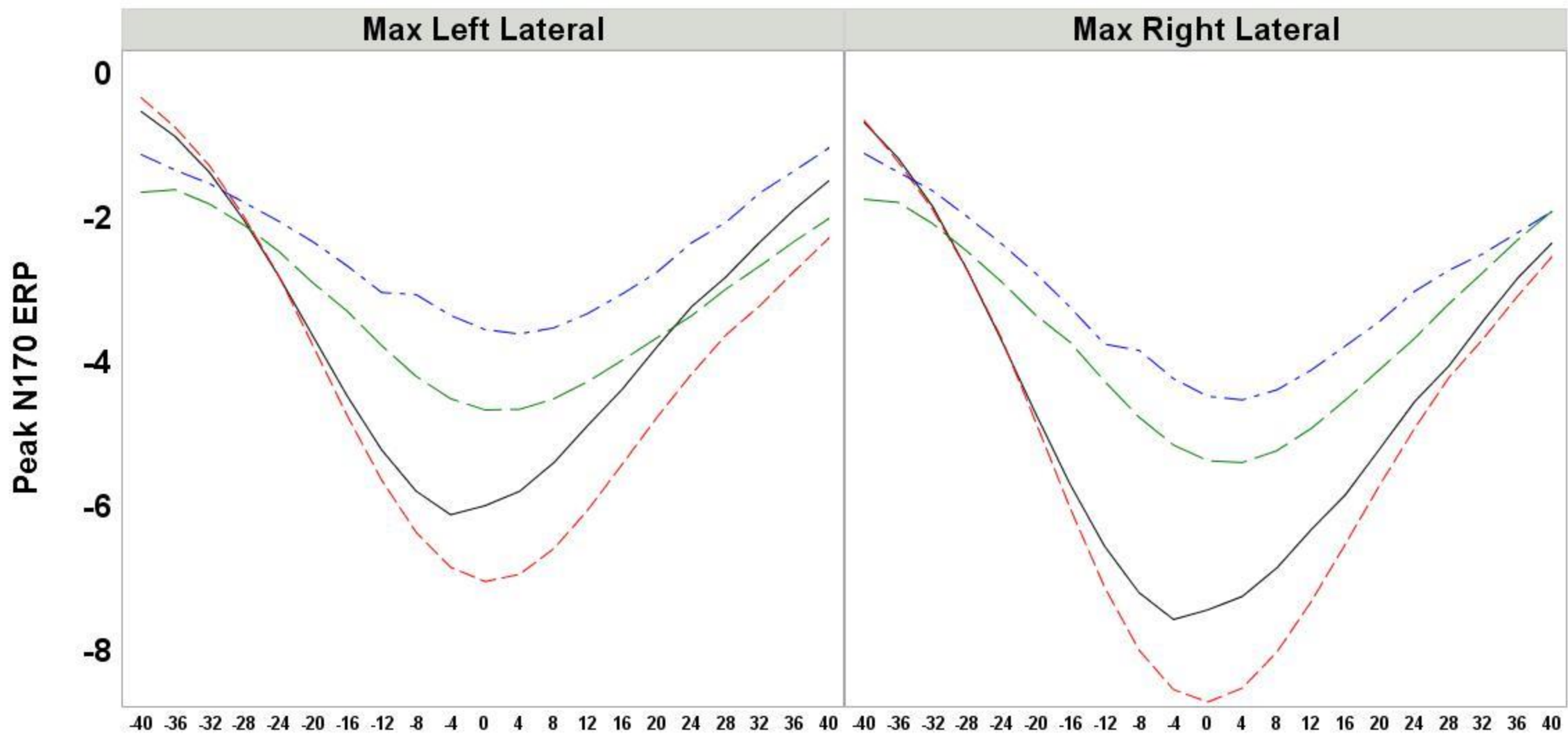


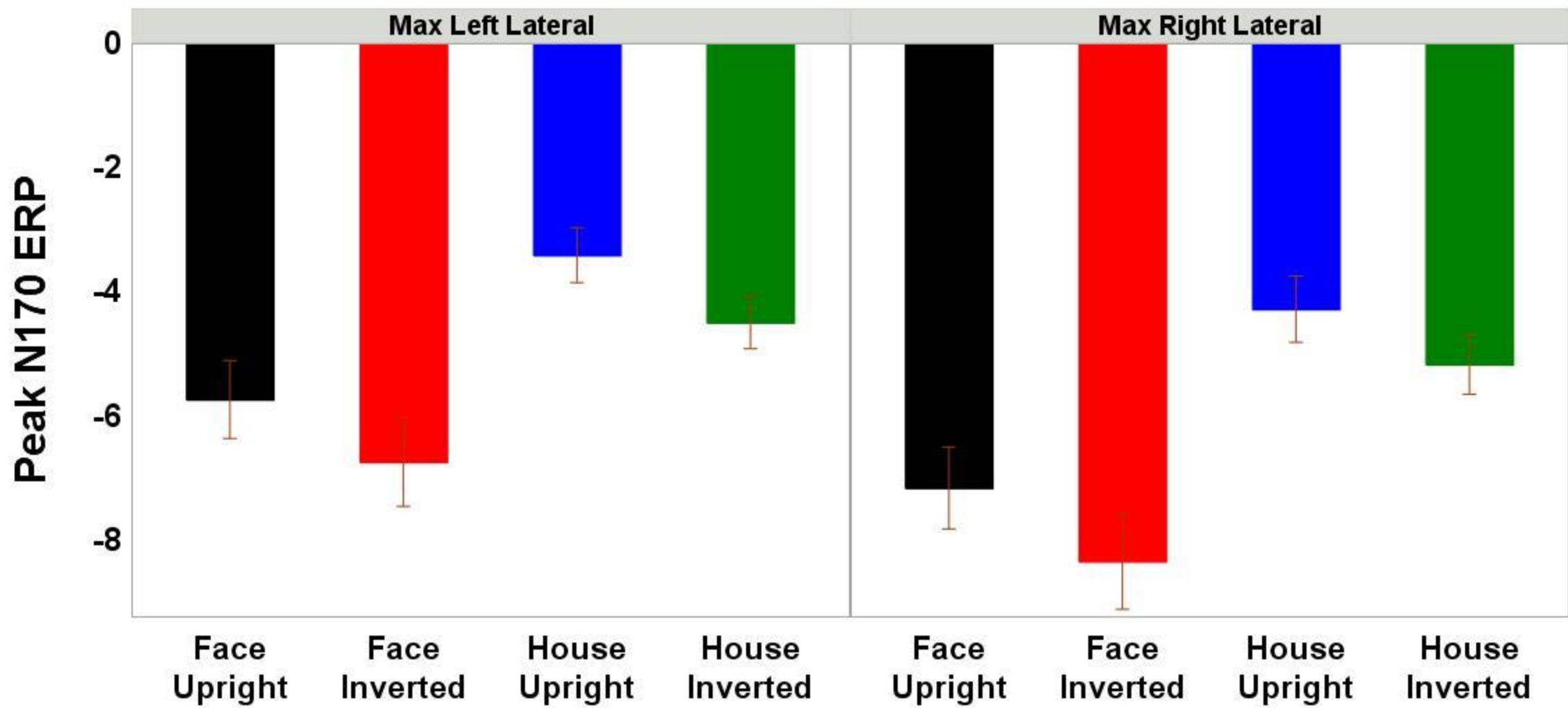
Faces (177 ms)

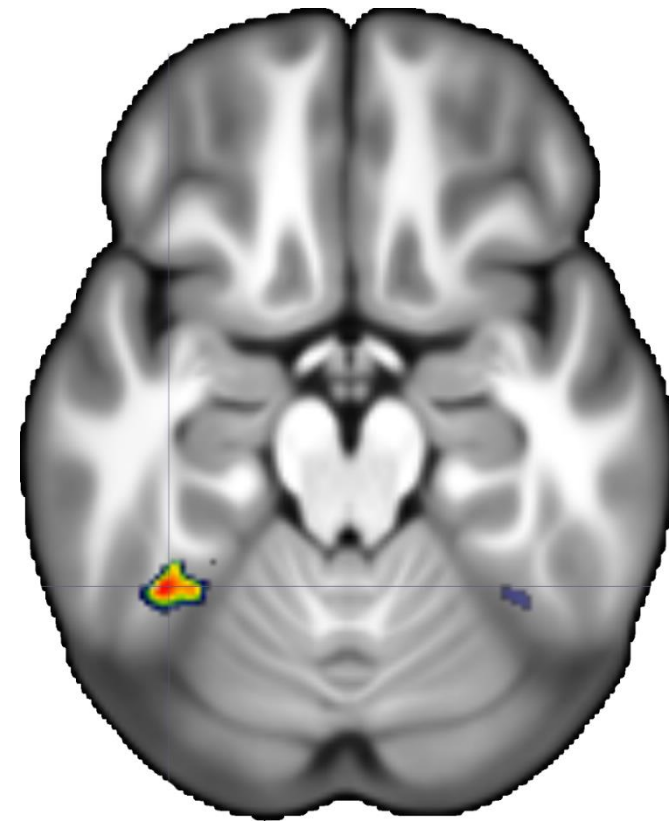
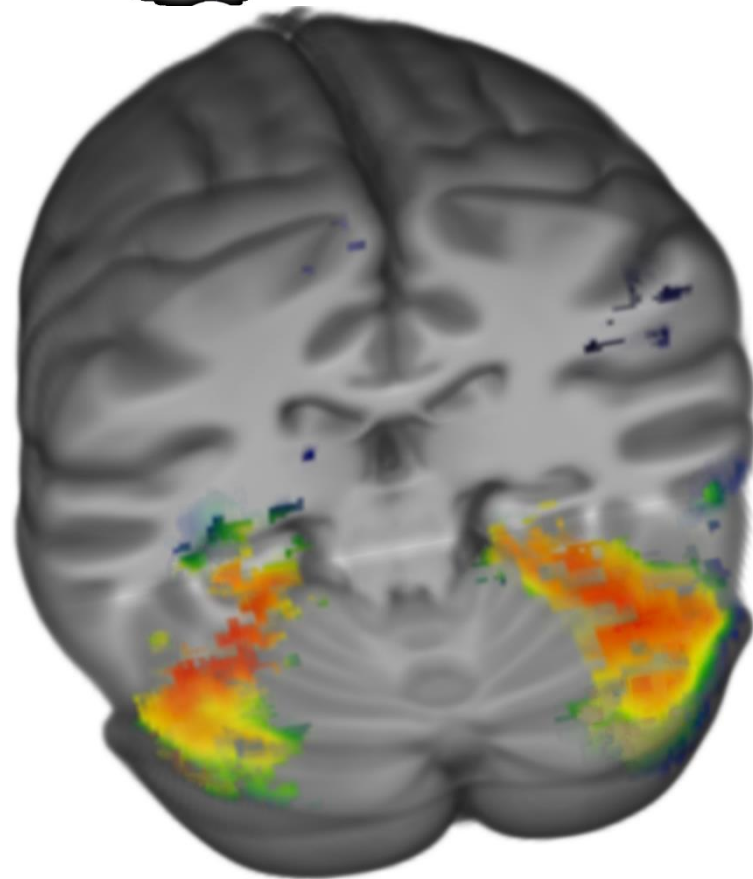
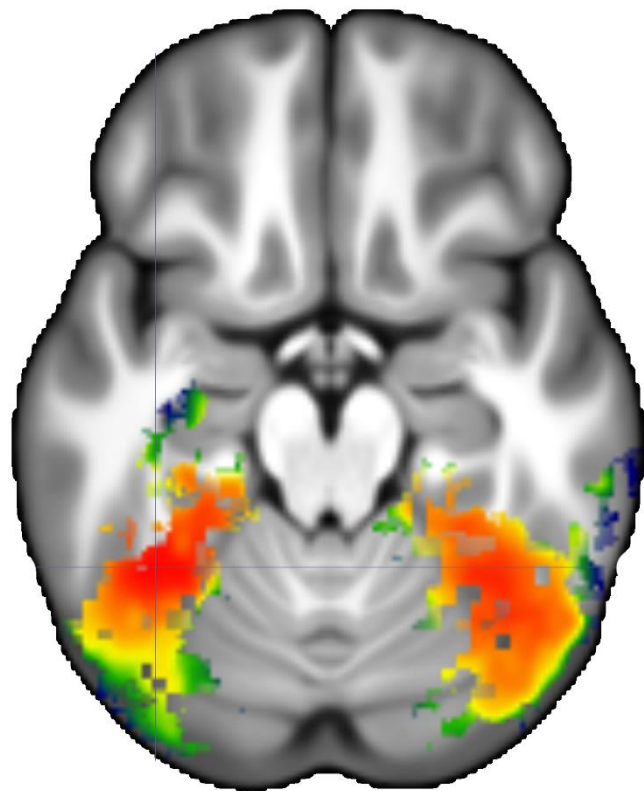
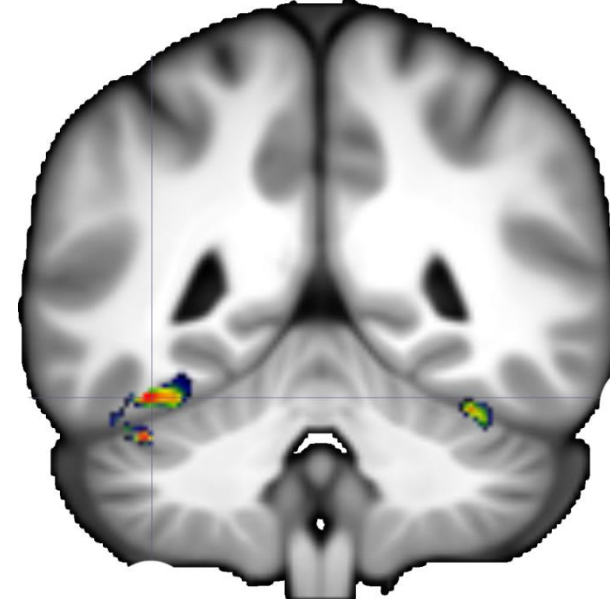
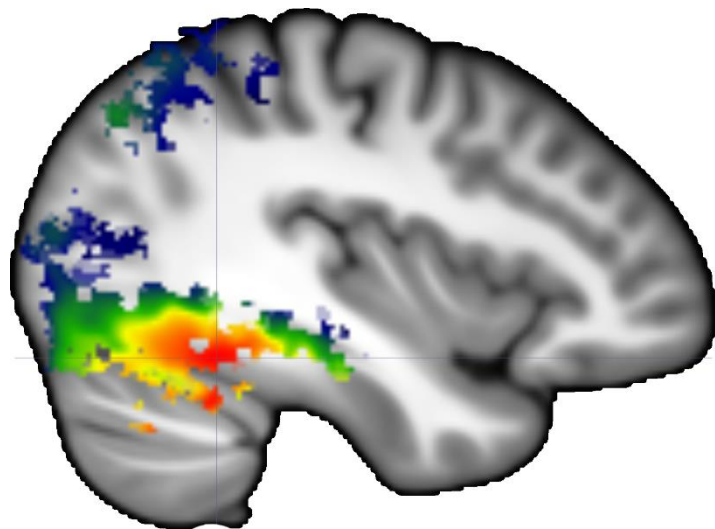
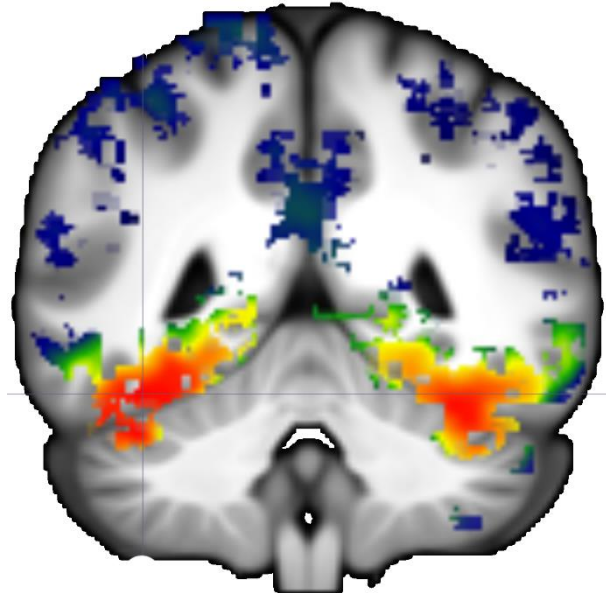


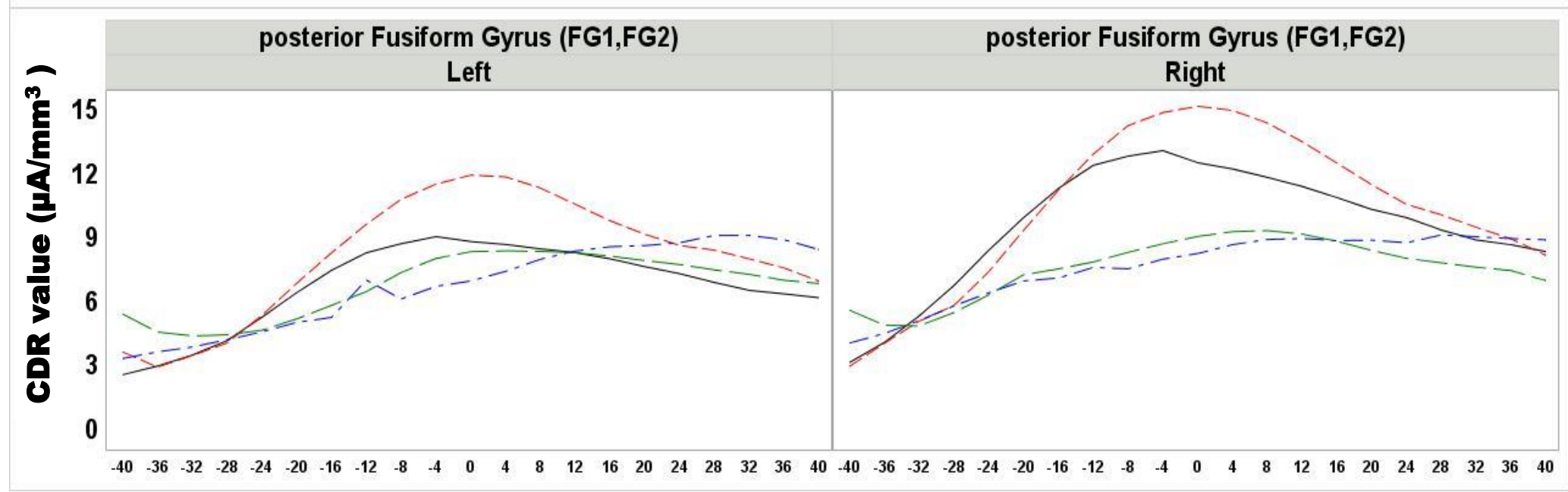
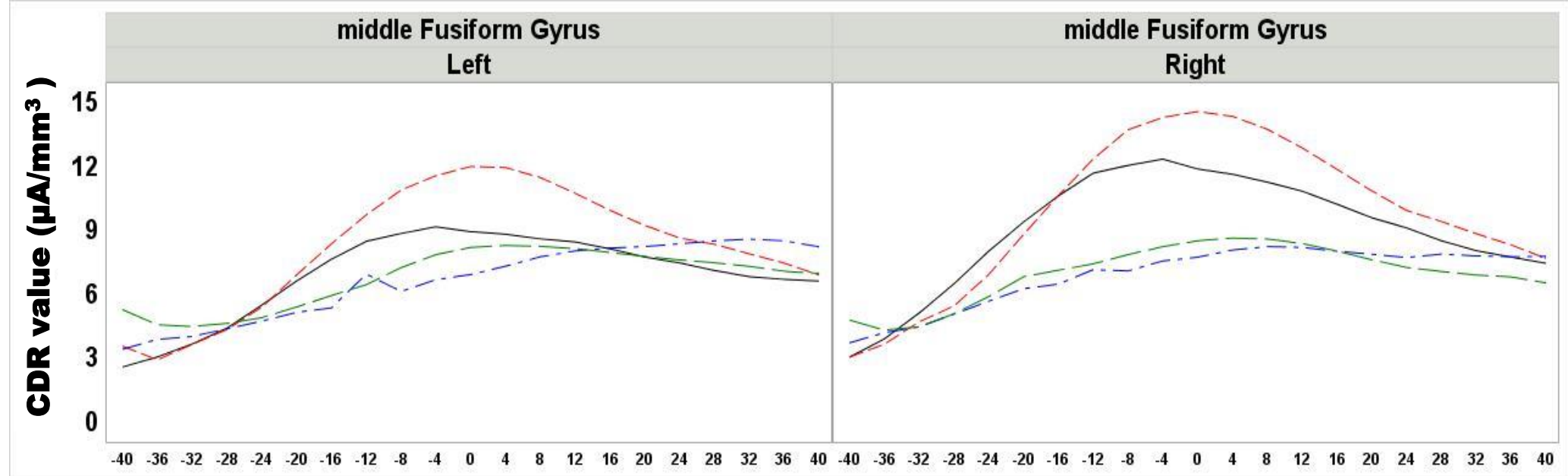
Houses (177 ms)



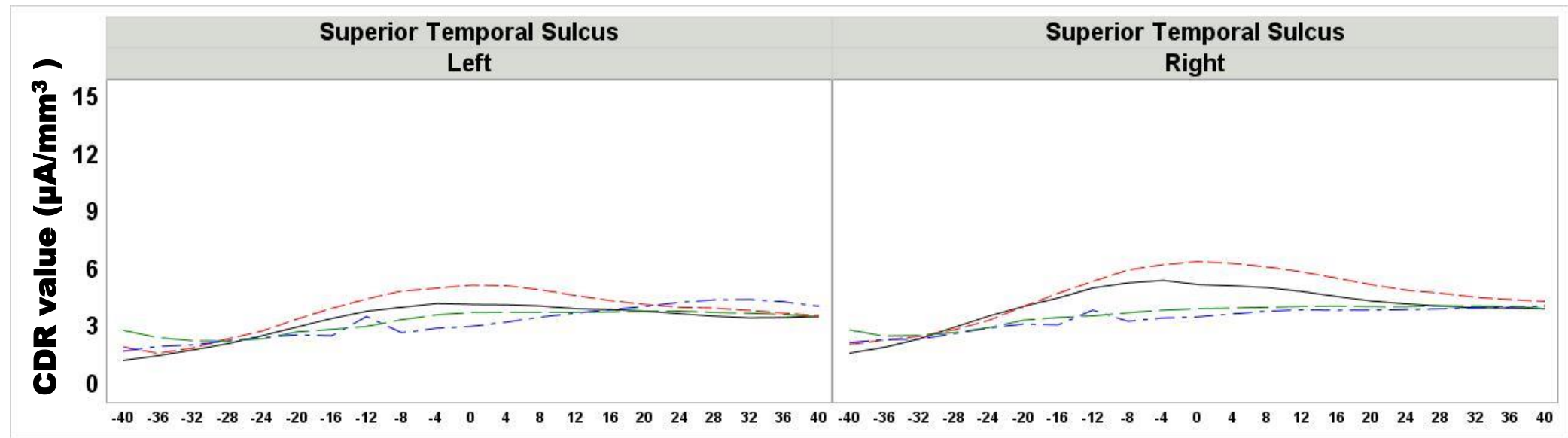
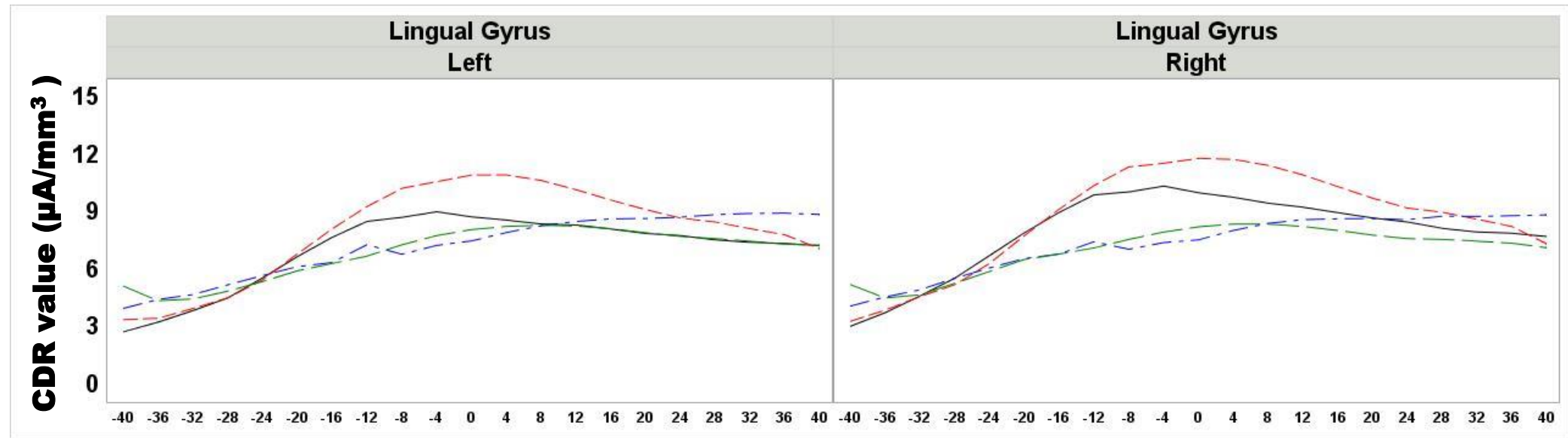




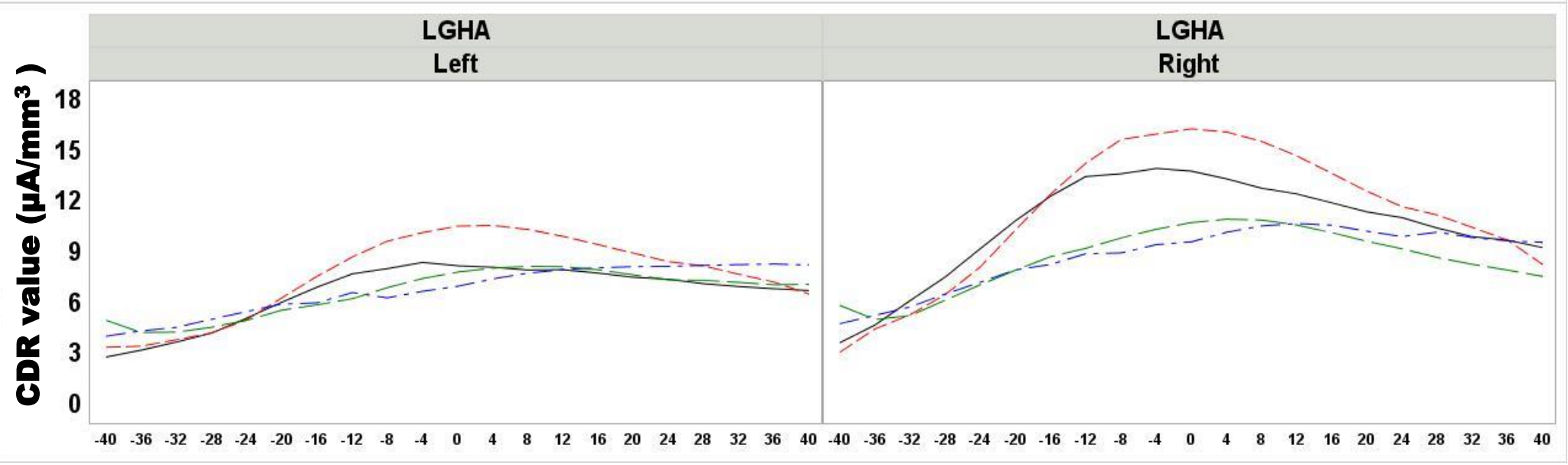
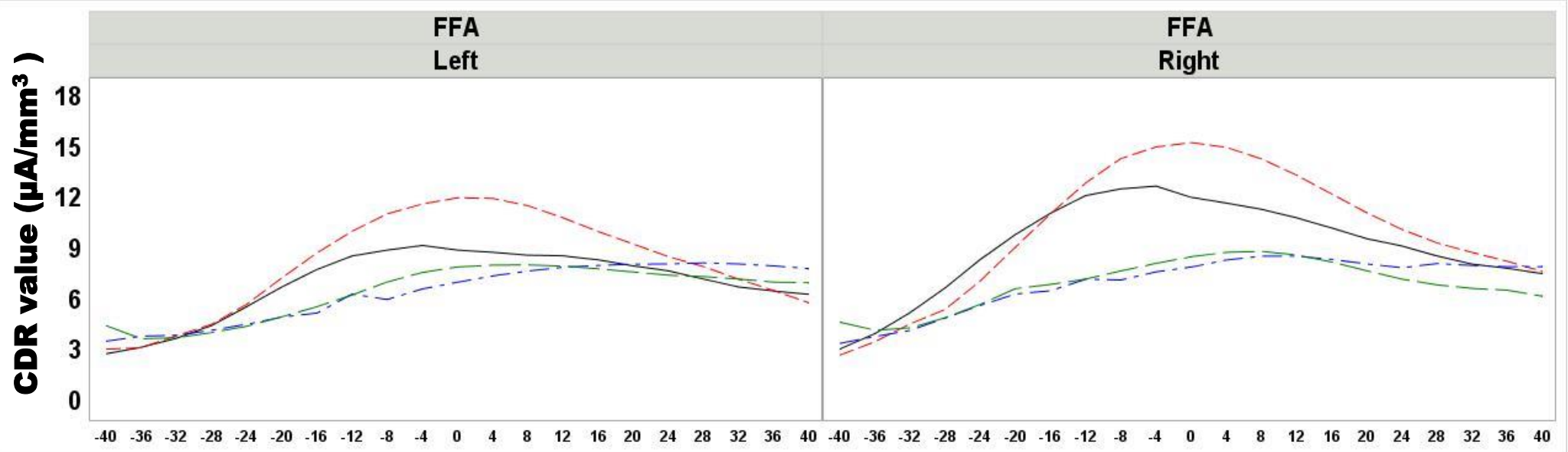




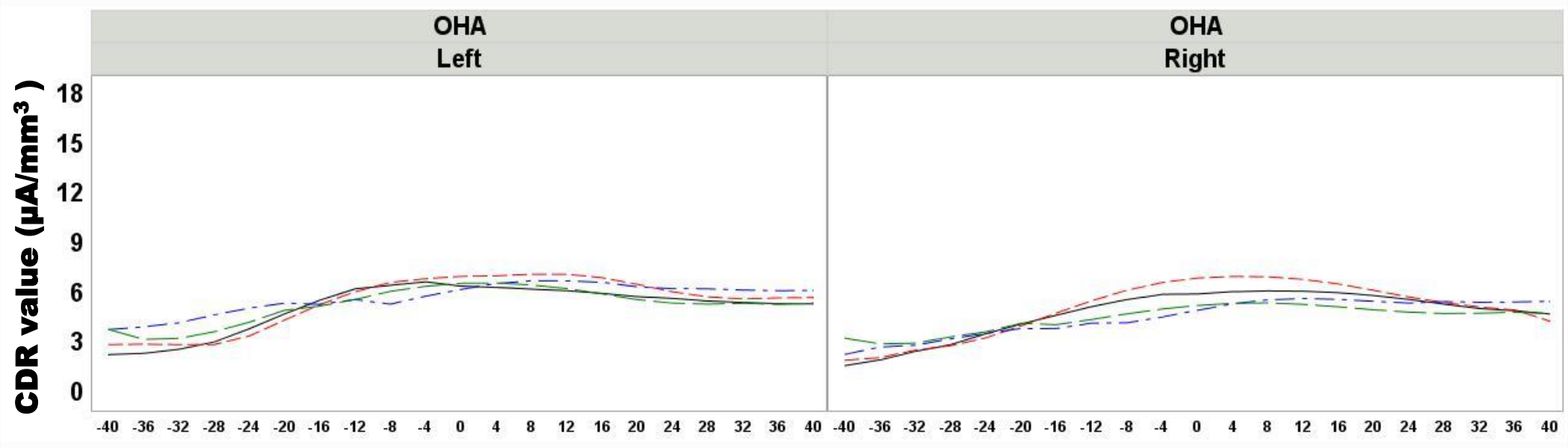
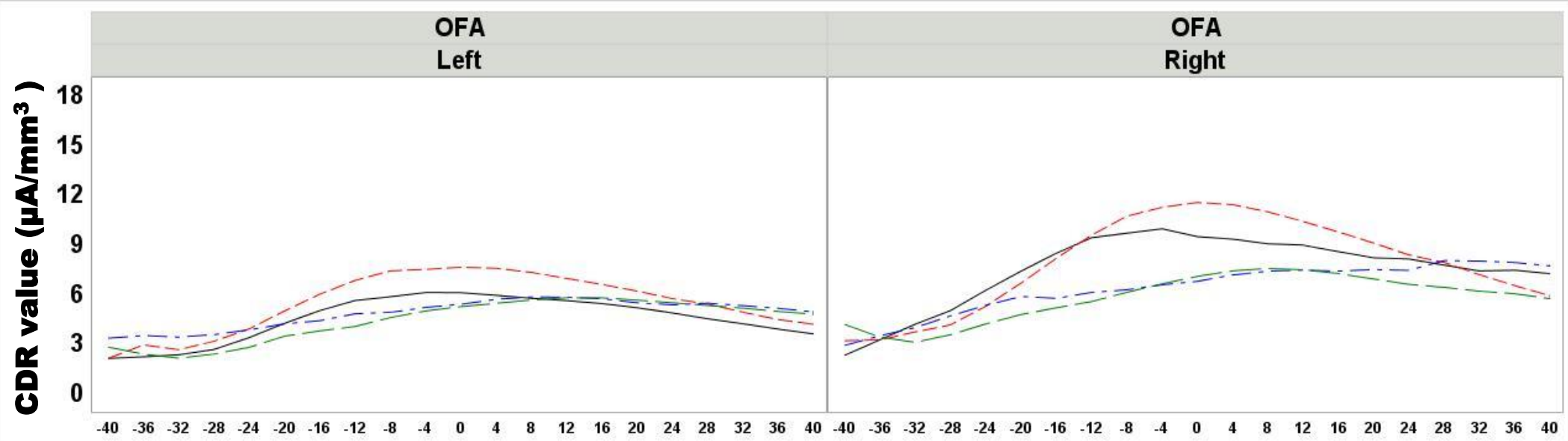
— upright face - - - - - upright house - - - - - inverted face - - - - - inverted house



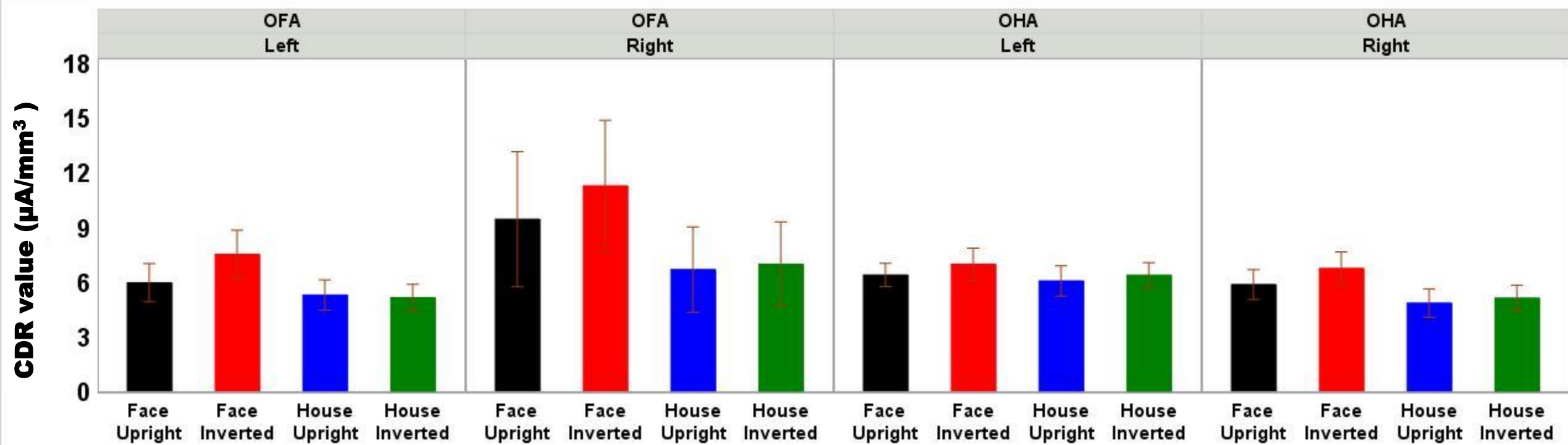
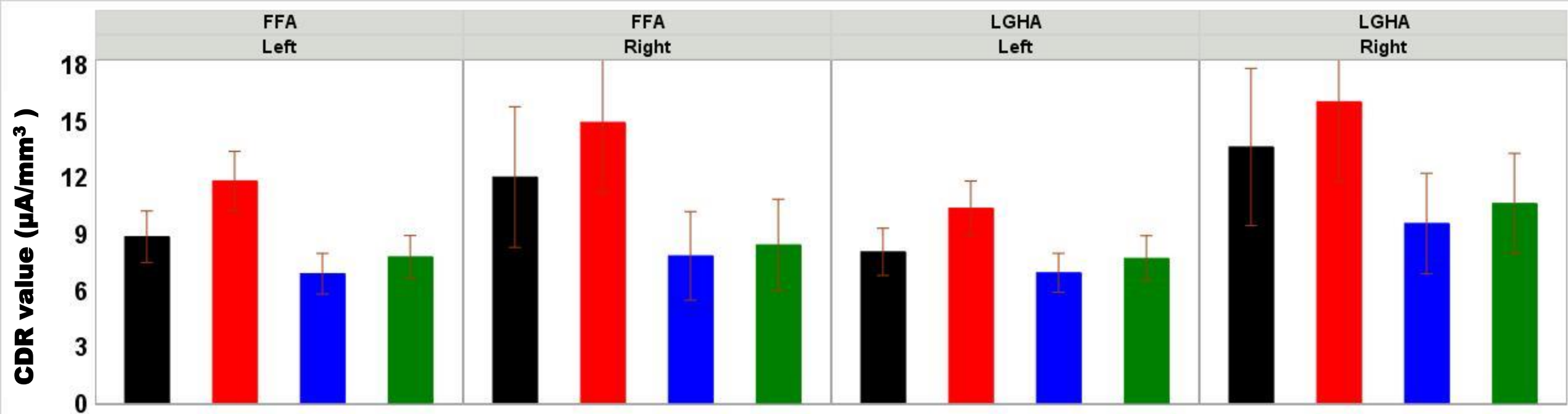
— upright face ··· upright house - - - inverted face - - - inverted house

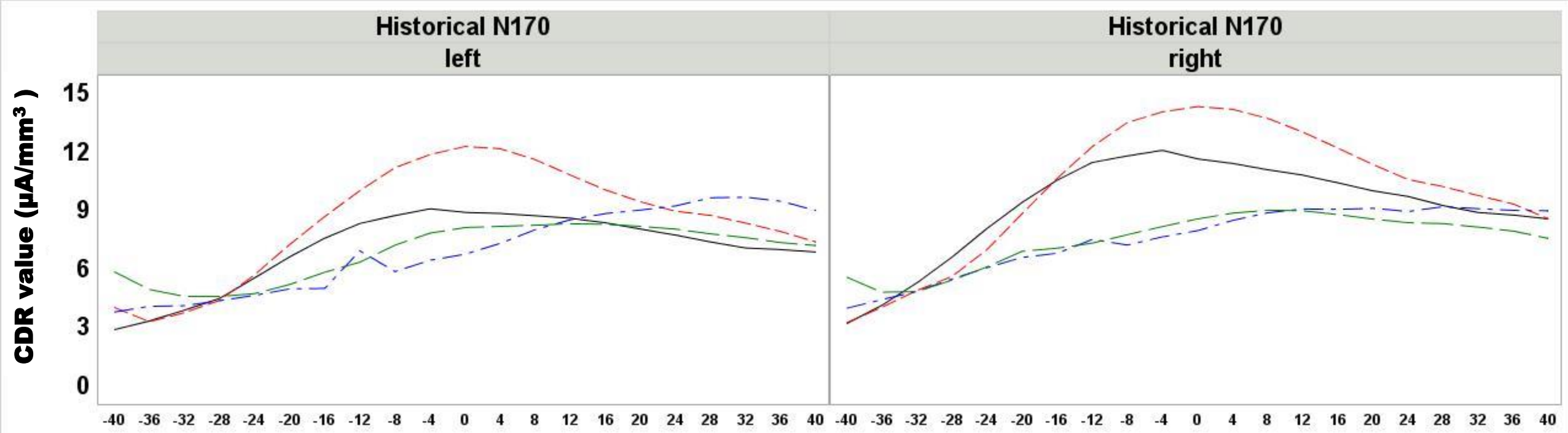
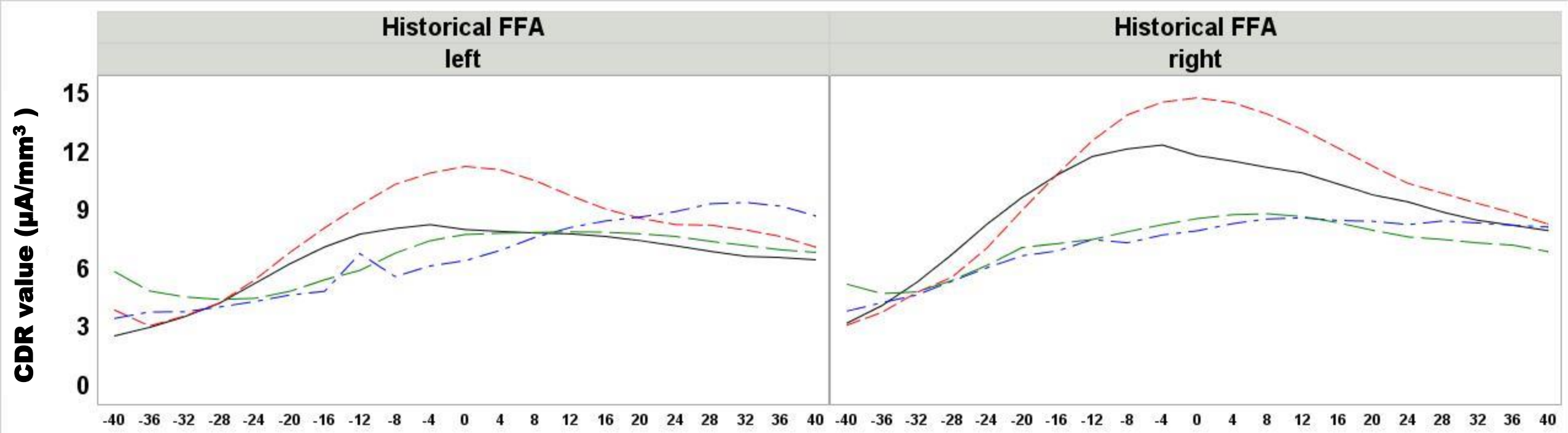


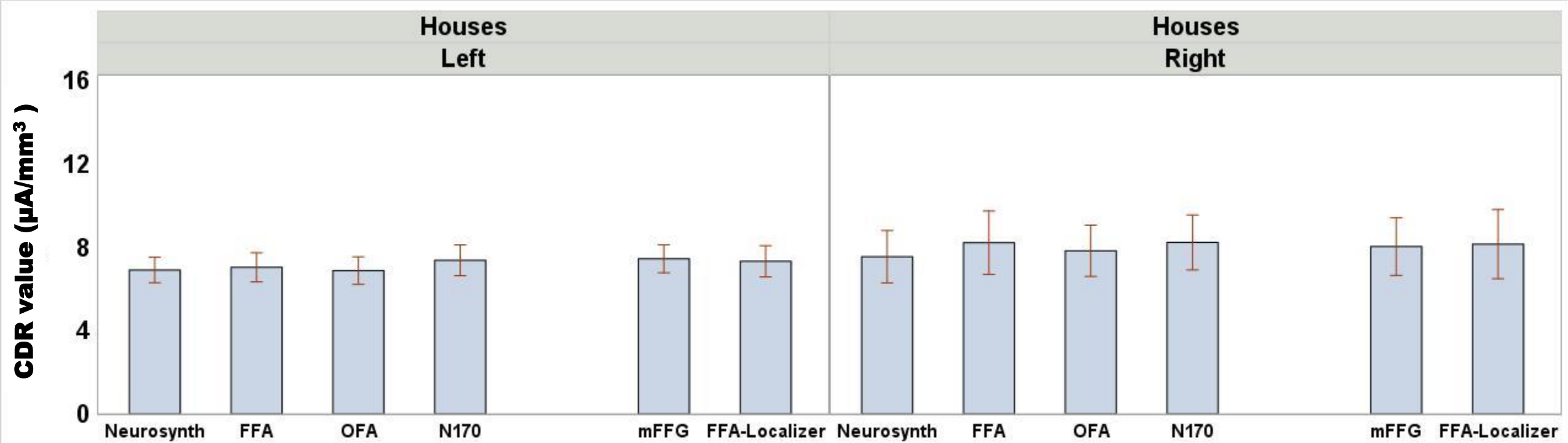
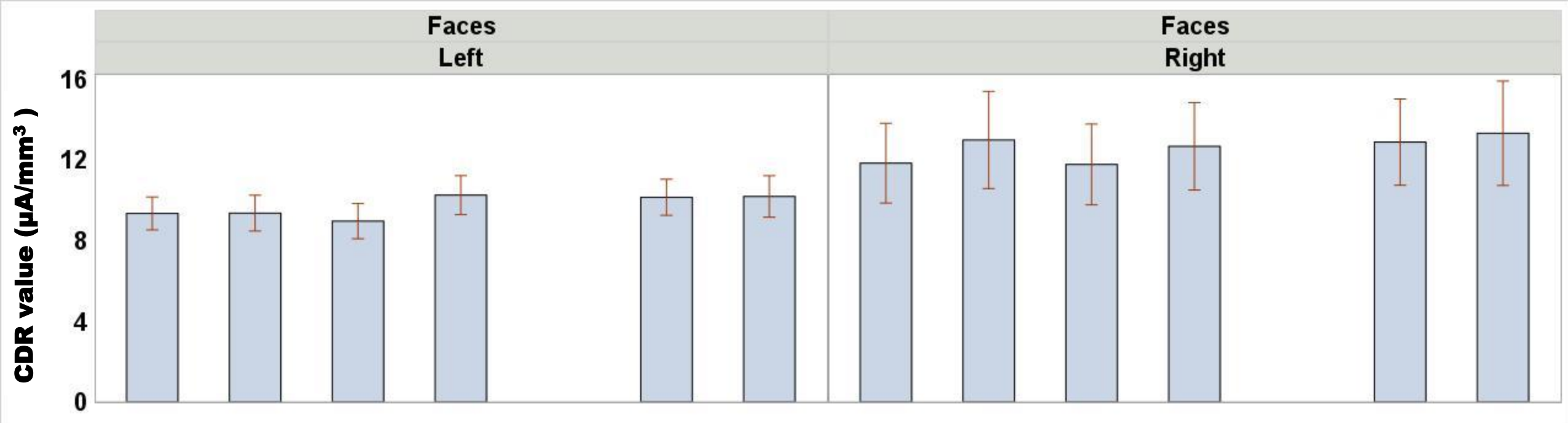
— upright face
 - - - - - upright house
 - - inverted face
 - - - - - inverted house

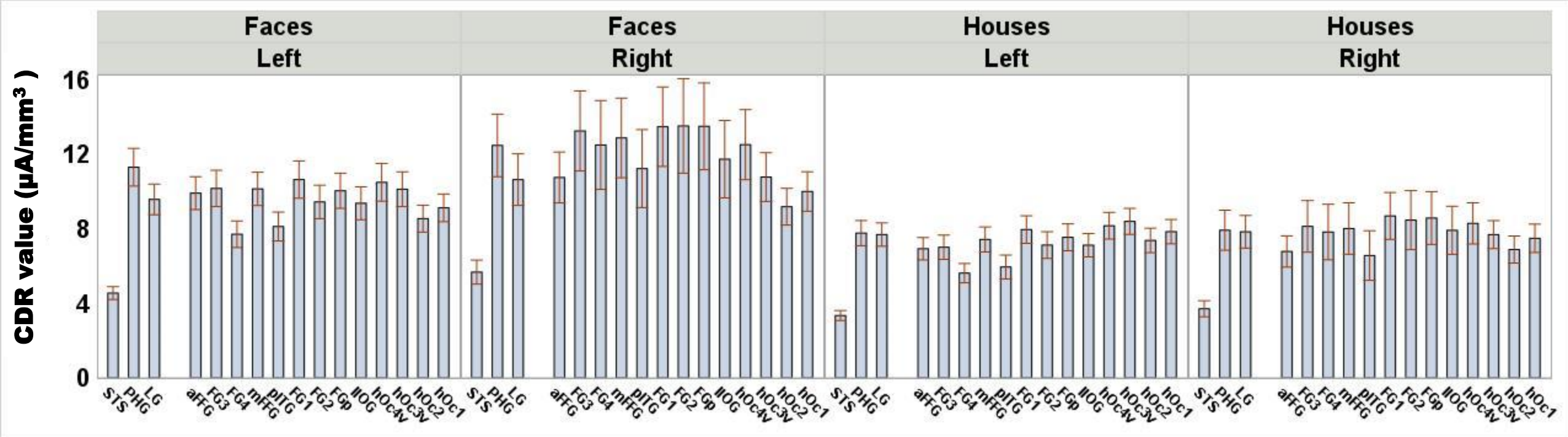
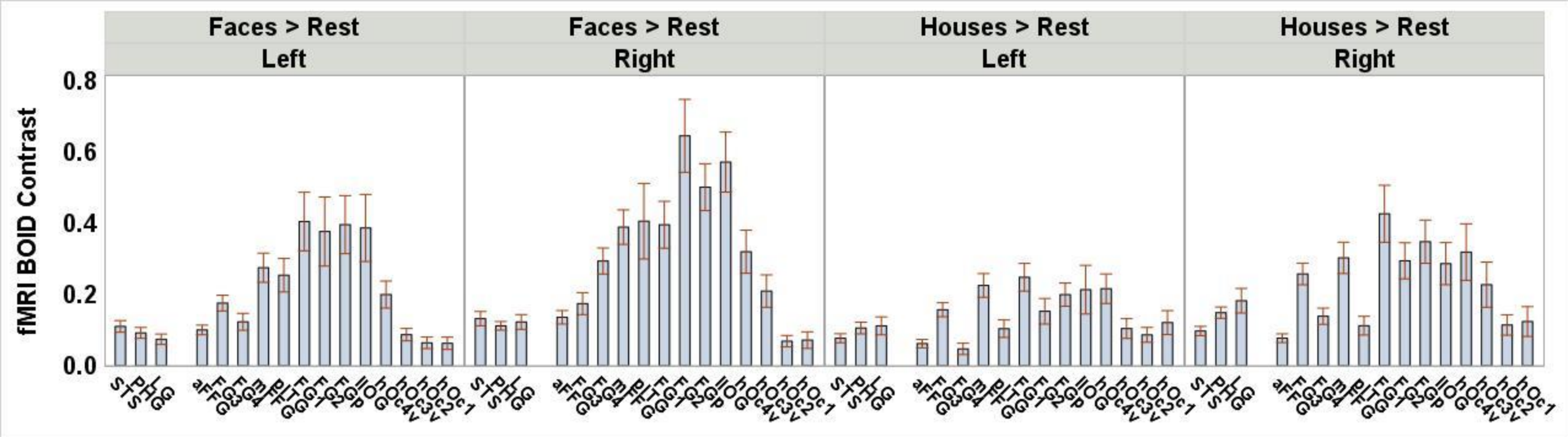


upright face
 upright house
 inverted face
 inverted house

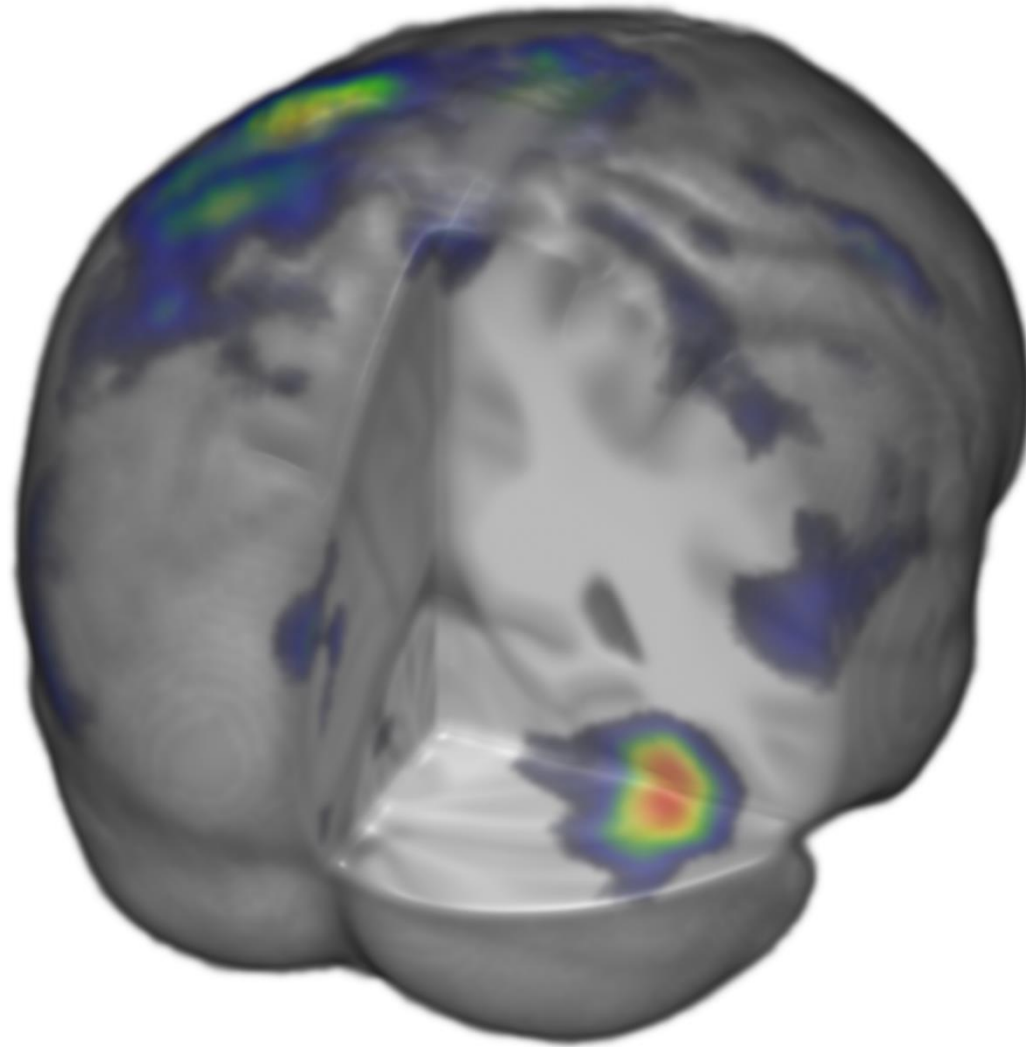




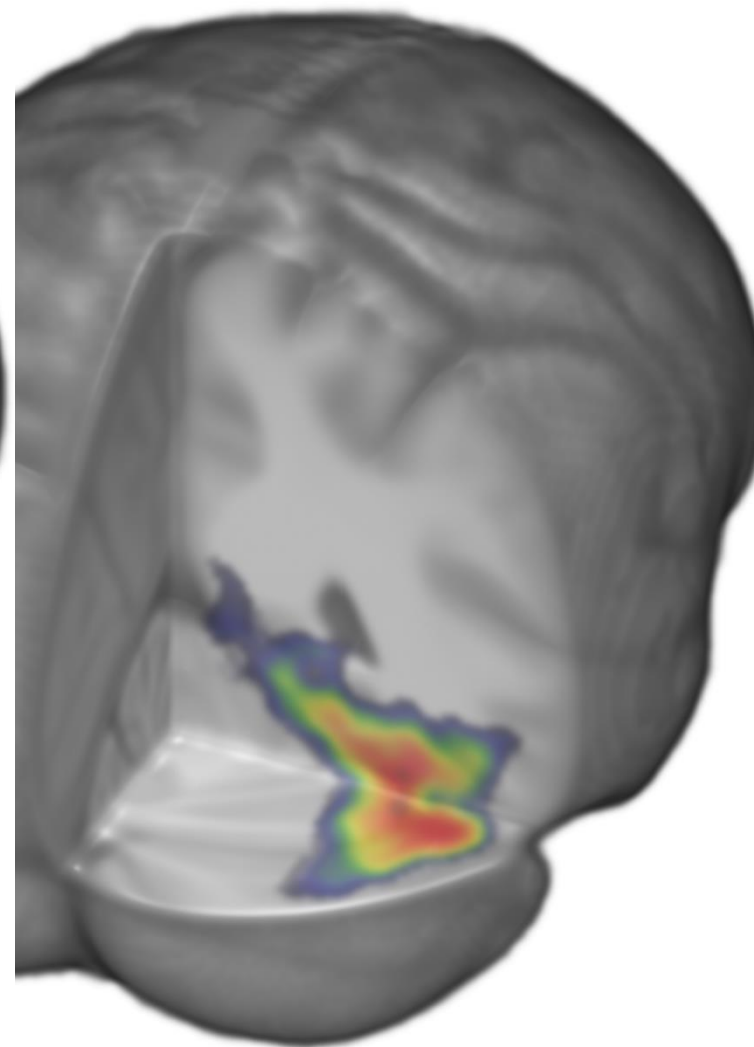




fMRI Faces > Rest



ERP CDR Faces



fMRI * CDR

